Crack pattern observations to finite element simulation

AN EXPLORATORY STUDY FOR DETAILED ASSESSMENT OF EXISTING REINFORCED CONCRETE STRUCTURES

Saurabh Dhanmeher
MASTER THESIS | STUDENT NUMBER: 4519566
Masters in Structural Engineering
(Specialisation: Structural Mechanics)

Thesis committee:

Dr. Max Hendriks(Chair)

Prof. Jan Rots

Dr. Arthur Slobbe

Dr. Yuguang Yang

Acknowledgement

The thesis study is conducted in collaboration with Nederlandse Organisatie voor Toegepast Natuurwetenschappelijk Onderzoek(TNO) as part of the curriculum for MSc in Structural Engineering at Technische Universiteit Delft.

The foremost acknowledgement goes out to my parents, for their eternal love and support in all my pursuits in life.

I would like to thank, Dr. Max Hendriks who informed me about the topic at TNO and as chairperson of the thesis committee has played a pivotal role is shaping my approach towards research. Special thanks go out to Dr. Arthur Slobbe, who took me under his wing at TNO and was a superb supervisor, mentor and guide. His vision and ideas are central to the work I have pursued in this thesis. I would also like to thank other committee members, Dr. Yuguang Yang, whose expertise in concrete and critical evaluation helped me a lot and Prof. Jan Rots, who provided valuable inputs during the final stages of the thesis.

Acknowledgement goes out to my near and dear friend Ir. Ameya Kamat, for all the discussions about image analysis which forms quite an important part of my thesis. Special thanks to my friend and housemate Alex Dreaves, who always offered a willing ear to listen to my ideas. Lastly a massive thank you to all my friends in Delft, who were always great company during the highs and lows throughout the course of my thesis work.

Saurabh Dhanmeher
November, 2017

Abstract

Uncertainties regarding structural safety of reinforced concrete structures may warrant a need for a detailed assessment. A detailed assessment using nonlinear finite element analysis is one of the alternatives which could help in decision-making about maintaining, upgrading or even demolishing and rebuilding of the structure. A reliable assessment should account for the existing damage in the structure, which may cause re-distribution of stresses within the structure, giving rise to unexpected failure modes. The existing approaches in nonlinear finite element analysis which account for the effect of already undergone damage in concrete, pose a number of limitations which either makes structural analysis ambitious or the uncertainty of concrete damage is not effectively accounted for. An alternative approach is adopted in this thesis, which is phenomenological and probabilistic in nature. Existing damage in concrete is conceived as a statistical field, which can be input into a finite element model, such that the existence of damage is taken as the starting point of the structural analysis. Focusing on indications of damage on the surface of concrete, i.e. crack patterns, an exploratory methodology based on image analysis is developed, to account for information obtained from crack pattern observation into nonlinear finite element analysis of reinforced concrete structures. The methodology is implemented on MATLAB and validated on damaged experimental specimens. Results of the computational analyses indicate good efficiency in predicting residual load carrying capacities and failure modes, alongside insightful numerical crack patterns. Through a critical examination of the obtained results and reflection upon the assumptions and simplification made in the methodology, recommendations for future research are provided.

Table of Contents

0. Introduction

0. 1 Background and motivation

Reinforced concrete (RC) structures are periodically assessed, e.g. by visual inspection, for a satisfactory performance during their lifetime. Uncertainties regarding the structural safety may arise due to a number of reasons, like an increase of traffic load or the discovery of damage in the structure. In an event of such uncertainty, an added opinion along with standard assessment methods may have to be sought, which will help responsible authorities in their decision-making concerning maintaining, upgrading or even demolishing and rebuilding of the structure. A more detailed assessment of the structure using finite element analysis is one of the alternatives to predict the structural behaviour and estimate the residual load carrying capacity.

This thesis focuses on detailed assessment by nonlinear finite element analysis, with uncertainties regarding the structural safety due to damage of the concrete. For a reliable estimation, the effect of already undergone damage (i.e. pre-damage) should be taken into account, since it may cause re-distribution of stresses within the structure and hence, may significantly impact the overall structural response under future loading.

Damage in the concrete can be present due to a variety of reasons, e.g. load history, deterioration mechanisms and accidental loading. Different approaches exist to account for this damage in nonlinear finite element simulations of RC structural members:

- Approach 1: Modelling the physical process which causes the damage.
- Approach 2: Performing a phased analysis.
- Approach 3: Adopting reduced material properties.

The first approach can be seen as a definitive way to account for pre-damage as it most closely captures the true physics of the problem. However, it poses certain difficulties. Generally, damage in concrete is caused by multiple physical processes working simultaneously. Therefore, it is often difficult to determine the precise source of damage. Furthermore, the physical processes themselves are dependent on a number of uncertain parameters like environmental conditions and material micro-structure. Accurately taking these parameters into account demand huge computational costs, due to which the analysis of the global structural behaviour may become unfeasible.

The second approach entails numerically loading the member under study, in multiple phases. In first phase, load is applied until a similarity is observed between the real and numerical crack pattern. The condition of the member at the end of phase 1 is considered as the pre-damaged state. In the subsequent phases, the pre-damaged member is checked for various load combinations as required. The usefulness of this approach is severely limited by the inherent uncertainty of the load history on the structure. Hence, speculations have to be made about the load which gave rise to the observed crack pattern.

The third approach involves testing cores drilled from the existing structure. The strength and stiffness obtained from these tests are then considered as a safe limit for the material properties used in the analysis. However, since the number of cores which can be drilled from a structure are limited, it is difficult to account for the spatial variability of damage, which is a prime cause of nonlinearity in the behaviour of concrete structures.

An alternative approach to the ones mentioned above, is explored in this thesis, based on an assessment framework recently proposed at TNO [1]. Within this framework is a suggestion for a material model for concrete based on total strains [see Appendix A], which is aimed at allowing direct incorporation of the effects of pre-damage in a finite element model, thereby eliminating the need for a phased analysis. The damage input, could be distributed as a statistical field over the domain under study, in order to account for the spatial variability. The finite element model is set up such that, the existence of pre-damage is taken as the starting point of the structural analysis. The obtained structural responses could then be used to draw conclusions about the safety and reliability of the structure. A major advantage of such a phenomenological and probabilistic approach is that it would eliminate the need to model complex physical processes, thereby providing a feasible way to study the global structural behaviour. However, a simplification of reality by focusing on the phenomena but overlooking the micro-physics of damage is bound to have a penalty of reduced accuracy, which needs investigation.
Also, following pertinent questions arise, which need addressing:

- How to define damage?
- How to account for pre-damage and its associated uncertainty?
- How to model pre-damaged structural members?

0. 2 Objectives and research question

The aim of this study is to contribute towards the development of a generic modelling approach that brings the information obtained from crack patterns into a finite model and enables the study of the effects of pre-damage of concrete, on the structural behaviour. Specifically, it aims at generalising the material model suggested at TNO, by implementing it in a finite element analysis framework and exploring its effectiveness in simulating experiments on pre-damaged RC members found in literature.

The following desired characteristics of the material model for damaged concrete are drawn:

- Input parameters as a function of measurable damage indicators based on fundamental mechanisms and experiments in literature.
- Meaningful results on the structural level.
- Practical to use for real-life RC structural members.
- Able to handle multiple types/sources of concrete damage.
- Damage input suited for probabilistic calculations

The following research question is set to be discussed through the results of the study:

- **How can the information obtained from visually observed crack patterns in RC structures be included in finite element analyses?**

The question is addressed by exploring ways to correlate the observed damage in RC structural members, specifically, surface crack patterns, to mechanical properties of concrete. These correlations are then used as damage input at the constitutive level in finite element simulations, to obtain the global structural response of the member. The effectiveness of this approach is discussed along with possibilities to extend the range of its application.

0. 3 Approach

In order to answer the main research question, the following steps are performed:

- Conducting a literature review investigating a few well-known causes of concrete damage.
- Characterising damage based on literature review to identify possible measurable inputs.
- Reviewing literature to explore methods to translate measurements to input data.
- Studying nonlinear finite element analysis of concrete fracture.
- Exploring the trial version of the material model implemented on DIANA [2].
- Implementing a nonlinear finite element analysis framework on MATLAB [3], which incorporates the desired material model for damaged concrete. The motivation for this step arises, from the need to provide flexibility in incorporating different algorithms, to couple damage evaluation with the finite element model.
- Verification and calibration of the implemented code by comparing results with DIANA.
- Validating on experimental tests using the developed tool.
- Drawing conclusions on the basis of obtained results.
- Suggesting possibilities for future research.

0. 4 Scope

The study is exploratory in nature and mainly focuses on damage in concrete which can be visually observed on the macro-scale. The observed crack patterns are assumed to reflect the damage occurring inside the structure. The study is limited to analysis of structural members damaged due to the load history experienced by the structure. Mechanical loads exerted on laboratory specimens are assumed to satisfactorily represent the load history. First, experiments conducted on the shear behaviour of vertically pre-cracked RC beams [4] are considered. Subsequently, focus is directed towards studying a more realistic case of pre-damage in RC members. Experiments investigating the shear capacity of RC members [5] are selected for this task. All the selected specimens are treated as 2-d plane stress problems. Figure 0. 1 provides a general outline of the thesis work.

Besides load history, damage in concrete due to time dependent deterioration mechanisms are studied in order to establish a generic outlook towards concrete damage [see appendix B]. The validation for it is, however, out of the scope of this thesis work.

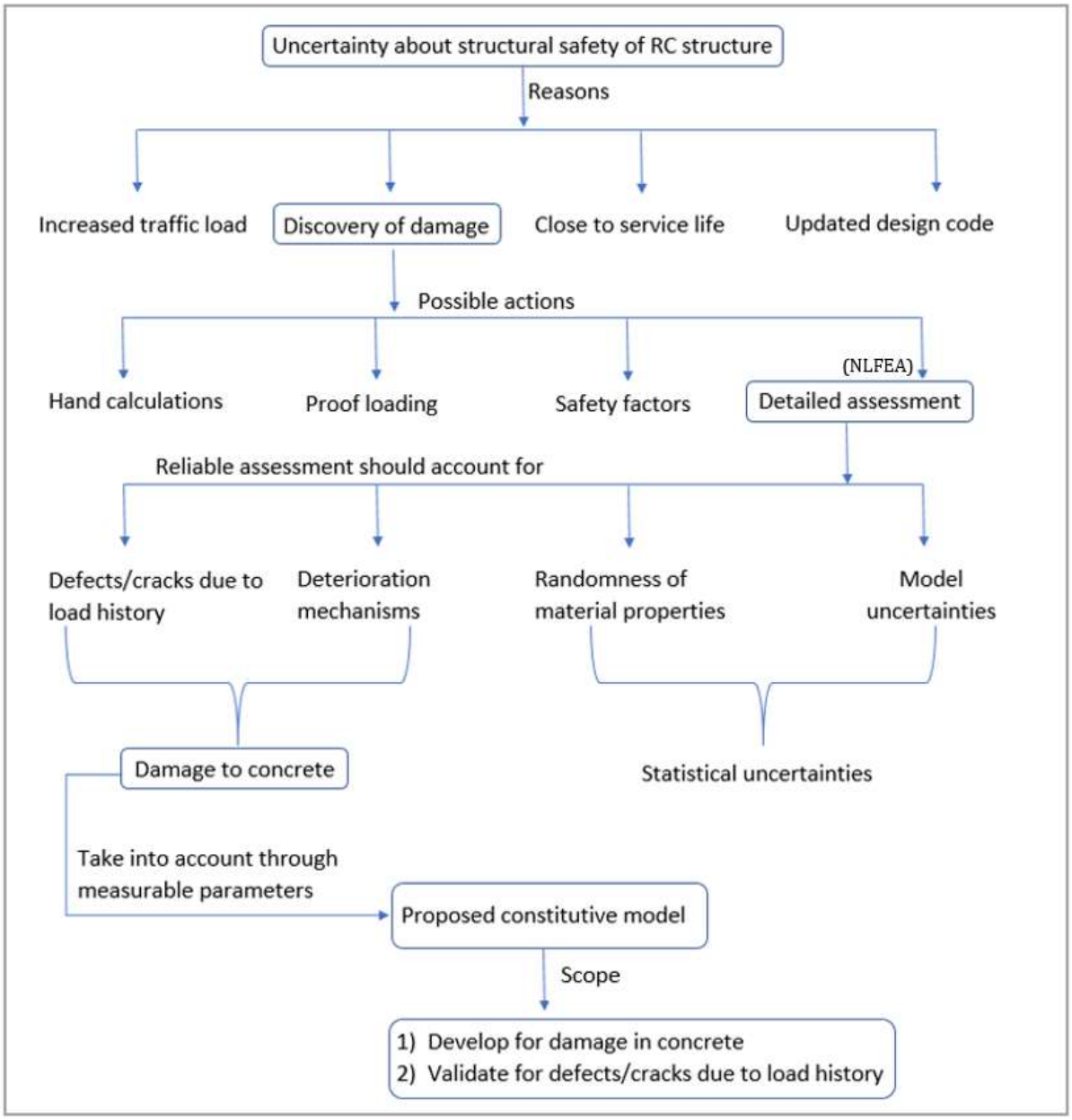

Figure 0. 1 Thesis Outline

0. 5 Structure of the report

The report is structured in the following format:

Chapter 1. Literature review: General discussion on damage in RC structural members and its visually observable characteristics. Exploration of assessment methods to translate measurement of damage characteristics to input data with a detailed discussion on fractal analysis of concrete surfaces.

Chapter 2. Methodology for modelling damaged RC members: Step-wise description of the methodology for finite element modelling of damaged RC members using the adopted approach. Discussion of assumptions made for each step.

Chapter 3. MATLAB Implementation: Setting up of a MATLAB based finite element framework. Verification tests to ensure proper implementation of the code. Full-scale computational analysis of RC structural members.

Chapter 4. Computational analysis of experimental specimens: Discussion of computational analyses of the selected experimental specimens including description of the experiment, finite element modelling, results and sensitivity study.

Chapter 5. Conclusions and recommendations: Addressing of the set research question. Conclusions based on the obtained results and suggestions for future applications.

Appendix A: Description of established crack concepts and total strain based formulation for finite element analysis, which serves as a point of departure for the adopted approach.

Appendix B: Literature review on damage in concrete due to time-dependent deterioration mechanisms.

1. Literature review

1. 1 Introduction

The primary aim of this chapter is to characterise damage in reinforced concrete such that correlations can be set up between visual observation of the structure and material properties of concrete. Literature on some typical forms of damage seen in RC was reviewed and is summarised in section 1.2. Detailed description of the studied mechanisms can be seen in Appendix B. Fractal analysis of concrete surfaces was reviewed as a method to translate the observations to usable data, which is discussed in the section 1.3.

1. 2 Damage in reinforced concrete

Reinforced Concrete (RC) is a composite construction material made up of concrete and reinforcing steel. The concrete itself is a composite material which derives its material properties (strength and stiffness) from its constituent elements, i.e. aggregates, cement and their interface. At an elementary level, damage in concrete implies degradation of its constituent elements and weakening of the interaction between them. This could occur due to the external load applied on the structure or the internal stresses developed within the structure due to deterioration of the material. Generally, the stressing and consequent damage of the RC structures is caused by a combination of mechanisms, which may depend on a number of factors like temperature, porosity, water-cement ratio, etc. Hence in reality, it is often difficult to attribute the cause of damage to specific mechanisms and to quantitatively describe the change in material properties. However, due to the fact that the tensile strength of concrete is drastically lower than its compressive strength, damage in concrete is generally accompanied by cracking on the surface. In many cases, the patterns formed by these cracks along with other distinguishable features can provide an indication of the damage causing mechanism. Figure 1. 1 to Figure 1. 6 exhibit some typical damage mechanisms, distinguishable features and crack patterns observed in RC structures. Table 1. 1 summarises these typical damage mechanisms in concrete and their distinguishable features. More information on the mechanisms is provided in Appendix B.

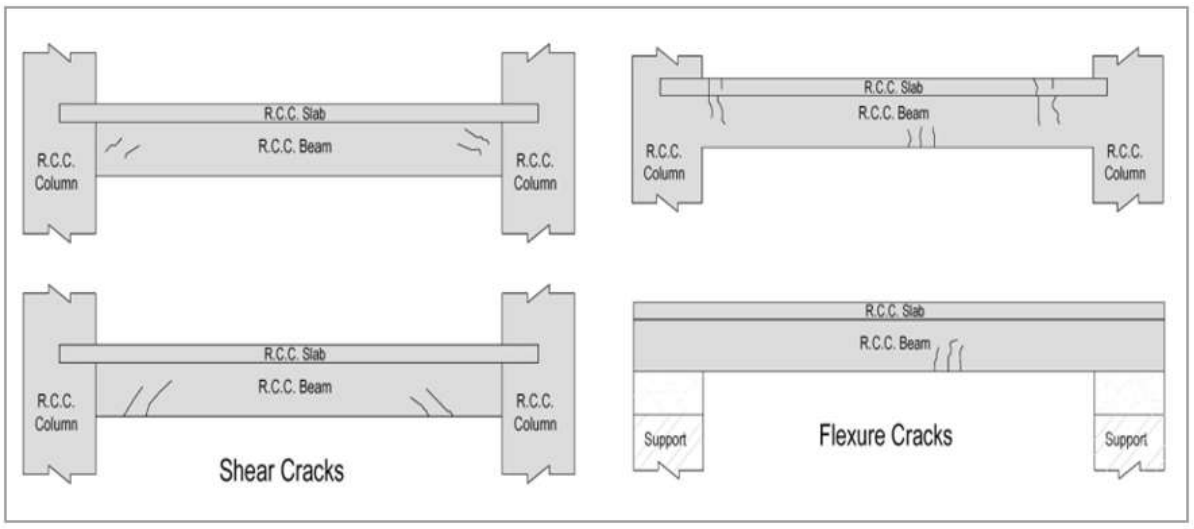

Figure 1. 1 Cracks in RC members due to external load [6]

Figure 1. 2 Map-cracking due to alkali-silica reaction and cracks preferentially oriented along the main reinforcement [7]

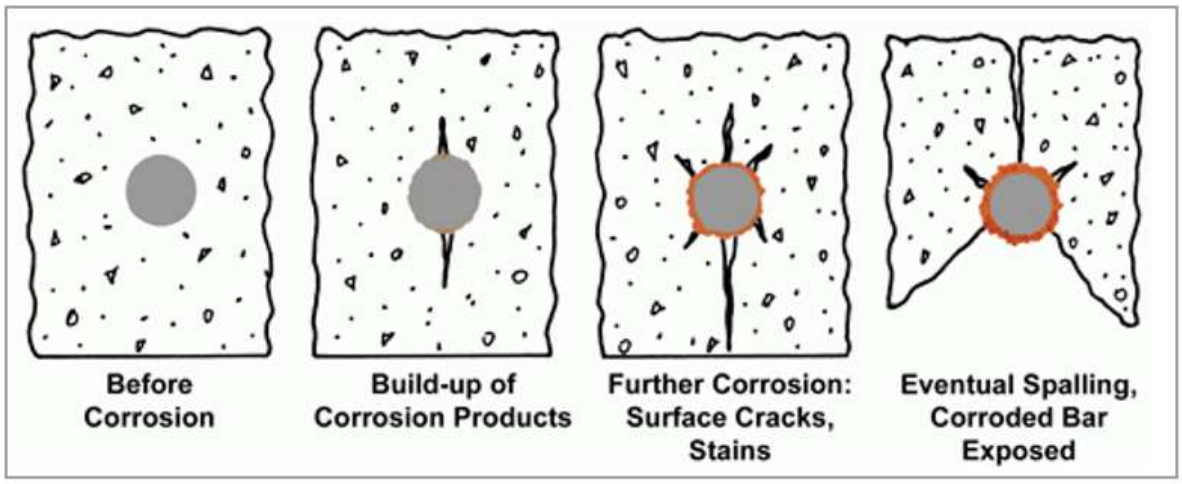

Figure 1. 3 Evolution of corrosion damage in RC [8]

Figure 1. 4 RC member affected by reinforcement corrosion [9]

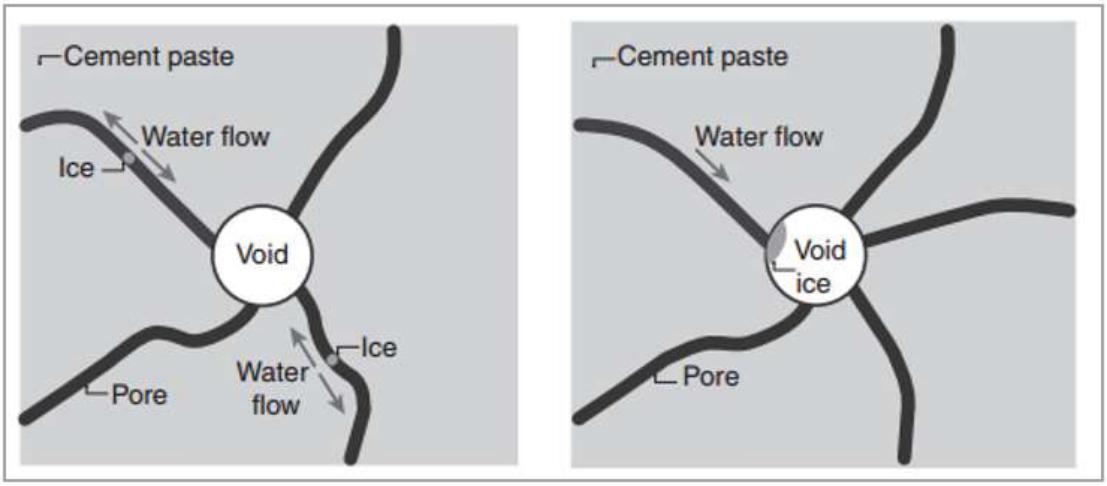

Figure 1. 5 Freeze-thaw mechanism in the cement paste [10]

Figure 1. 6 Surface scaling of concrete due to freeze-thaw cycles [11]

Cause of damage	Internal characteristics	Visible characteristics	Relevant measurable parameters
Mechanical loading	• Micro-cracking in interfacial transition zones	• Cracks in areas of high tensile stress	• Crack width • Crack orientation
Reinforcement Corrosion	• Loss of rebar area • Internal cracks along reinforcement	• Cracks with rust stains • Spalling of concrete cover	• Weight loss along rebar
Freeze-thaw cycles	• Freezing and thawing of water in the micro-structure	• Delamination due to surface damage • Cracking due to internal damage	• Degree of saturation of drilled cores
Alkali-silica reaction	• Formation of silica-gel in the aggregates and cement paste • Expansion of gel due water absorption	• Map-cracking • Cracks with desiccated silica-gel	• Damage Rating Index (petrographic study) • Stiffness of drilled cores

Table 1. 1 Summary of typical damage mechanisms in concrete and distinguishable features

1. 3 Quantitative assessment of observed concrete damage

As seen in the previous section the surfaces of damaged areas of RC structures exhibit complex crack geometries. Fractal geometry could serve as a useful tool to characterise such complex patterns and provide a novel way of assessing the effect of pre-damage in existing structures [12]. The term 'fractal' was coined by Benoit Mandelbrot, to characterise objects which exhibit statistical self-similarity, i.e. a small portion of the object can be considered as a scaled copy of the whole, in a statistical sense [13]. Since its inception, fractal geometry has found applications in many fields of science and engineering [14]. Research suggests that concrete fracture surfaces possess fractal characteristics which can be correlated to the mechanical behaviour of the structure [12] [15]. In this section, these fractal characteristics are described and their correlation with mechanical properties is discussed by reviewing experimental literature on RC structural members.

1.3.1 Fractal dimension

In fractal analysis, the most basic parameter used to characterise the geometry of the object under study is called the fractal dimension(D). It provides a quantitative measure of the complexity of a pattern, when observed from different scales. The most popular algorithm to estimate D is the box-counting algorithm which considers the space filling properties of an object as a measure of its complexity [15]. The method involves covering the object with a virtual grid of boxes of size r. Next, the number of boxes N(r) required to completely cover the object are counted. As the box size tends to zero, the ratio, log(N(r))/log(1/r) converges to the measure of D.

Therefore, fractal dimension is defined as,

$$D = \lim_{r \to 0} \frac{\log N(r)}{\log(1/r)}$$

The ratio log(N(r)) vs. log(1/r) is plotted for a range of box sizes and the slope of the least square fit line is taken as the estimate of the fractal dimension of the object. The process is demonstrated in Figure 1. 7 for four artificial crack patterns.

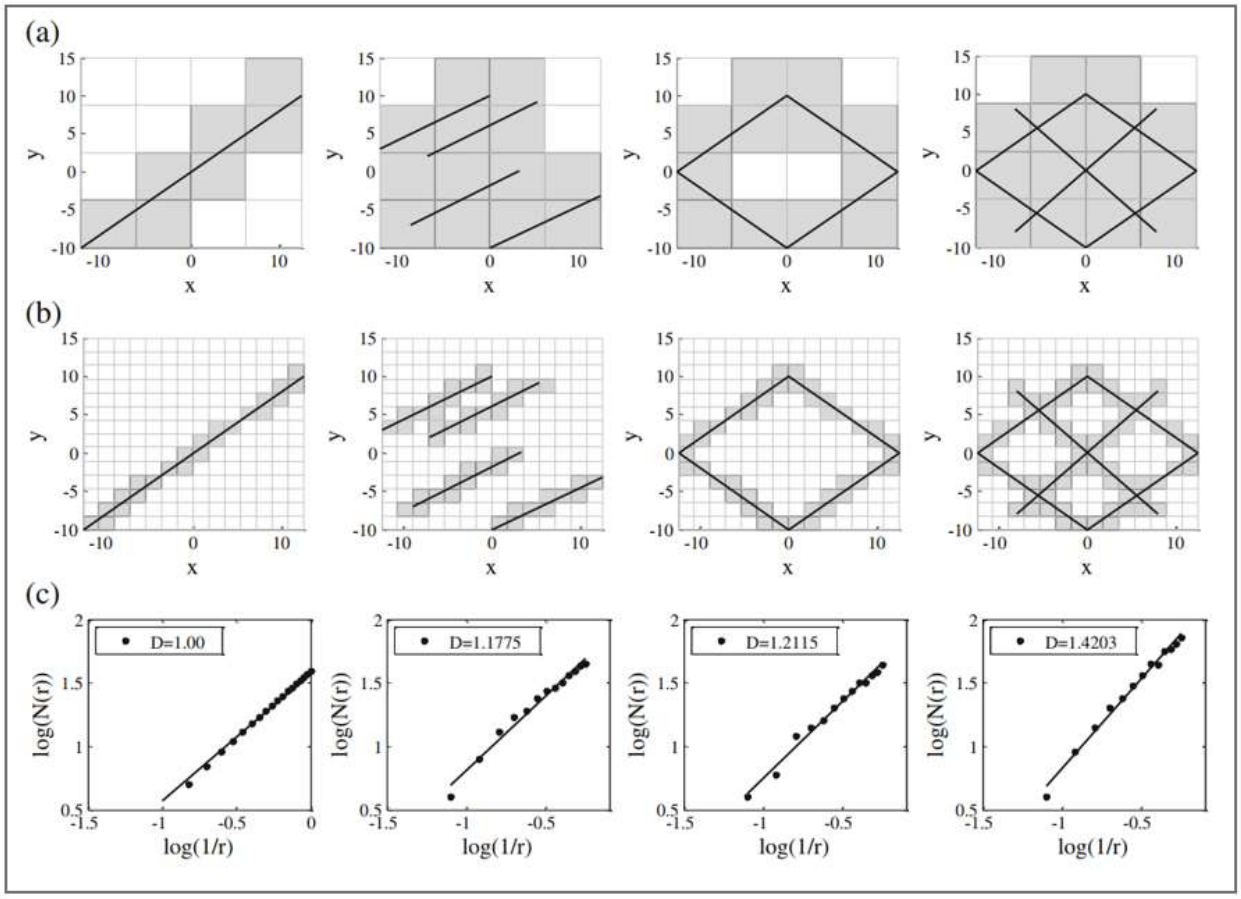

Figure 1. 7. Estimation of fractal dimension [15]

It can be observed in Figure 1. 7 that for a straight line the value of D is equal to 1, which is the minimum value taken by the fractal dimension of a curve embedded in a 2-d space. For distributed lines it takes a higher value. When the same distributed lines are arranged in a quadrilateral shape the value jumps from 1.1775 to 1.2115. This is because more area is required to cover the same total length, thereby increasing the number of boxes required to cover the curve. Upon addition of a cross to the quadrilateral, D further jumps to a higher value. The value of 2 will be taken up when the curve covers the entire domain and passes through all the boxes. Hence, the maximum value of fractal dimension for an object embedded in a 2-d space is 2.

D quantitatively describes the distribution of a pattern under study and takes up higher values for patterns which cover more area. In the experimental setup described in [15] these observations were used to infer that larger values of D may correspond to structural elements significantly damaged and the following damage index was proposed for structural health monitoring of RC structures,

$$DI = \frac{D_i - D_1}{2 - D_1} \qquad (0 < DI < 1)$$

Where, D_i and D_1 are the fractal dimension of the current state and reference state respectively. 2 represents the maximum value of D_1

Two full-scale shear walls were tested in [15] for cyclic lateral loading. The experimental setup for one of the walls can be seen in Figure 1. 8.

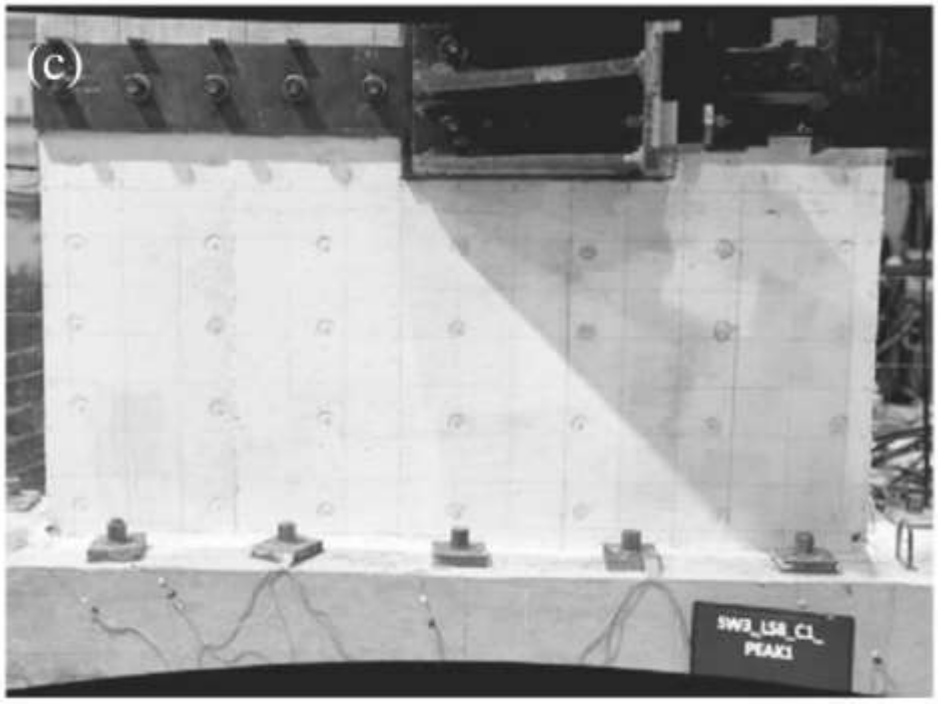

Figure 1. 8 Experimental setup for cyclic lateral loading [15]

The residual stiffness loss of the walls was computed as,

$$RSL = 1 - \frac{K_i}{K_1}$$

Where, K_i and K_1 are the lateral secant stiffness loss of the wall at the current state and reference state respectively. The fractal dimension of the residual crack pattern after each load step were computed and compared against the RSL for each load step. Figure 1. 9 shows a representative load step(LS5) for one of the walls in which the crack patterns are extracted from the image of the experimental setup. Figure 1. 10 demonstrates the estimation of the fractal dimension using the box-counting algorithm for the same.

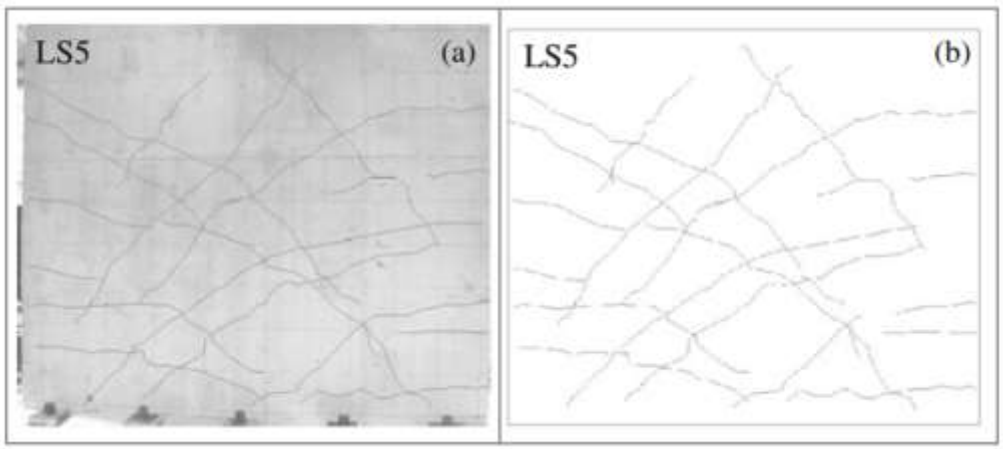

Figure 1. 9 a) Photograph of experiment b) Extracted crack pattern [15]

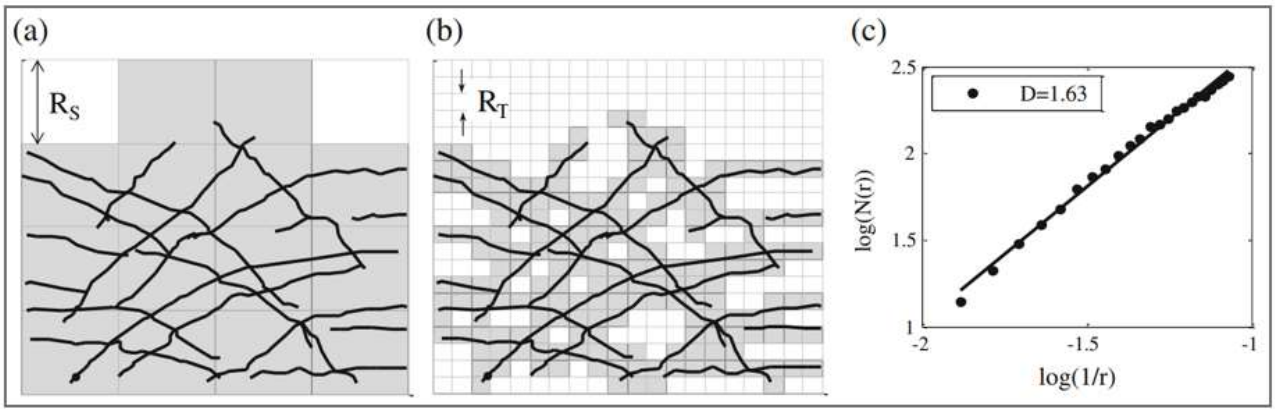

Figure 1. 10. Estimation of fractal dimension of extracted crack pattern [15]

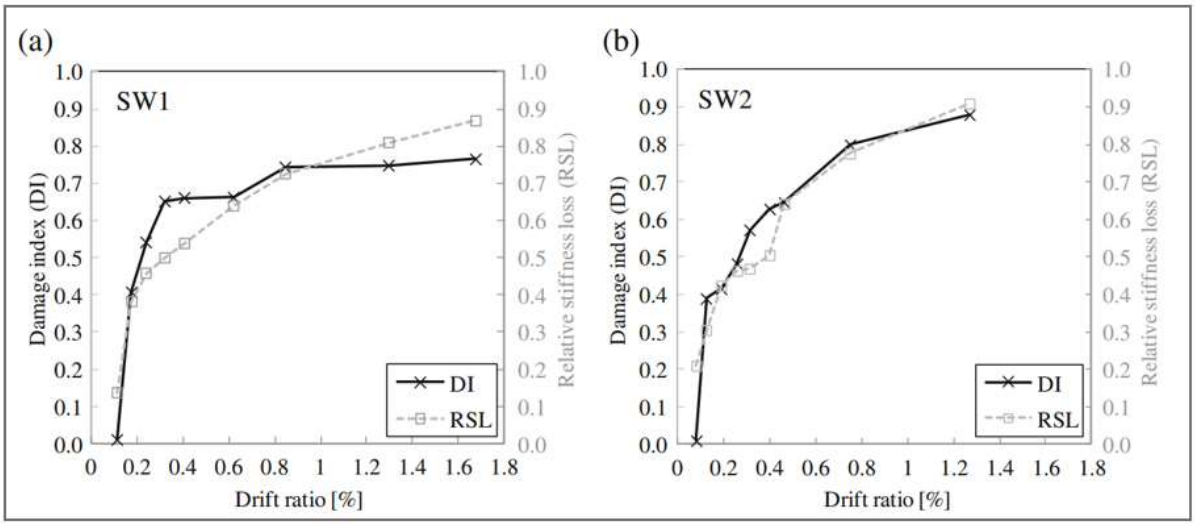

Figure 1. 11. Comparison of damage index(DI) and relative stiffness loss(RSL) at every load step for both specimens [15]

It can be observed in Figure 1. 11 that there is a close fit between the variation of stiffness and the damage index based on fractal dimension of residual crack pattern of the shear wall.

In another experiment conducted in [12] an RC beam was tested under three-point bending. The experimental setup can be seen in Figure 1. 12.

Figure 1. 12 Experimental setup of three-point bending test [12]

The fractal dimension of the residual crack pattern was computed using the box-counting algorithm and was compared against the first three orders of natural frequency of the beam computed using frequency spectrum analysis. Figure 1. 13 shows a representative crack pattern at a particular load step (load step 6) while, Figure 1. 14 shows the comparisons of natural frequency versus the fractal dimension of the cracks for all load steps.

Figure 1. 13 Crack pattern after load step 6 [12]

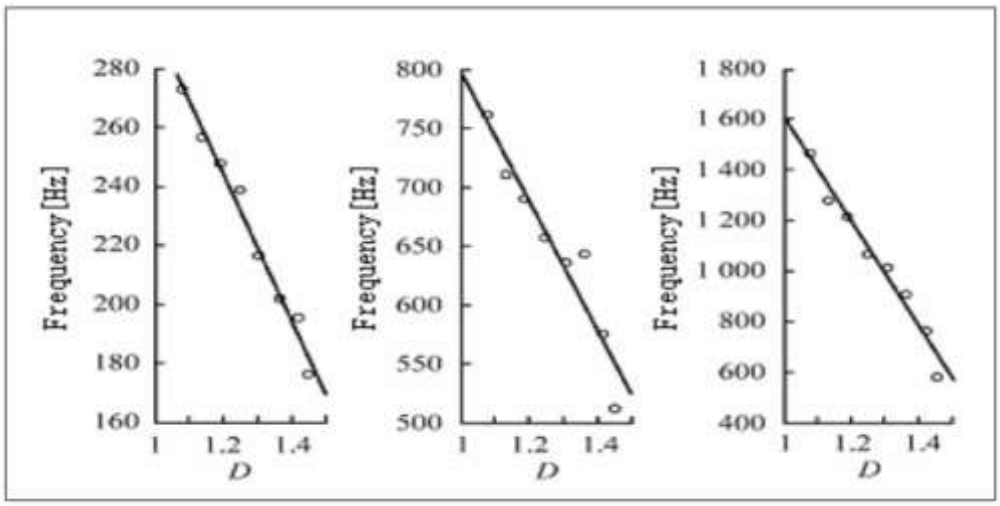

Figure 1. 14 Comparison of first three orders of natural frequency of RC beam against the fractal dimension of residual crack pattern after every step [12]

It can be seen from Figure 1. 14 that a negative linear correlation was reported between fractal dimension and the fundamental natural frequency of the beam.

1.3.2 Multifractal analysis

Multifractal analysis is a generalisation of the box counting algorithm in which fractal dimension D, instead of being a global parameter is now a local parameter called singularity strength α which may change from box to box [16]. A generalised dimension D_q is considered, which is a function of a real valued moment q. The variation of q controls the scale at which the measure of D_q is taken. The measure can be spread over the domain under study, via a set of normalised measures, which define the local scaling [16].

The analysis can be divided into three steps,

- **Evaluation of weight associated with each box**

The expression for D_q is given by,

$$D_q = \frac{1}{q-1}\lim_{r\to 0}\left(\frac{\log\sum_{i=1}^{N}(P_i{}^q)}{\log(r)}\right)$$

Where, q is the real valued moment order, r is the box size, i is the box number, N is the number of boxes and P_i is given by,

$$P_i = \frac{(N_i)}{\sum_{i=1}^{M}(N_i)}$$

Where, N_i is the mass of object inside the ith box, and M is the number of boxes containing at least one unit of mass. Therefore, P_i is the weight associated with the ith box. For a 2-d binary image, unit mass is equivalent to one black pixel. Thus, P_i becomes the probability of existence of a black pixel inside a box.

❖ **Evaluation of normalised measures and multifractal spectrum**

In multifractal analysis it is also possible to determine number of boxes having similar local scaling, that is same α and define f(α) as the fractal dimension of boxes with singularity α [16]. The curve f(α) is called the multifractal spectrum and provides information about the range of singularity strengths present in the measure at different scales of measurement. In order to construct the multifractal spectrum as proposed in [17], a family of normalised measures is introduced as,

$$\mu_i = \frac{(P_i{}^q)}{\sum_{i=1}^{N}(P_i{}^q)}$$

The normalised measures are a function of box size r and the moment order q and take up values between [0,1]. Using these normalised measures, the following functions are evaluated.

$$\alpha(q) = \lim_{r\to 0}\left(\frac{\sum_{i=1}^{N}[\mu_i * \log(P_i{}^q)]}{\log(r)}\right)$$

$$f(q) = \lim_{r\to 0}\left(\frac{\sum_{i=1}^{N}[\mu_i * \log(\mu_i{}^q)]}{\log(r)}\right)$$

By making log-log plots over varying box sizes, α(q) and f(q) can be evaluated for a range of values of q. Plotting f(q) vs. α(q) gives the multifractal spectrum f(α).

❖ **Visualisation of data**

For the artificial crack pattern (a)CASE0, seen in Figure 1. 15, plots for probability measure P_i and normalised measure μ_i, are seen in Figure 1. 16. Plots for multifractal spectra f(α) and generalised dimension D_q are seen in Figure 1. 17 for all artificial patterns.

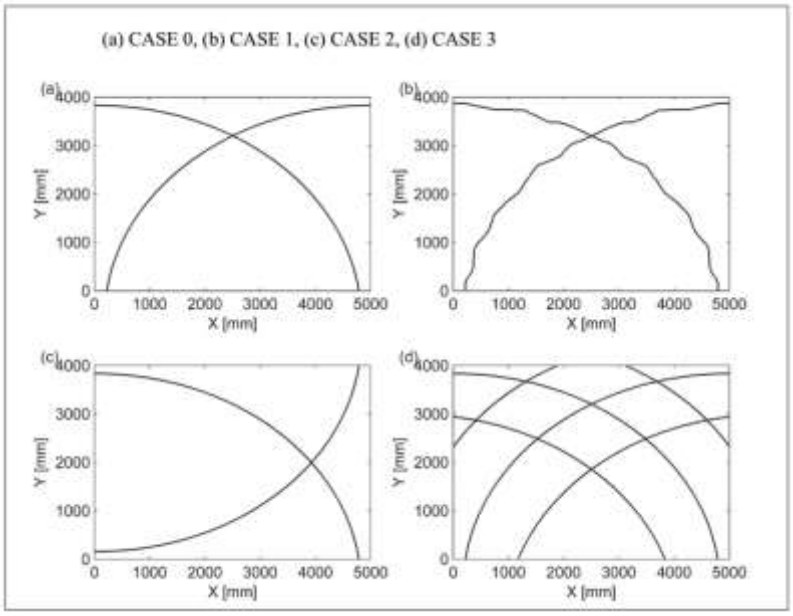

Figure 1. 15 Artificial crack patterns for multifractal analysis [16]

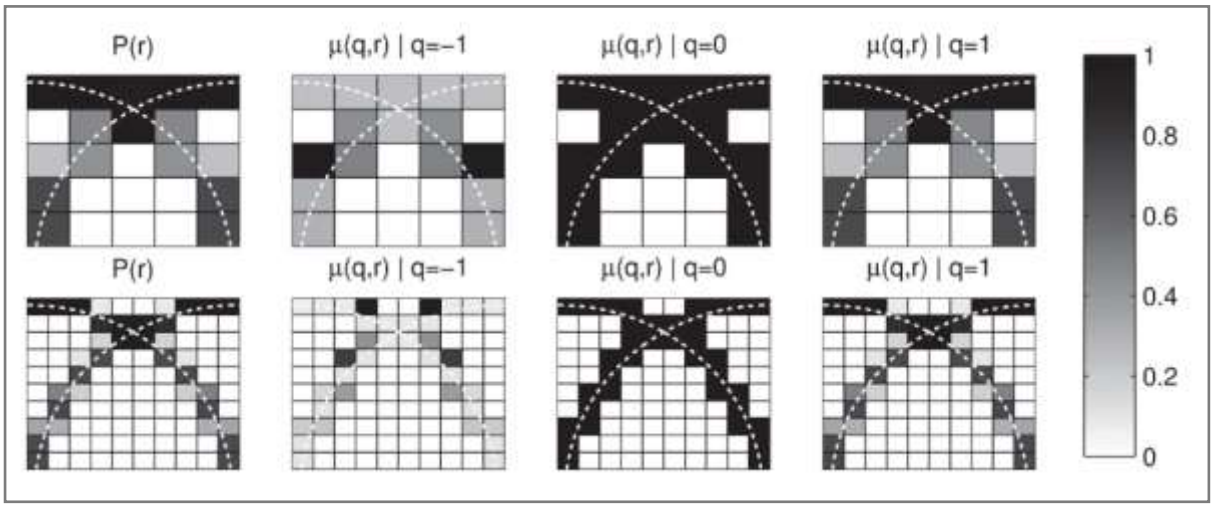

Figure 1. 16 Probability and normalised measures for two different box sizes [16]

In Figure 1. 16 it is observed that boxes with more points of the crack within them have higher probability measures, as can be expected. The effect of variation of q is illustrated by considering three values of q. For q equal to -1, boxes with lower number of crack points have higher measure. For q equal to zero each box has the same measure irrespective of the number of crack points. For q equal 1, boxes with higher number of crack points have higher measure. This is because, the negative values of q highlight the lower probability events whereas the positive values of q highlight higher probability events.

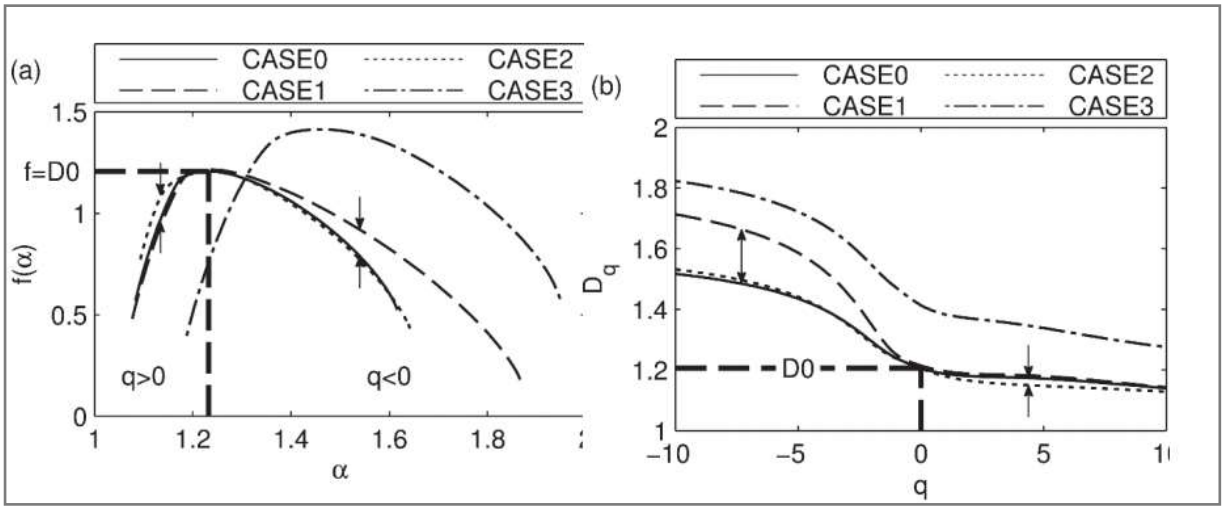

Figure 1. 17 a) Multifractal spectra for all artificial crack patterns b) Generalised dimension D_q vs q for all artificial crack patterns [16]

This is understood by comparing results for different artificial cracks patterns seen in Figure 1. 15. Between CASE0 and CASE1, the general shape remains the same but the local features vary. It is seen in Figure 1. 17 that minor variation is observed for positive values of q, whereas high variation is seen for negative values of q for both the multifractal spectra and generalised dimension. Thus, negative values of q emphasize local scaling. For positive values of q, the effect

of local scaling gradually disappears and the general shape of the pattern is emphasized more. This is confirmed by comparison of CASE2 with CASE0 in which the general shape is changed but the local features are kept the same. The multifractal spectra and generalised dimension differ significantly only for positive values of q. For CASE3, $f(\alpha)$ and D_q differ from CASE0 for all values of q, indicating a change in the general as well local features of the crack pattern.

At q equal to zero, the generalised dimension D_q equals the box counting dimension. The fractal dimension D discussed in the previous section is recovered as D_0. Thus, multifractal analysis is a refinement over a mere box counting analysis and is capable of reflecting the variations of local features of cracks at different scales.

1. 4 Discussion

Damage in concrete was characterised according to observable crack patterns and distinguishable features as seen in Table 1. 1. The internal characteristics most fundamentally reflect damage in RC. However, for existing structures, they are often difficult to assess. Also, taking their effect into account on a structural level implies huge computational costs. The visible characteristics are the next immediate consequence of the internal characteristics and can be assessed to extract information about the structural damage. Although, since the fundamental physics of the evolution from undamaged material to damaged state is overlooked, the analysis is simplistic. Also, the extracted damage information is uncertain in nature and must be complemented with statistical methods to translate into input. However, the feasibility to perform analysis of the global structural behaviour, is seen as a decisive advantage. Here, a trade-off is made between accuracy and computational feasibility.

Fractal analysis as a form of damage assessment in RC structures was reviewed, in which fractal geometry is applied to statistically characterise surface crack patterns. It is noted that the fractal dimension of residual crack patterns computed using the box-counting algorithm appears to capture the global damage evolution by jumping to higher values with increase in damage. Thus, it could be conceived as a global damage parameter in structural analysis. However, it is not capable of capturing the local densities of damaged zones. The multifractal parameters - generalised dimension (D_q) and normalised measures(μ_i) can provide a refinement over this limitation as they quantitatively describe both the global and local statistical distribution of the crack pattern. Image analysis algorithms can be utilised to obtain images which represents the true distribution of cracks as closely as possible. This is an essential step in a successful implementation of this technique for damage assessment. The technique has been widely used to relate surface cracking of metals to its fracture toughness. However, its application to concrete fracture is relatively new and a thorough investigation of its applicability is needed. However, literature indicates that concrete surface cracks do possess fractal characteristics of self-similarity over a wide range of scales. A laboratory experiment to further study the relation between the multifractal measures and stiffness loss due to cracks can be conceived, in which the surface of the member under study is painted such that the crack distribution is readily captured in photographs. A clear understanding of this relation could be followed by linking fractal parameters to mechanical properties of the concrete material.

2.Methodology for modelling damaged RC members

2. 1 Introduction

The global strategy conceived, in order to accomplish finite element analysis of a damaged RC members, is described in this chapter. The central idea of the approach is to capture the geometry of the observed crack pattern on the surface of the structure in terms of digital pixels of a photo, which can then be evaluated to extract usable information for input into a finite element framework including a constitutive model for damaged concrete. The main features of the strategy are:

- Image analysis to store damage information
- Framework for finite element analysis
- Coupling between image analysis and FE framework

Each feature is described in a separate section, in the above order. A range of assumptions and simplifications are made along each step of the procedure, in order to explore the utility of this approach. These are discussed in the corresponding sections. Complete details of the adopted finite element framework are described in the next chapter. Here, only the focus of the study, i.e. the constitutive model for damaged concrete is discussed. An overview of the procedure can be seen in Figure 2. 1.

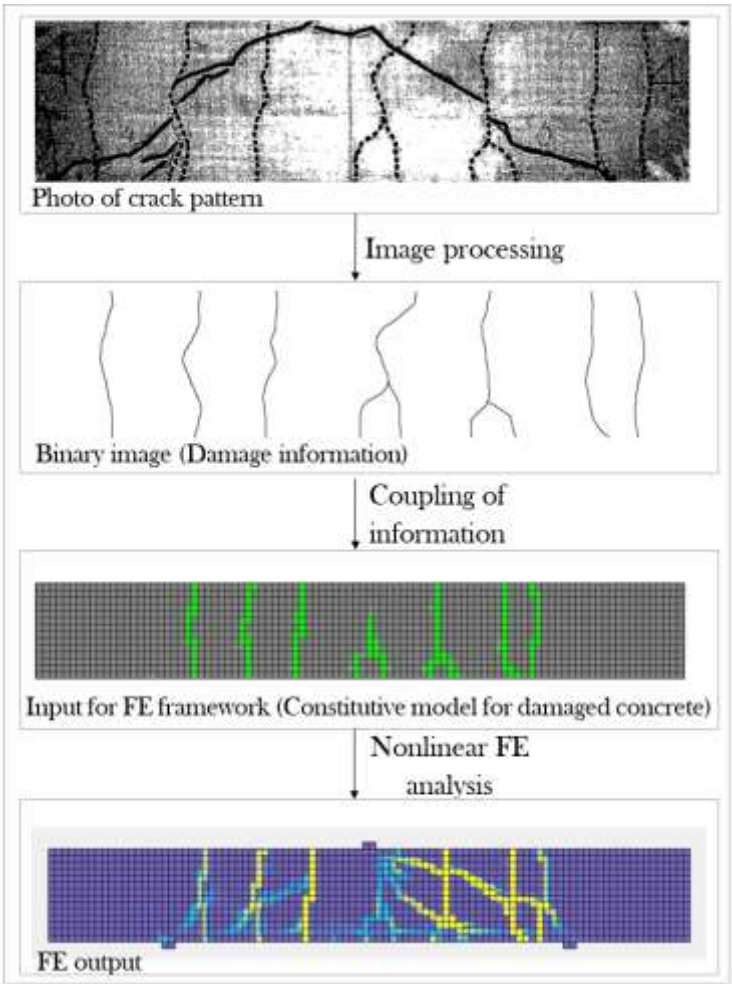

Figure 2. 1 Overview of the global strategy for finite element analysis

2. 2 Image processing to store damage information

Digital image processing is the use of computer algorithms to process images in order to retain the required information, such that it can be extracted for later use. A full correlation is assumed between surface crack patterns captured in photographs and the damage occurring inside the structure.

In Figure 2. 1, the pre-damage due to cracks is represented by dotted lines in the photo of crack pattern. Although, only an estimation of the true geometry, visually, it still holds valid information regarding the trajectories of the cracks. This is segmented out using an image processing software [18] and stored in the form of a binary image.

In reality however, surface crack patterns are extremely complex geometrical figures and convey new detail at every scale of observation. Therefore, definitive information about crack-widths and pattern distribution, can only be extracted from high-quality images which capture the true geometry of the pattern. Thus, the efficiency of this step depends on the resolution of the camera. Effectively, this necessitates assumptions about the missing information depending on the available image, capability of the finite element framework and the required level of

sophistication. These requirements are addressed after the description of the constitutive model for damaged concrete.

2. 3 Constitutive model for damaged concrete

The total strain based smeared cracking approach [see Appendix A] serves as a point of departure for the constitutive model for damaged concrete. The considered formulation, provides an augmentation to the total strain based smeared cracking model discussed in the Appendix A. The add-on feature is a possibility to evaluate pre-damage at the beginning of the analysis via a set of input parameters (pre-damage variables), such that damaged and undamaged concrete are described under the same framework. This is in the spirit of definition of material damage formulated in damage mechanics [19], which is a branch of continuum mechanics that aims to incorporate changes in the micro-structural level of the material via a finite number of scalar or tensor-valued internal variables [20].

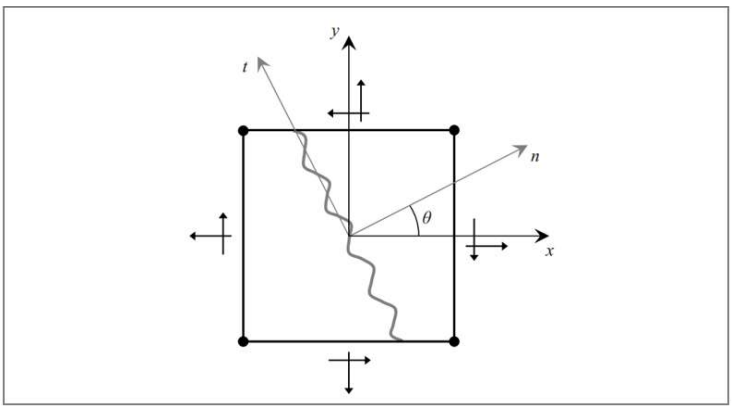

Figure 2. 2 Axes of cracking for a concrete element [21]

For a cracked(damaged) concrete element seen in Figure 2. 2, matrix $\mathbf{D}_{\mathrm{nt}}$ which sets the relation between stresses and strains in the nt-axes system takes the following secant form,

$$\mathbf{D}_{\mathrm{nt}} = \begin{bmatrix} \frac{(1-d_1)E}{1-\nu^2(1-d_1)} & \frac{\nu(1-d_1)E}{1-\nu^2(1-d_1)} & 0 \\ \frac{\nu(1-d_2)E}{1-\nu^2(1-d_2)} & \frac{(1-d_2)E}{1-\nu^2(1-d_2)} & 0 \\ 0 & 0 & \frac{\beta E}{2(1+\nu)} \end{bmatrix} \qquad (2.1)$$

Here, ν is the Poisson's ratio of concrete. β is termed as the shear retention factor, which governs the sliding behaviour along the crack interfaces by accounting for phenomena such as aggregate interlock [20]. d_1 and d_2 are treated as damage variables. d_1 is the stiffness reduction in the n-direction (normal to the crack) and d_2 is the stiffness reduction in the t-direction (tangential to the crack). The influence of these variables in the constitutive relationship along a particular direction i, is schematically shown in Figure 2. 3.

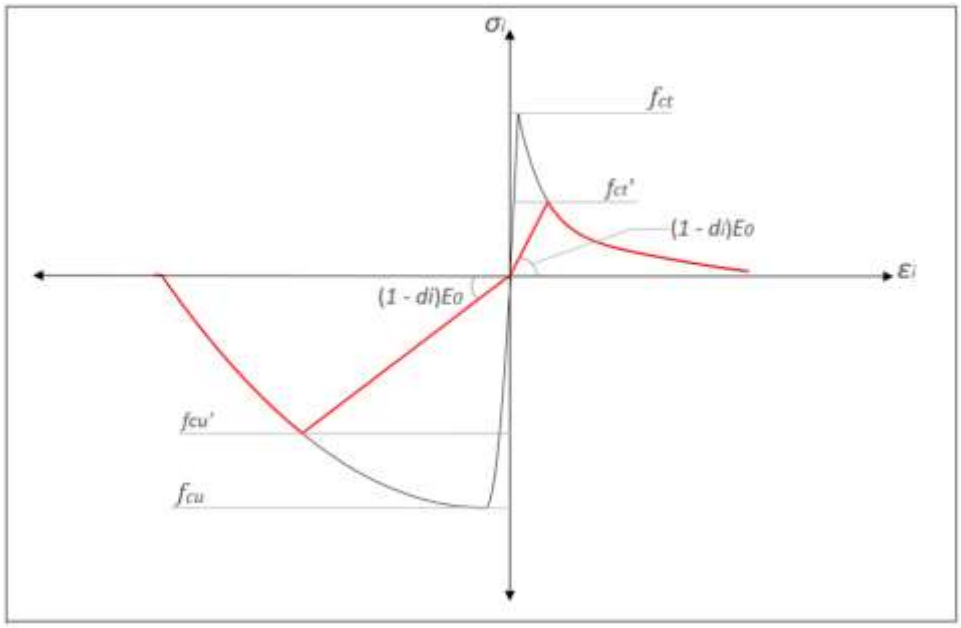

Figure 2. 3 Constitutive law for damaged concrete derived from the undamaged state

It can be inferred from Figure 2. 3 that,

$$(1 - d_i)E_0 = E' = \frac{\sigma_i}{\varepsilon_i}$$

Thus, the mechanical properties of the damaged material follow from the reduction in strength and stiffness of the undamaged state. Therefore, scalar variables d_1 and d_2 control the integrity of the material, by taking up values between 0 (undamaged state) and 1(completely damaged state) and therefore represent the magnitude of damage. The angle θ between the x-axis and n-axis represents the direction of damage and can be conceived as an additional input parameter.

The above formulation is adopted for an orthogonal axis system. This is schematised in Figure 2. 4. The following notations are adopted for the damage variables:

- d_{nt}: Tensile damage in the normal direction
- d_{nc}: Compressive damage in the normal direction
- d_{tt}: Tensile damage in the tangential direction
- d_{tc}: Compressive damage in the tangential direction
- θ: Orientation of damage

The input for d_1(d_{nt} or d_{nc}) d_2(d_{tt} or d_{tc}) and θ, is addressed in the next section of the chapter. The assumptions made in this section can be summarised as follows:

- Damage, i.e. cracking and crushing of concrete, is characterised by reduction in initial stiffness(E_0)
- The reduction is described by scalar variables
- Tensile damage(cracking) is characterised by reduction in tensile strength(f_t)
- Compressive damage(crushing) is characterised by reduction in compressive strength(f_c)
- Concrete material behaviour is described by a total strain based smeared cracking approach in an orthogonal axis system.

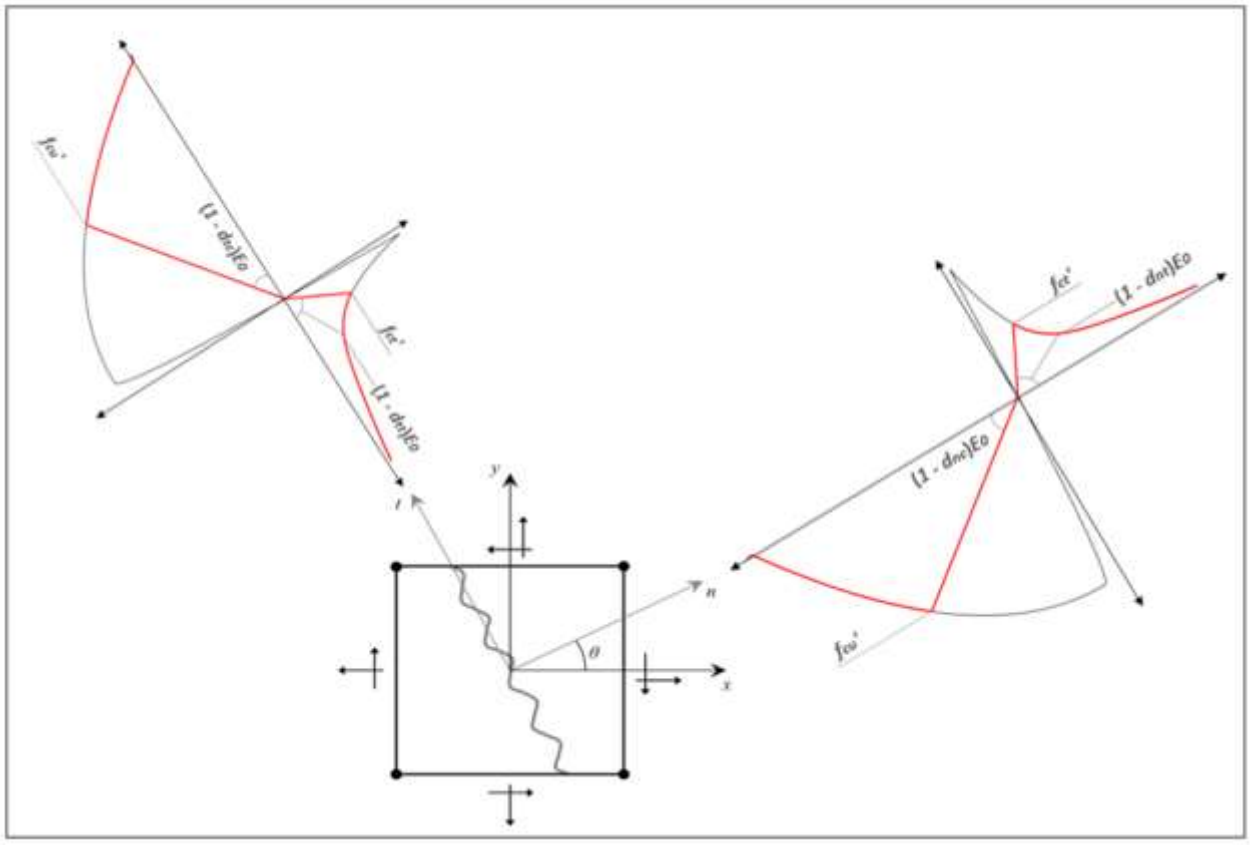

Figure 2. 4 Adopted formulation for damaged concrete

2. 4 Coupling between image analysis and FE framework

Though the presented model above enables damage input for compression, in this thesis an assumption of purely tensile damage in the RC structure is adopted, which implies:

- Concrete is assumed to be uncrushed due to the mechanical load exerted on the RC structure.
- The reduction in compressive strength due to cracking is ignored.
- Compressive damage variables d_{nc} and d_{tc} are set to zero.

Two input approaches for variables d_{nc}, d_{tc} and θ are conceived, based on two different characterisations of stiffness reduction due to observed cracks. These are described in the following sub-sections.

2.4. 1 Single crack input

In this type of input, the stiffness loss is evaluated over every single crack individually. Damage variable d_{nt} is co-related to the width of crack, using the crack stress-crack opening relationship employed in the FE framework. The orientation of damage θ, is estimated from the observed crack pattern and the variable d_{tt} is set to zero, implying no tensile loss along the direction tangential to the crack.

Thus, the quantities of interest from image analysis are, crack-width and crack-orientation. The process of extraction of crack-orientation from a binary image containing estimated crack-

trajectories (Figure 2. 1) is discussed first. Following that, extraction form a binary image containing real cracks is addressed. Next, requirements for crack-width extraction form real and estimated crack pattern images are considered.

❖ **Extraction of crack-orientations:**

The binary image set up in Figure 2. 1 is covered with a virtual grid of boxes for a range of box-sizes. This process is visualised in Figure 2. 5.

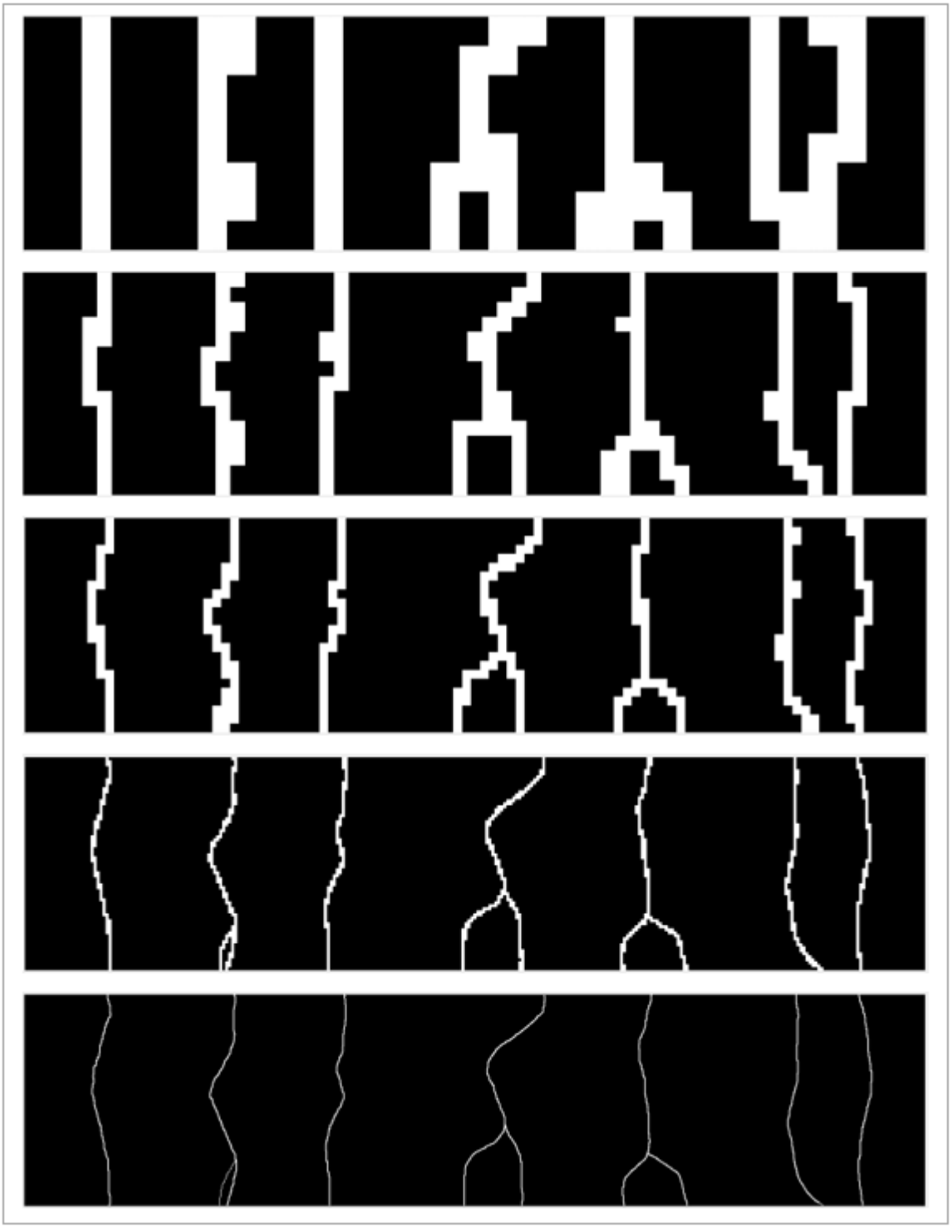

Figure 2. 5 Binary image covered by a virtual grid of boxes

As the box-size decreases, the covering is refined successively, thereby capturing the detail inside each box more accurately. Depending on the required degree of sophistication, a suitable box-size is chosen and equated to the size of finite element. The crack-orientation is extracted from each box using a suitable technique, and coupled with the corresponding finite element. The gist of the process is depicted in Figure 2. 6. Here, the best fit line along the black pixels inside each box is taken to be an estimate for the crack-orientation of the corresponding element.

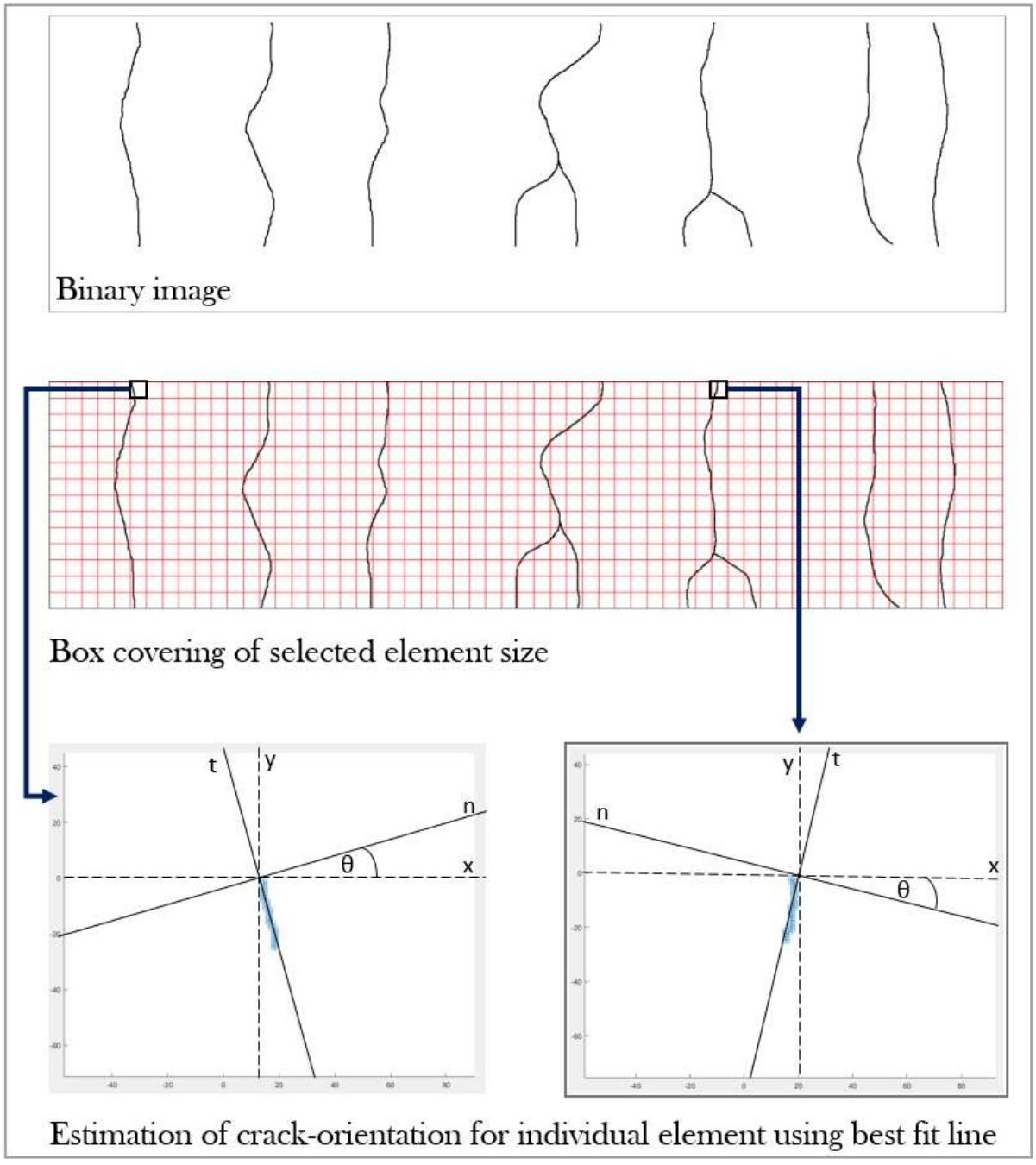

Figure 2. 6 Estimation of crack-orientation using best fit line method

Similar technique can be employed for an image of a real crack pattern. For an orthogonal cracking system as adopted in the previous section, only one direction of damage per element

can be handled by the constitutive formulation. Hence, the estimation described here is compatible with the FE framework. However, for a multi-directional cracking formulation, a more complex estimation technique could be employed, which accounts for element cracking in multiple directions.

❖ **Extraction of crack-widths:**

At the structural scale of observation, which is the scale of interest in this study, the width of an individual surface-crack along any interval, is much smaller compared to the size of the structure. Hence, a demand for high-resolution exists, for an image which is capable of capturing the geometrical features, required to extract crack-width information. A high-resolution image of a pre-damaged RC member is shown in Figure 2. 7. The image contains (5616 x 3744) pixels.

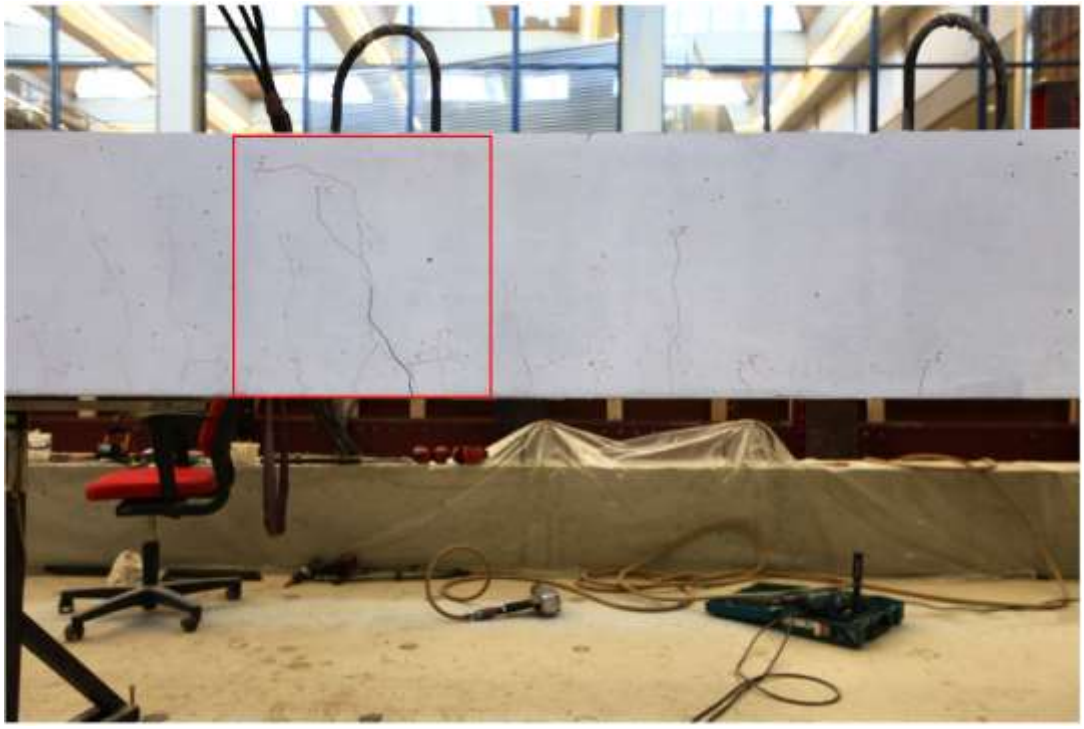

Figure 2. 7 High resolution photo of pre-damaged RC member

Focusing in the area marked by the red box, for the current scale of observation only one real crack is visible, while the red lines are crack trajectories drawn by hand on the member. Upon successive zooming the real crack geometry is traced as seen in Figure 2. 8.

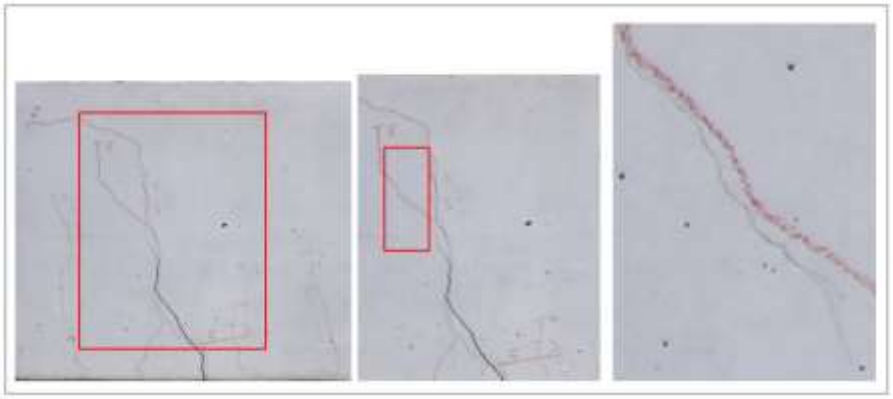

Figure 2. 8 Real crack geometry traced by successive zooming

The procedure of subdivision into boxes, as for extraction of crack-orientation can be adopted and an algorithm for extraction of crack-width can be implemented based on the distribution of crack-pixels inside the box. The idea is visualised in Figure 2. 9.

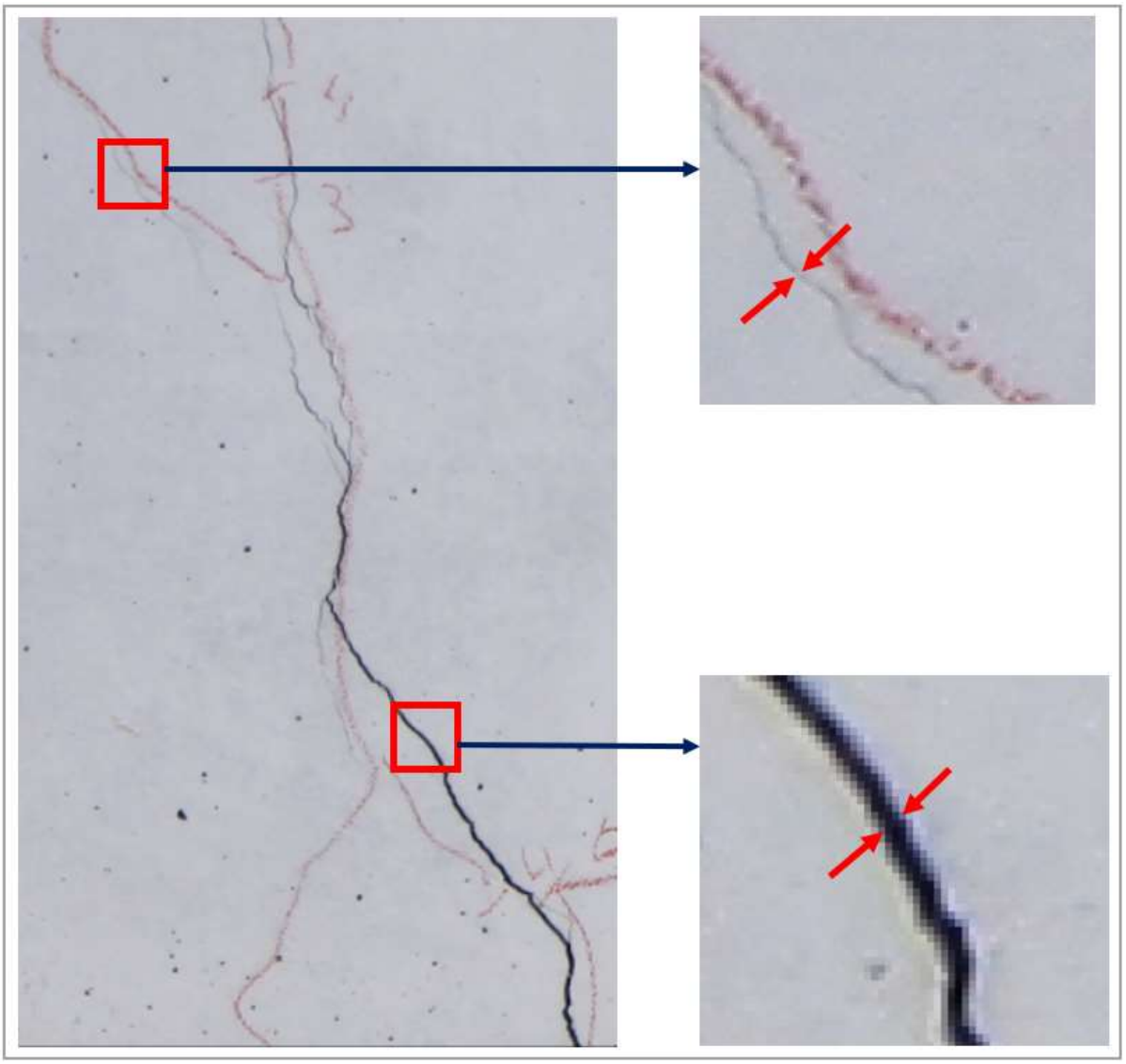

Figure 2. 9 Estimation of crack-width(schematisation)

Since, one pixel now becomes the smallest unit of measurement of width, an image resolution of at least (1x1) pixel for the smallest width desired to be captured in the analysis is required. Only using a high-resolution camera may not always fulfil this requirement, i.e. extremely small cracks which are desired to be accounted in the analysis may not be captured in a single a photograph. Multiple high-resolution photographs from the same range can be taken, in order to construct a binary image required to extract crack-widths. However, this is not explored further in this study. Instead a simplified assumption of binary cracking is adopted. This means, elements through which the cracks pass, are considered to be fully damaged ($d_{nt}=1$), irrespective of the width of the crack. Elements over which cracks do not cross over, are considered undamaged($d_{nt}=0$).

2.4. 2 Damage zone input

In this type of input, the loss of stiffness due to cracks is evaluated over a zone of elements. Therefore, the distribution of the entire crack pattern is considered more relevant than width and orientation of individual cracks. For a sophisticated analysis, magnitude of damage (d_{nt} and d_{tt}) for each element could be obtained from a statistical distribution of surface features, e.g. multifractal analysis. The definition of damage from the statistical distribution then needs to be correlated to the damage variables defined in the constitutive model for damaged concrete. A simplified input could involve adopting identical values for d_{nt} and d_{tt} for all the elements of the zone. Both the ideas are schematised in Figure 2. 10.

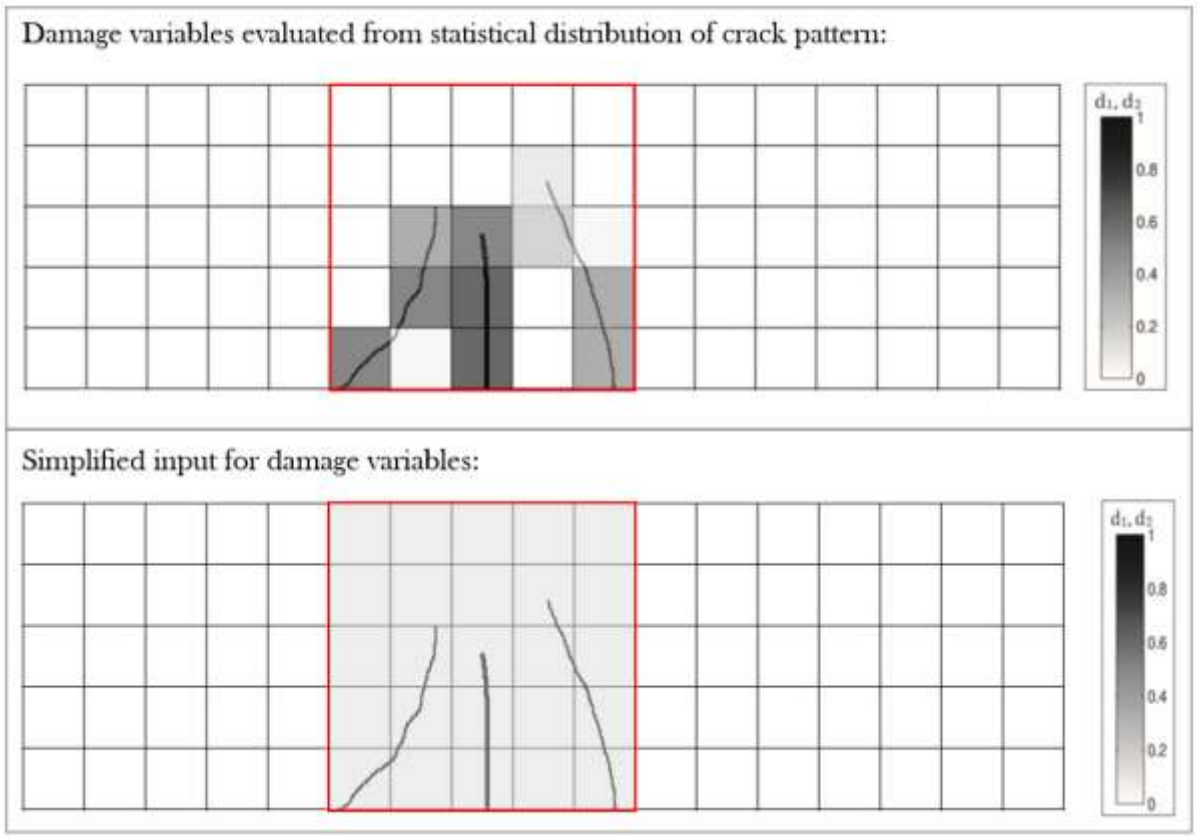

Figure 2. 10 Damage zone input(schematic)

Direction of damage for each element comprising the zone, instead of being an input parameter, is now fixed by aligning it with the direction of the major principal strain obtained after the first loading step or with the direction of first rotation.

The sophisticated input relies on the distribution of damage. Therefore, a photo of the real crack-pattern is imperative for this type of input if it is to be coupled with image analysis. Such a coupling is not considered in this study. As will be considered in chapter 4, a simplified input is adopted, in order to explore the behaviour of the damaged member under this type of input.

2. 5 Discussion

The overall methodology for modelling damaged RC members was presented. A total strain based smeared cracking model, with damage variables is adopted. The central assumption is that the crack patterns observed on the surface of the structure can be co-related to the damage inside the structure. This damage is represented by a set of internal scalar variables which control the strength and stiffness of an element in a particular direction. This gives rise to a field of damage which can be interpreted as single crack input or damage zone input.

The rationale behind adopting either types of input is different. In the single crack approach, the magnitude and direction are evaluated from crack-width and crack-orientation respectively. The variable θ is fixed independently as an input parameter. Thus, physically appealing definition for the damage variables are sought. However, the size of the specimen or more specifically the size of the element through which the crack passes is not addressed in the measure for damage. Therefore, this type of input requires an apriori rational choice of element size which is small enough to represent a localised crack of bandwidth 'h'. It can therefore be reasoned, that in the extreme case, when the size of the bandwidth is zero, the single crack input becomes equivalent to the discrete crack concept [see Appendix A]

In the zone input, damage can be treated as a statistical field measured over the domain under study. The crack pattern inside this domain is then discretised into boxes and the measure of distribution of crack points inside each box is used to construct a damage field. The size of the finite element can be equated to the maximum box-size considered in the damage calculations. This serves as a scale invariant link between the measure of damage and the input for the finite element analysis. However, the information about the direction of localisation of cracks is overlooked and the definition for damage variables becomes physically less meaningful.

The first approach, accounts for local effects of crack-width and crack-orientation in a transparent manner. High resolution images contribute to a more efficient evaluation of damage. Although, since width and orientation of cracks are averaged out over the element size, a binary image estimating the required damage information can be constructed. Thus, a high-resolution image is not a stringent requirement for this approach. However, it requires selection of a proper element size to arrive at meaningful results. Moreover, since the prediction of residual load carrying capacity is the ultimate objective, in cases with complex surface crack patterns, this type of input may lead to an over-refined analysis. Hence, this approach is most suitable in cases of pronounced local cracking. The second approach is more suitable in cases of damage domains consisting of a number of small cracks. However, local features of crack-width and orientation cannot be incorporated in the constitutive model in a transparent manner. Moreover, a true image of the crack pattern is imperative for this type of approach in order to couple it with image analysis.

Obtaining, the required image to efficiently carry out the structural analysis as described in the methodology can be a challenge. Also, the assumption of co-relation between surface damage and internal damage seems reasonable only for 2-d situations. For 3-d situations, damage information can be obtained from other detection techniques, e.g. acoustic tomography and can be incorporated in the same framework to replace image analysis.

3. MATLAB implementation

3. 1 Introduction

A finite element analysis framework was implemented on **MATLAB** [3] following the methodology discussed in the previous chapter. The implementation is discussed in this chapter. The global scheme of calculation is elaborated. The specific stress-strain curves adopted for analysis are enlisted and general finite element considerations are described. Next, a few elementary verification tests are described in which results are compared with **DIANA** [2] to ensure proper implementation. A simple eight-cell reinforced concrete structure is also tested to further verify the code. Following that, a full-scale RC beam, later treated as an experimental specimen is modelled and the results are discussed. The features of the implemented algorithm for image analysis of damaged domain are described. The discussion can be summarised in the following format:

- Global solution procedure (section 3.2)
- Constitutive model for concrete and reinforcement (section 3.3 - 3.4)
- Finite element considerations for 2-D plane stress problems (section 3.5)
- Verification of the code (section 3.6)
- Algorithm for image analysis (section 3.7)

3. 2 Global scheme

For the derivation of a matrix based finite element formulation from the strong form of the equilibrium equation, [22] was referred. Standard displacement control was chosen for the analysis wherein deformations are prescribed at chosen nodal points of the finite elements. The displacements at free degrees of freedom are computed using the global stiffness matrix which is built using the current state of the structural system. The derivative of the displacement field provides the strains at the integration points, using which stresses are evaluated from the constitutive relationship. The stresses at integration points are then converted to equivalent nodal forces and the system is checked for equilibrium. A full Newton Raphson technique for incremental iterative analysis was used, in which the current state of the system is evaluated for every new calculation of free displacements. The global scheme of the implementation is outlined in Figure 3. 1.

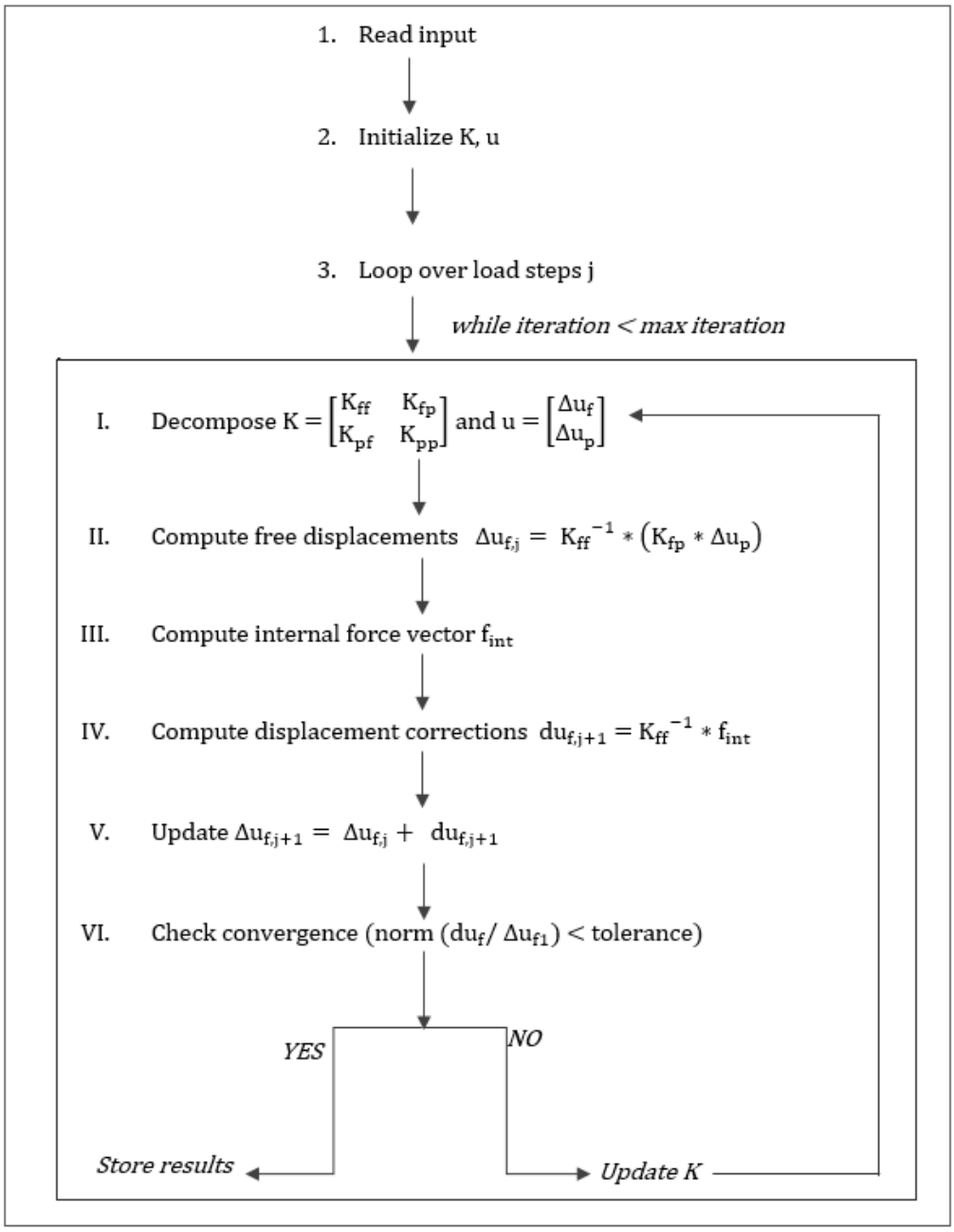

Figure 3. 1 Global scheme of implementation

3. 3 Constitutive model for concrete

3.3. 1 Damage parameters

A schematic representation of the implemented constitutive model for concrete can be seen in Figure 3. 2. As discussed in chapter 2, section 2.3, strains are monitored in an orthogonal axis system, using a set of internal variables. The direction of the nt-axes system is either set up via an input parameter 'θ' or can be derived from the direction of the principal strains after the first loading step or first rotation. The damage variable d_1 in the normal direction has two components 'd_{nt}' and 'd_{nc}' for tension and compression respectively. Similarly, reference components 'd_{tt}' and 'd_{tc}' are adopted for damage variable d_2 in the tangential direction. Unloading is assumed to follow a secant path.

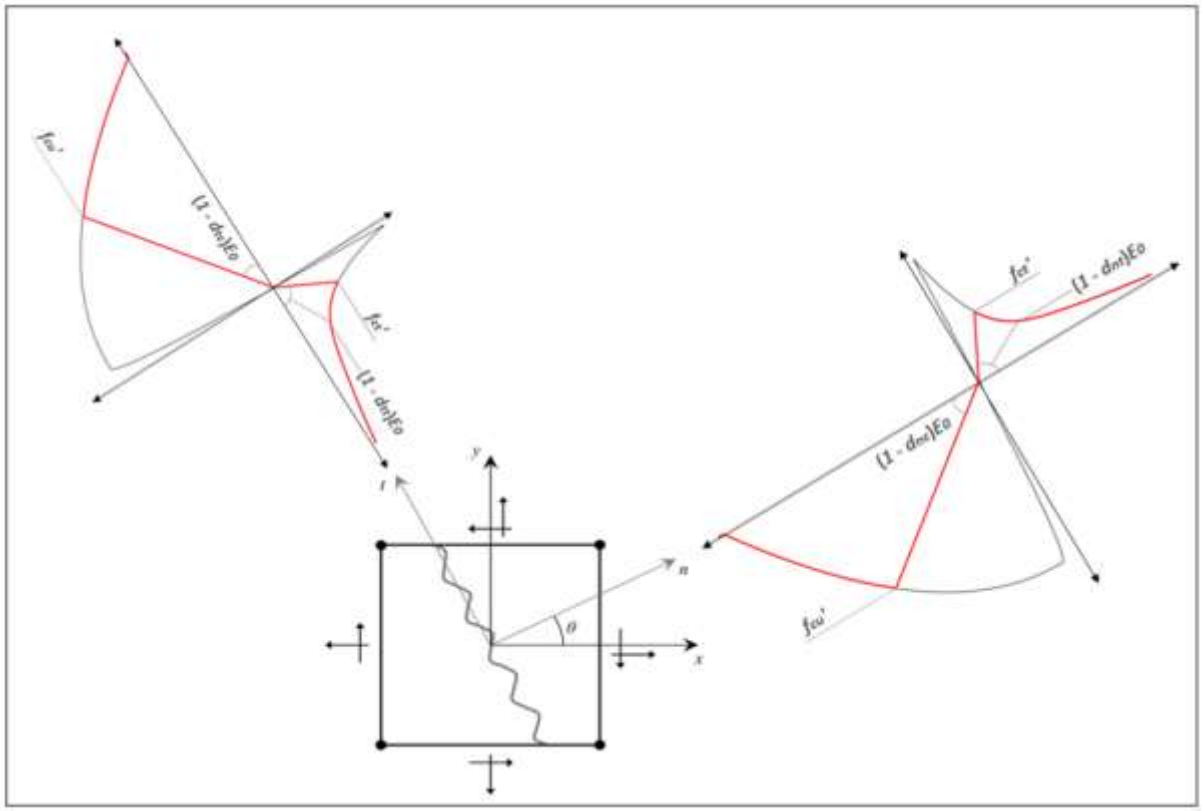

Figure 3. 2 Implemented constitutive model for concrete

For the numerical definitions of the constitutive model, i.e. nonlinear stress-strain relations after cracking/crushing, implementations in DIANA [2] and guidelines for nonlinear finite element analysis of concrete structures [23] were referred. A few relations in tension, compression and shear were implemented and verified for elementary tests. The relations used in the final analyses are described in the following paragraphs.

3.3. 2 Behaviour in tension

The stress-crack opening relation for normal weight concrete given in [24] was adopted for behaviour in tension after initiation of cracking (Figure 3.3).

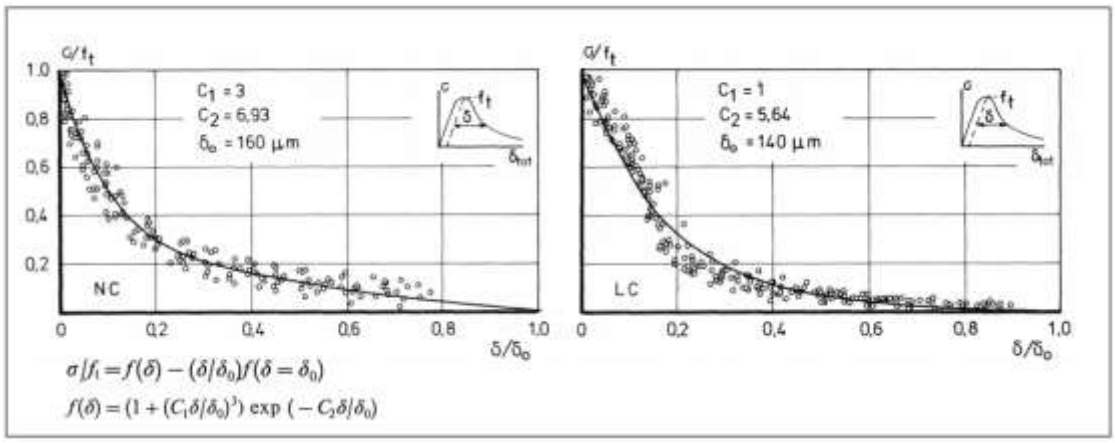

Figure 3.3 Stress-crack opening relations for normal weight(left) and light weight concrete(right) [24]

The area under the curve is termed the fracture energy in tension(G_f). It is related to ultimate strain value through the following relation,

$$\delta_{tot} = \varepsilon_{ult} = 5.136 * \frac{G_f}{h * f_t}$$

Where, crack bandwidth 'h' enters the description of the material which is the length over which the crack is smeared out [see Appendix A].

3.3. 3 Behaviour in compression

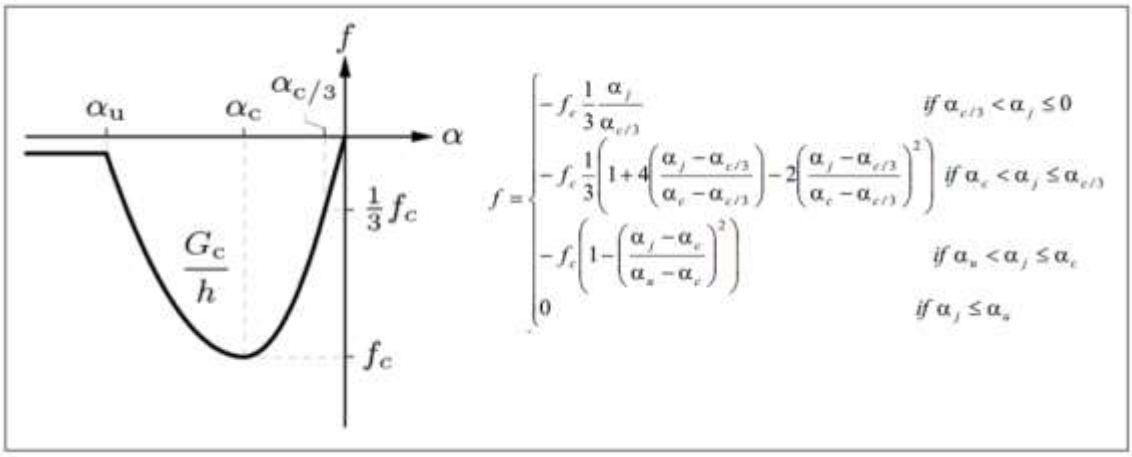

Figure 3.4 Parabolic compressive curve [2] [23]

The parabolic compressive curve given in [2] and [23] was adopted for compressive behaviour. The curve accounts for the initial linear elastic regime, but only the area under the curve after which the material begins to soften, is termed the fracture energy in compression(G_c). The characteristic values seen on the curve are related via the following relations,

$$\alpha_{c/3} = -\frac{1}{3}\frac{f_c}{E}$$

$$\alpha_c = 5\alpha_{c/3}$$

$$\alpha_u = \alpha_c - \frac{3}{2}\frac{G_c}{h * f_c}$$

Similar to the tensile behaviour, expression for ultimate strain in compression(α_u), contains the crack-bandwidth, h.

3.3. 4 Behaviour in Shear

In the linear elastic stage, the behaviour in shear is governed by the shear modulus (G) given by,

$$G = \frac{E}{2(1+\nu)}$$

For a fixed crack approach, a shear retention factor β needs to be defined which controls the residual shear stiffness after cracking(G_d), providing the relation,

$$G_d = \frac{\beta E}{2(1+\nu)}$$

The following shear retention relations were implemented:

- **Constant shear retention**: A certain percentage of shear stiffness is retained after cracking. Thus, $0 < \beta < 1$.

- **Damaged based shear retention**: The decay of shear stiffness is related to the decay of tensile normal stiffness. Thus, β takes the value $(1 - d_{nt})$.

- **Aggregate size based shear retention**: The decay of shear stiffness is related to the normal crack strain. Upon crack-opening greater than or equal to half the mean size of the aggregate, all contact is assumed to be lost. Therefore, the relation for β reads,

$$\beta = 1 - \left(\frac{2}{d_{agg}}\right)\varepsilon_{cr} * h \qquad (0 \leq \beta < 1)$$

Where, d_{agg} is the mean aggregate size and ε_{cr} is the crack normal strain.

For a rotating crack approach, the following expression for β ensues in order to enforce co-axiality between principal stresses and strains [25],

$$\beta = \frac{(\sigma_{11} - \sigma_{22})}{2(\varepsilon_{11} - \varepsilon_{22})}$$

Where, σ_{11}, σ_{22} are principal stresses and ε_{11}, ε_{22} are principal strains.

3.3. 5 Poisson's effect

A possibility to use a damaged based Poisson's ratio reduction after cracking was implemented. The Poisson's ratio of the material was assumed to decline at the same rate as the normal and tangential tensile stiffness. The Poisson's effect in 2-d was modelled by considering it as an 'extra' strain. The strain values obtained from the interpolation of the displacement field were pre-multiplied by the following matrix,

$$P = \begin{bmatrix} \frac{1}{1-\nu^2 p_1 p_2} & \frac{\nu p_2}{1-\nu^2 p_1 p_2} & 0 \\ \frac{\nu p_1}{1-\nu^2 p_1 p_2} & \frac{1}{1-\nu^2 p_1 p_2} & 0 \\ 0 & 0 & 1 \end{bmatrix}$$

Where, $p_1 = (1 - d_{nt})$; $p_2 = (1 - d_{tt})$

The stresses were then calculated using the obtained effective strain values. In case of no reduction after cracking, p_1 and p_2 are equal to 1 throughout the analysis.

3.3. 6 Estimation for crack bandwidth h

For the estimation of crack bandwidth suggestions in [2] were followed. The crack bandwidth for square elements was assumed to be equal to $\sqrt{A}$, where, A is the area of the element. This assumption was later verified by comparing results of numerical crack patterns.

3. 4 Constitutive model for reinforcement

An embedded reinforcement formulation was used to model the effect of reinforcement. The basic assumption of this formulation is that the strain in the reinforcing bar is the same as that of the concrete fibre it is aligned with [22]. Thus, the value of axial strain in the steel bar is borrowed from the strain values of the mother concrete element which it is embedded in. Uniaxial elasto-plastic stress-strain curve based on the von Mises yield criterion and strain hardening assumption was implemented as seen in Figure 3.5.

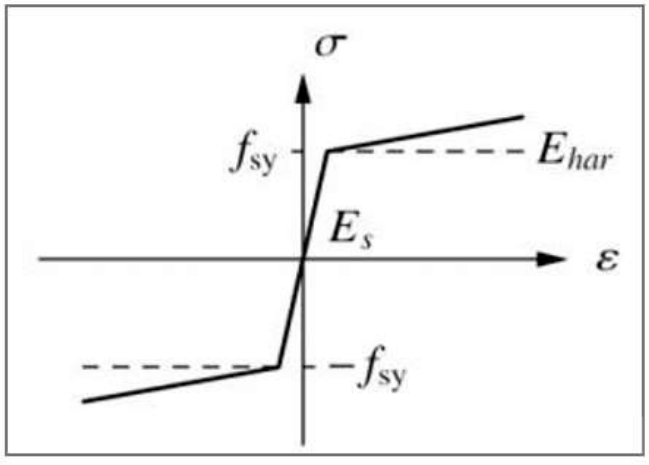

Figure 3.5 Constitutive model for reinforcement [23]

3. 5 Finite element considerations

3.5. 1 Element types for concrete

The implementation is restricted to 2-d plane stress elements. An isoparametric formulation is adopted, which means, the geometry of the structure and the displacement field are discretised by the same set of functions, commonly known as shape functions. Implemented element types for concrete are:

- **Four-noded Quadrilateral (Q8MEM)** [2]

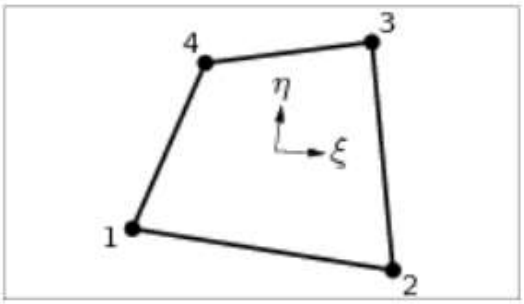

Figure 3. 6 Four-noded quadrilateral element [2]

The polynomials for displacement are given as,

$$u_i(\xi,\eta) = a_0 + a_1\xi + a_2\eta + a_3\xi\eta$$

Where i is the node number and (ξ, η) are isoparametric co-ordinates of the element.

- **Eight-noded Quadrilateral (CQ16M)** [2]

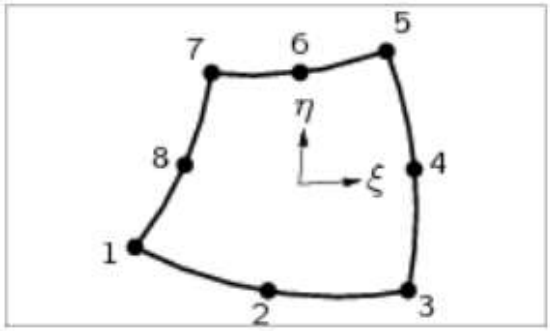

Figure 3. 7 Eight-noded quadrilateral element [2]

The polynomials for displacement are given as,

$$u_i(\xi,\eta) = a_0 + a_1\xi + a_2\eta + a_3\xi\eta + a_4\xi^2 + a_5\eta^2 + a_6\xi^2\eta + a_7\eta^2\xi$$

Where i is the node number and (ξ, η) are isoparametric co-ordinates of the element.

3.5. 2 Embedded reinforcements

As demonstrated in [2] the BAR embedded in Plane Stress technique [2] was used to incorporate the effect of reinforcement. Using the global nodal co-ordinates of reinforcement, ('location point' in Figure 3. 8) the co-ordinates for the 'integration points' were obtained in the local co-ordinate system of the mother element. These co-ordinates were used to borrow values from the strain field of the mother element. Using these strain values, stresses are computed from an independent constitutive law, in the direction of the reinforcement. The obtained stress values are then re-transferred as nodal forces to the mother element.

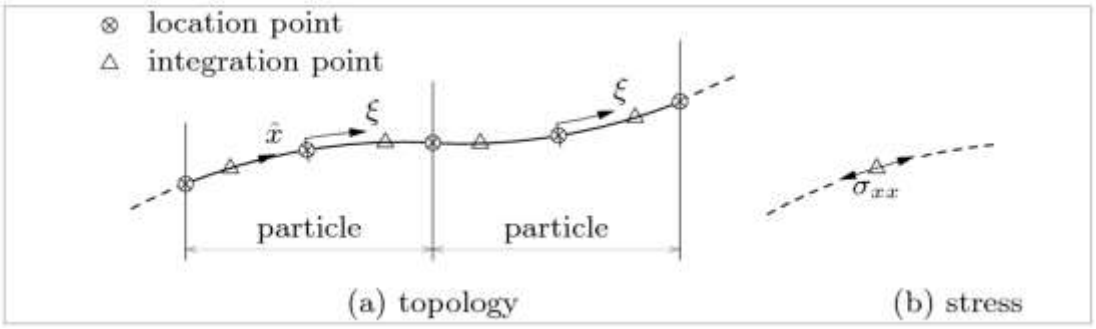

Figure 3. 8 BAR in Plane Stress [2]

3.5. 3 Integration schemes

A standard (2x2) and (3x3) Gaussian integration schemes (Figure 3. 9) were employed with the possibility to use either, for both implemented concrete element types.

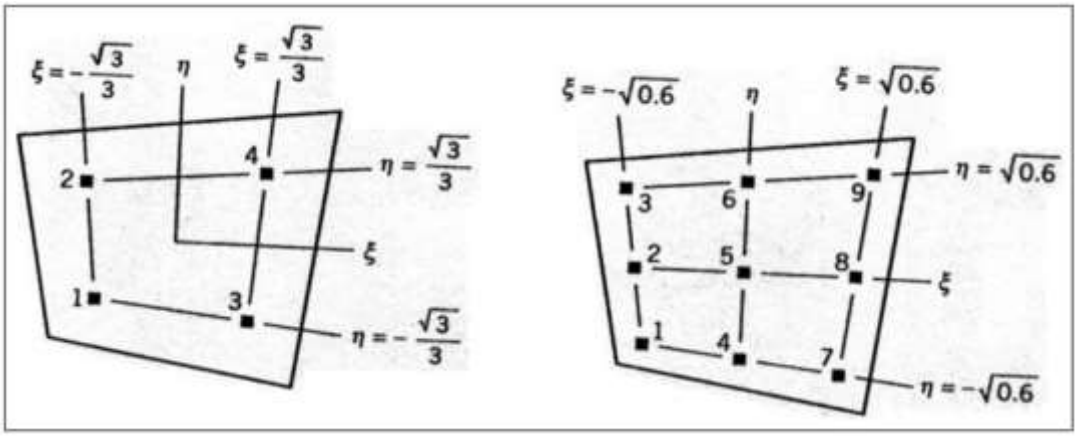

Figure 3. 9 (2x2) and (3x3) Gaussian quadrature [26]

3.5. 4 Visualisation of results

In order to aid visualisation, the obtained results were plotted for extrapolated nodal values of stresses and strains. The method to extrapolate stress and strain values to the nodes, described in [27] was adopted. Plotting was performed element-wise and nodal averaging was avoided.

3. 6 Verification

Effort was made to emulate the Total Strain-Based Crack Model(TSCM) implemented in DIANA. After satisfactory implementation of TSCM, the possibility for damage input was added to the algorithm. A number of verification tests were performed to ensure proper working of the MATLAB code. The tests are divided into three types:

3.6. 1 Elementary cell tests

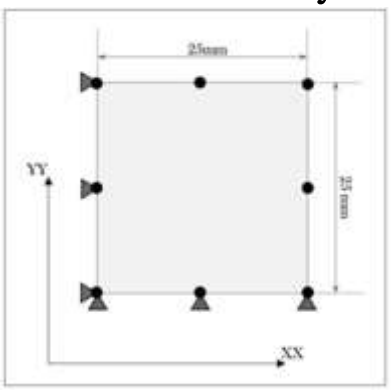

Figure 3. 10 Geometry and support conditions for elementary cell

A single finite element (elementary cell) was tested for uniaxial and biaxial load combinations. The results were compared by testing the same element in DIANA using the Total Strain Based Crack Model [2] with identical geometry, material properties and load steps. Geometry and support conditions of the elementary cell for axial loading are shown in Figure 3. 10. The material data and finite element descriptions are enlisted in Table 3. 1. The loading data and results are tabulated in the following section. For the integration point labels, refer Figure 3. 9

Thickness(t)	25 mm
Young's modulus(E)	30000 N/mm^2
Poisson's ratio(ν)	0.2 (No reduction)
Compressive strength (f_c)	30 N/mm^2
Tensile strength(f_t)	3.5 N/mm^2
Compressive fracture energy(G_c)	15 N/mm
Tensile fracture energy(G_f)	0.1 N/mm
Crack bandwidth(h)	25 mm
Crack orientation	Fixed
Tensile behaviour	Hordijk tension softening
Compressive behaviour	Parabolic softening
Shear behaviour after cracking	Constant (β=0.2)
Element type	CQ16M
Integration scheme	4-point Gauss
Convergence criteria	Displacement norm: 1e-6 mm Force norm: 1e-6 mm
Maximum no. of iterations	150

Table 3. 1 Material properties for elementary cell

DIANA MATLAB Units: Stress(S) – N/mm², Strain(E) – (%)

Load:
Uniaxial tension
(1 mm: 200 steps of 0.001)

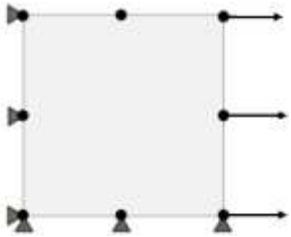

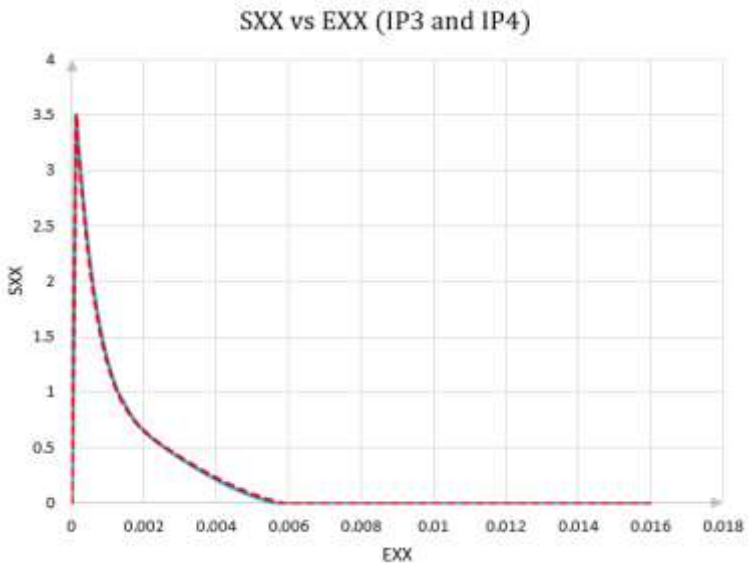

Load:
Uniaxial compression
(-4 mm: 200 steps of 0.001)

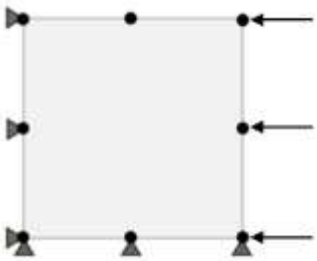

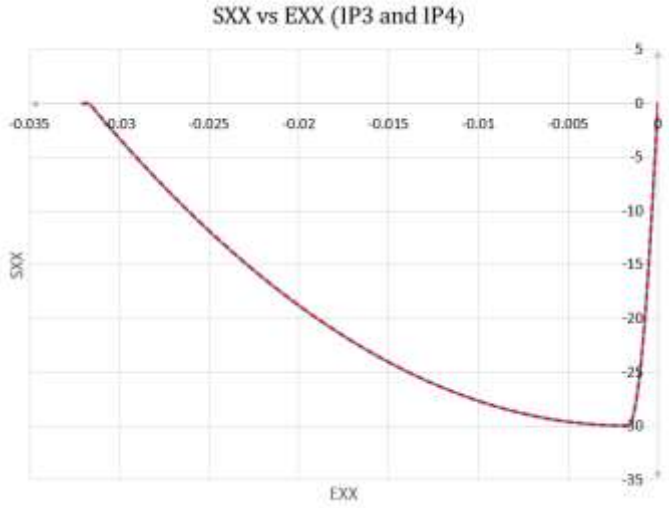

Load:
Tension-compression
Tension: 1 mm
Compression: -2mm
100 steps of 0.001

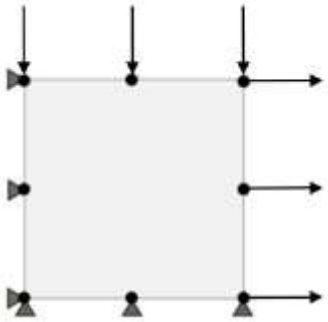

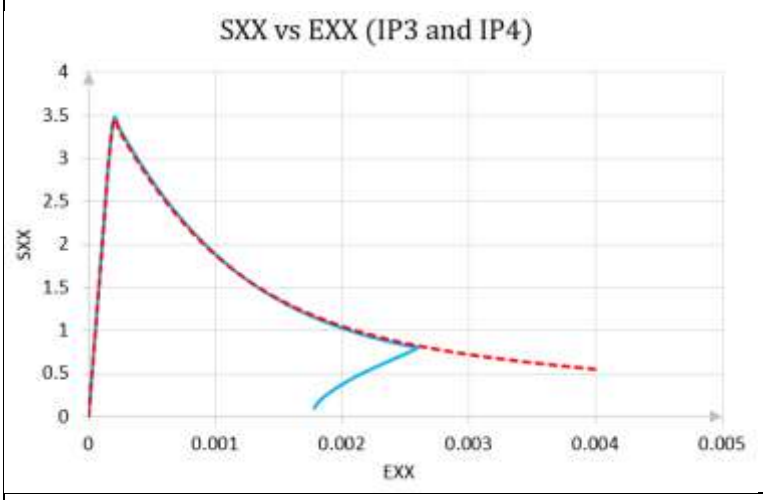

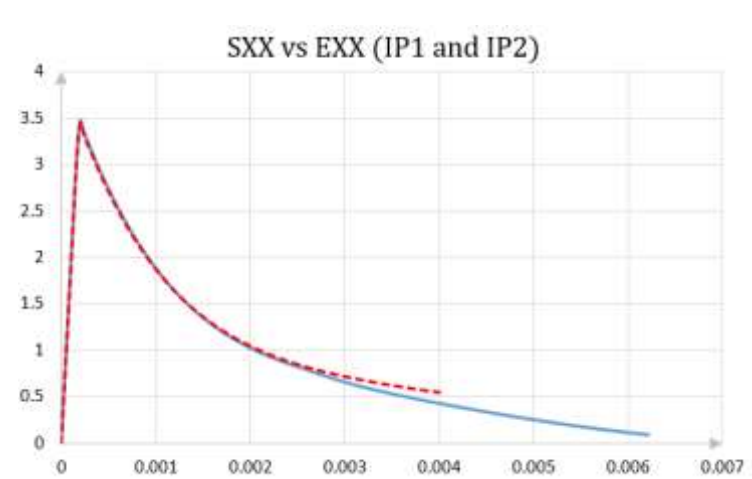

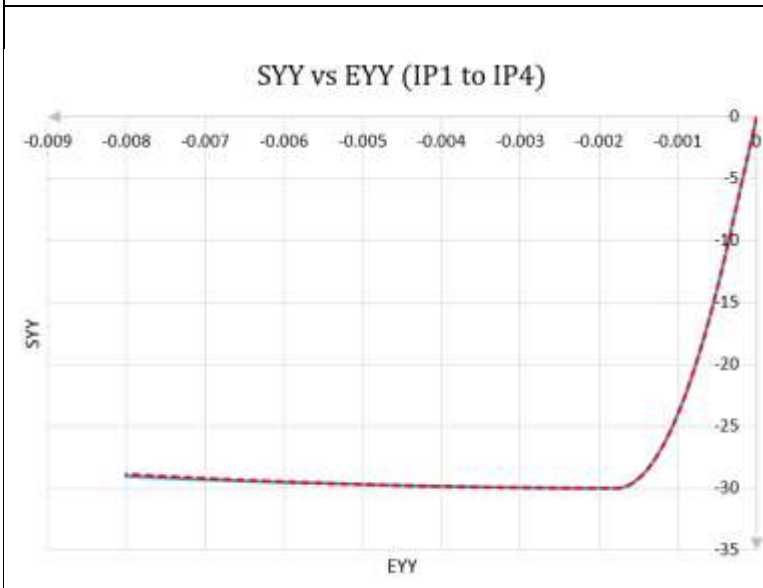

Table 3. 2 Axial test results for elementary cell

Comparative stress-strain plots for representative integration points show an overall good match with DIANA results (see Table 3. 2). However, numerical snapping back [22] of certain integration points, that is decrease in strain without complete yielding of any other integration points, as can be seen in Table 3. 2 for DIANA biaxial test, was also observed in certain compression test results of the MATLAB code. Specifically, this happened only when the residual compressive stiffness dropped below 0.04*E. A probable reason for this could be the ill-conditioning of the stiffness matrix for a single cell test in which failure is completely dominated by non-linear softening. Therefore, a residual stiffness of 0.05*E was adopted during compressive one cell tests.

Axial tests were also performed on the elementary cell with damage inputs. Table 3. 3 shows the results for a biaxial test with tensile and compressive damage varied between 0 and 1.

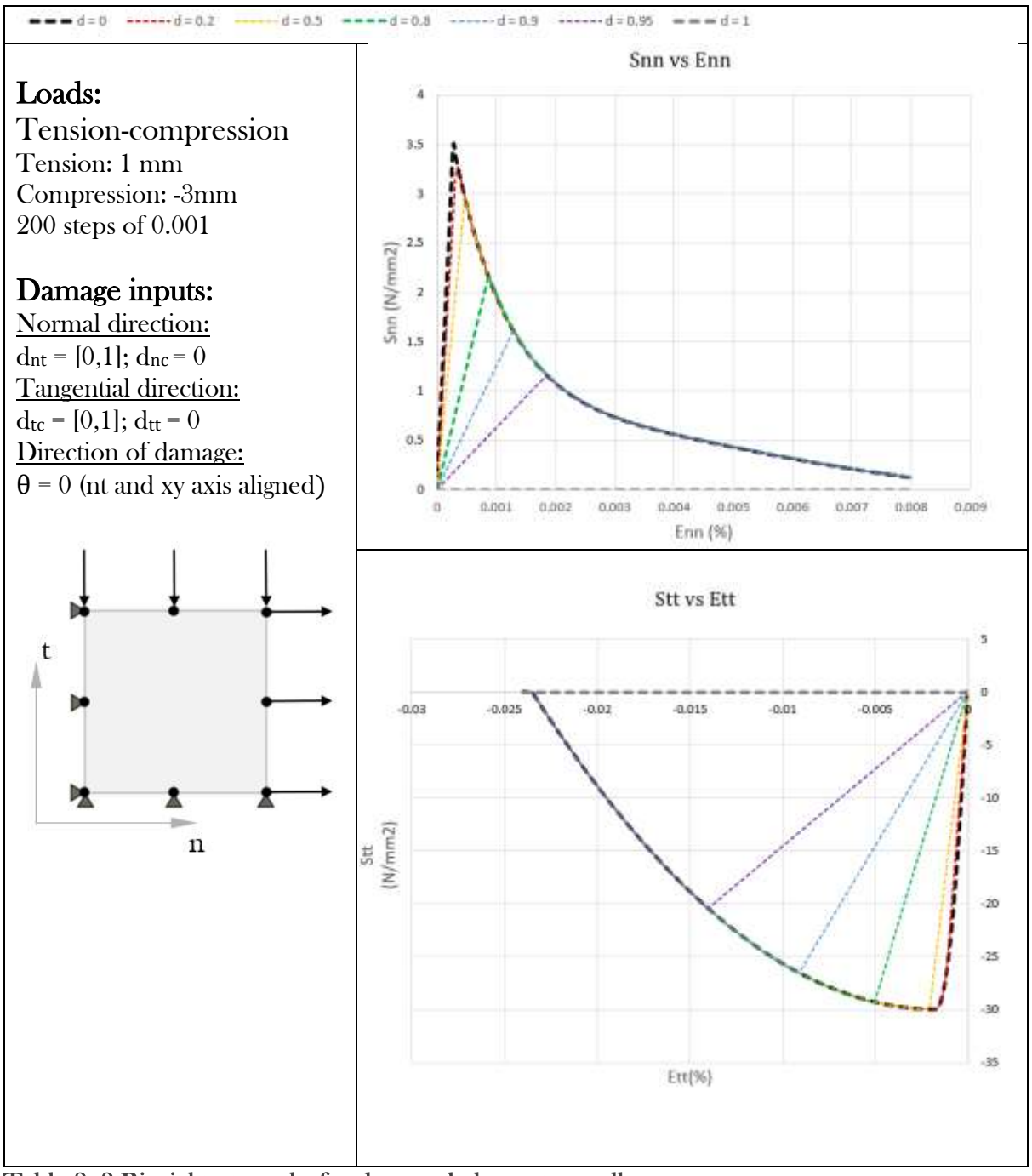

Table 3. 3 Biaxial test results for damaged elementary cell

3.6. 2 Eight-Cell test

In order to further verify the implementation, a small eight element RC structure was tested in bending. The geometry, loading and support conditions are seen in Figure 3. 11. A displacement of 0.5 mm was prescribed at the loading point in small increments (0.01*(25),0.005*(50)). Linear elastic rigid steel plates were used for support and loading. Material properties and finite element parameters for concrete in this test are identical to those of the elementary cell (Table 3. 1), expect the crack bandwidth which is taken equal to the element size as 12.5mm. Properties for the reinforcement are listed in Table 3. 4.

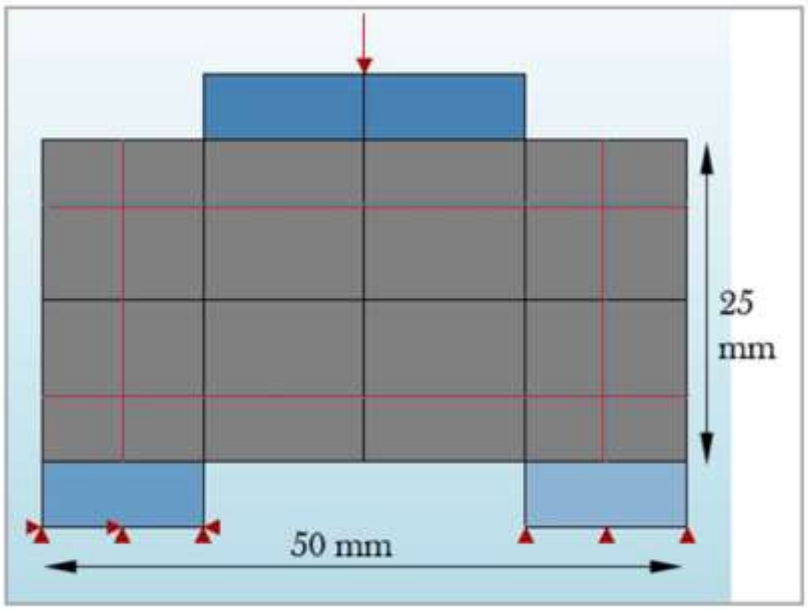

Figure 3. 11 Geometry, loading and support conditions for 8-cell test

Yield stress (fy)	250 N/mm^2
Young's Modulus (Es)	200000 N/mm^2
Hardening Modulus (Eh)	40000 N/mm^2

Table 3. 4 Reinforcement properties for eight-cell test

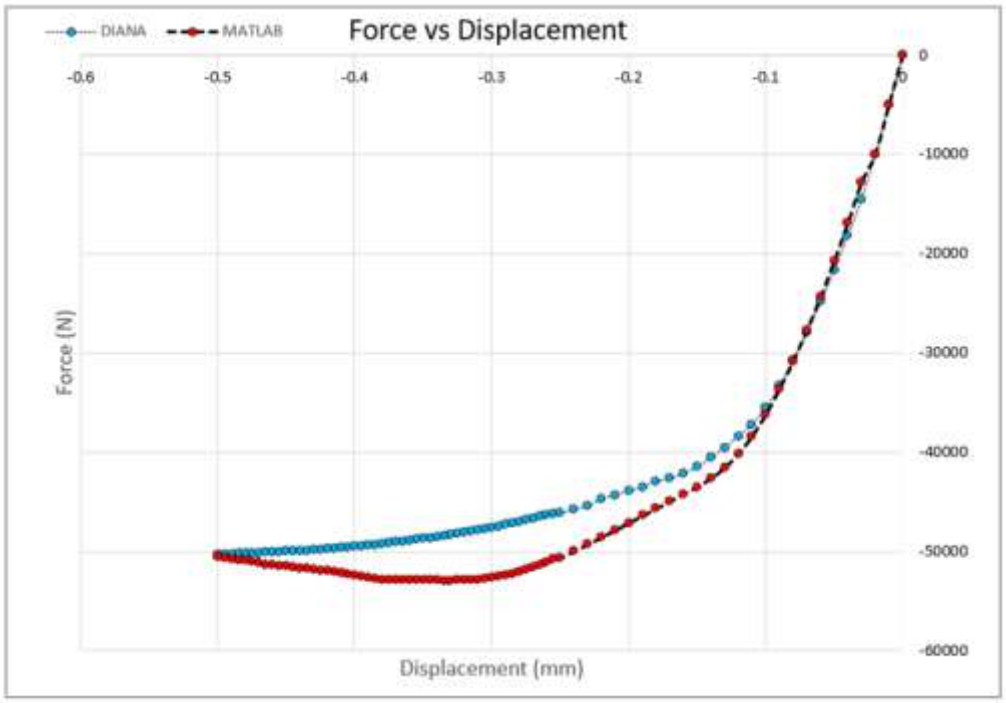

Figure 3. 12 Force vs. Displacement for eight-cell test

Figure 3. 12 shows a comparison of force versus displacement curves for the loading point with a displacement-norm tolerance of 1e-2mm and force-norm tolerance of 10e-2 N. Convergence was obtained for all steps. The two solutions drift-away slightly after the end of the linear regime. The overall agreement however, was considered to be satisfactory.

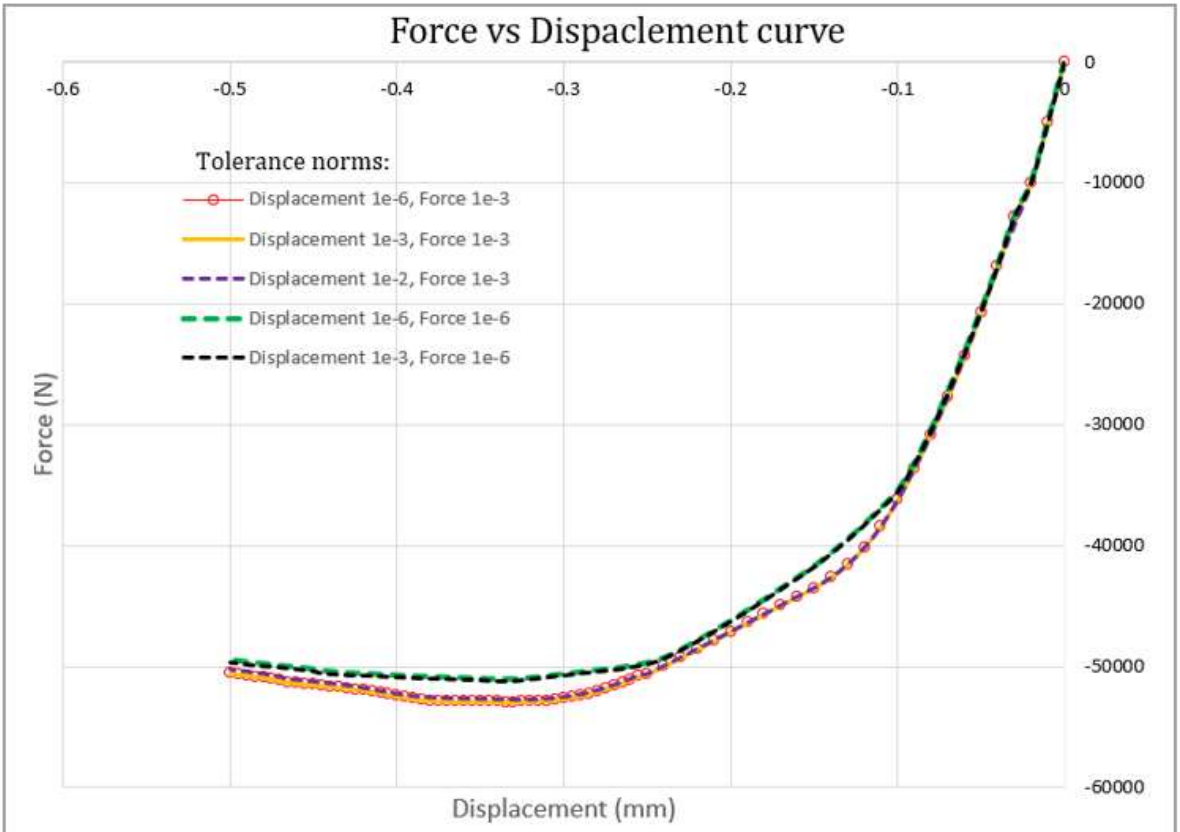

Displacement norm tolerance(mm)	Force norm tolerance(N)	Maximum iterations before convergence
1e-6	1e-6	30
1e-2	1e-2	1
1e-3	1e-3	2
1e-3	1e-6	1
1e-6	1e--3	10

Figure 3. 13 Sensitivity study for convergence criteria

A sensitivity study was conducted by varying the acceptable tolerance for convergence of the solution procedure. The number of iterations before convergence was noted for each load step. The results of the study are summarised in Figure 3. 13. As seen in the figure, the variation of tolerance norm did not appreciably change the solution. Additionally, it was observed that the force norm was most readily satisfied, although a relaxed force norm drifted away from the strictest criteria. A relaxed displacement norm on the other hand resulted in almost the same equilibrium path as the strictest norm but with lesser number of iterations. Therefore, 1e-3 mm displacement norm and 1e-6 N force norm were chosen as the convergence criteria as a balance between accuracy and computation time.

3.6. 3 Full-scale test

After finalising the implementation, computational analysis of a full-scale RC beam tested in [4] was undertaken.

Details of the specimen

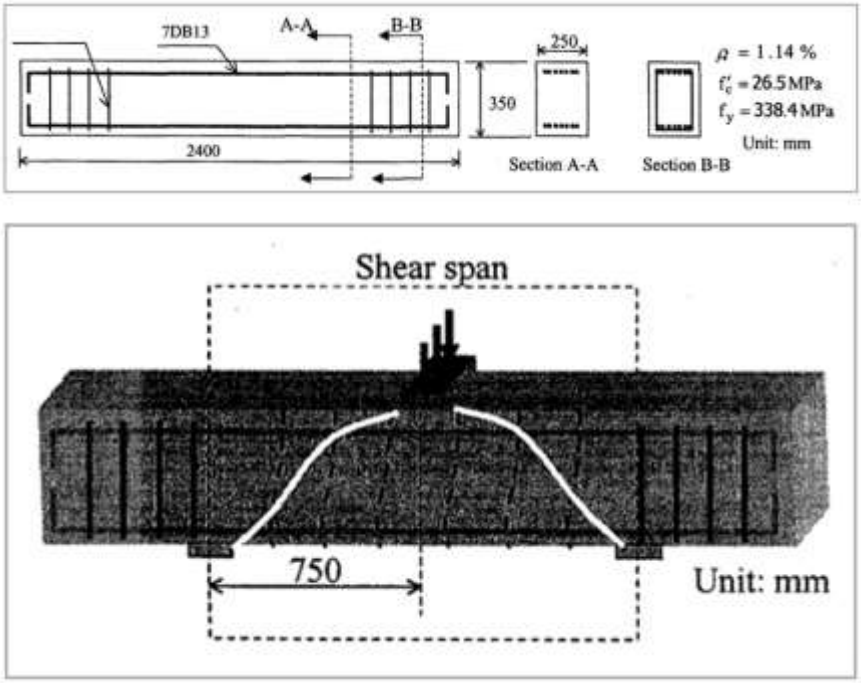

Figure 3. 14 Geometry, given material properties and support conditions for full scale test [4]

The geometry, material properties available in the experimental report, loading and support conditions can be seen in A conventional shear failure mode due to propagation of a single diagonal crack was observed in the experiment. The failure process was initiated by the first diagonal crack, appearing at the web, near the central region of the shear span. The experimental force-displacement curve and crack pattern at failure can be seen in figure1.

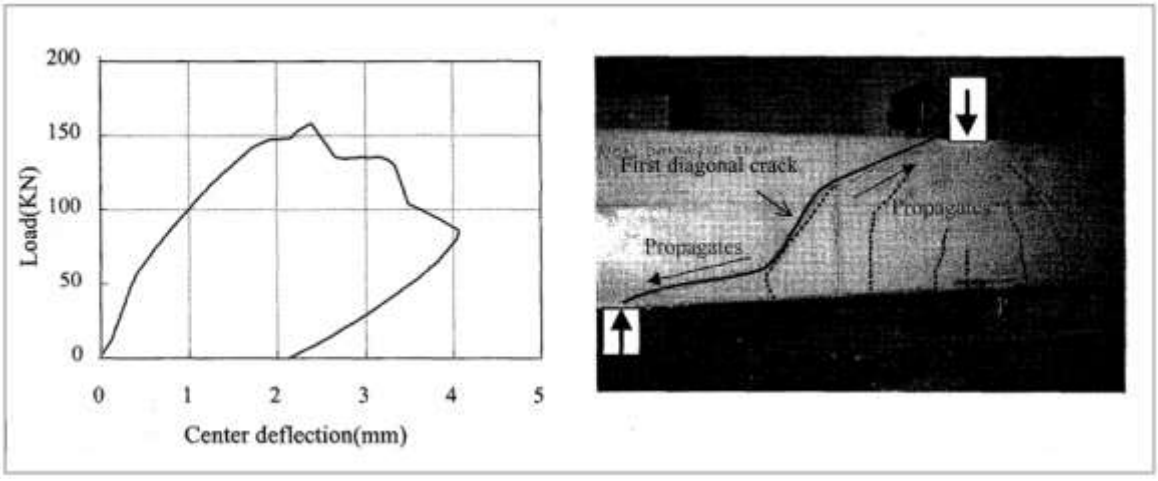

Figure 3. 15 Experimental load-displacement relationship and crack pattern at failure for full scale specimen.

A conventional shear failure mode due to propagation of a single diagonal crack was observed in the experiment. The failure process was initiated by the first diagonal crack, appearing at the web, near the central region of the shear span [4]. The experimental force-displacement curve and crack pattern at failure can be seen in figure1.

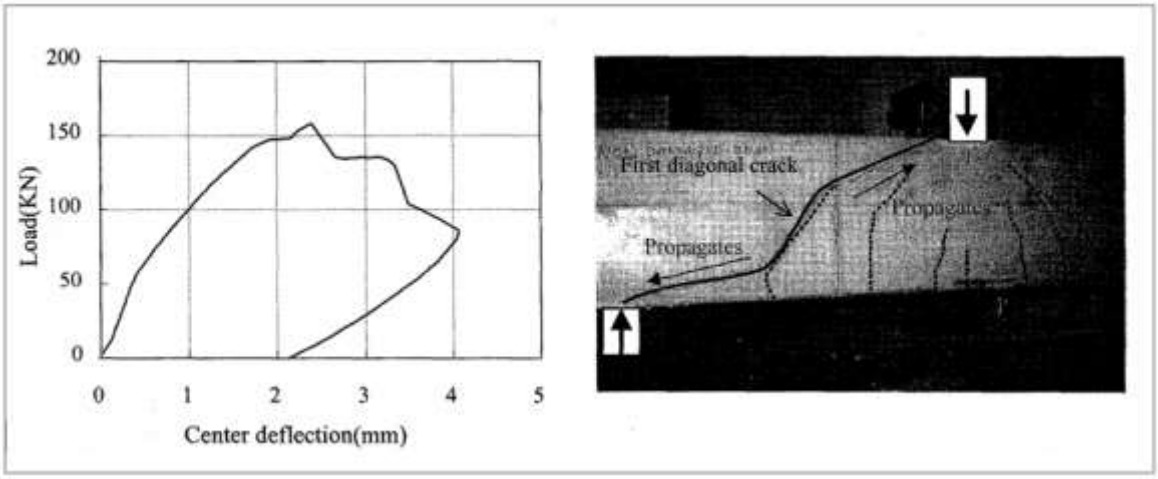

Figure 3. 15 Experimental load-displacement relationship and crack pattern at failure for full scale specimen [4]

Finite element modelling

The given compressive strength was treated as a characteristic value and the material parameters required to set up the finite element model were calculated using recommendations given in [23]. The Young's Modulus was estimated separately from the linear region of the force-displacement curve provided in the experiment. Table 3. 5 shows all the properties used in the computational analysis. The finite element mesh can be seen in Figure 3. 16.

Thickness(t)	250 mm
Young's modulus(E)	11577 N/mm^2
Poisson's ratio(ν)	0.15 (Damaged based)
Compressive strength (f_c)	26.5 N/mm^2
Tensile strength(f_t)	2.1 N/mm^2
Compressive fracture energy(G_c)	32.92 N/mm
Tensile fracture energy(G_f)	0.1316 N/mm
Element size	25 mm
Crack bandwidth(h)	25 mm
Crack orientation	Fixed
Tensile behaviour	Hordijk tension softening
Compressive behaviour	Parabolic softening
Shear behaviour after cracking	Constant (β=0.01)
Element type	CQ16M
Integration scheme	4-point Gauss
Convergence criteria	Displacement norm: 1e-3 mm Force norm: 1e-6 mm
Maximum no. of iterations	50
Yield stress for reinforcement (fy)	338.4 N/mm2

Young's modulus for reinf. (Es)	200000 N/mm²
Hardening modulus for reinf. (Eh)	4000 N/mm²

Table 3. *5* Material properties and finite element considerations for full-scale test

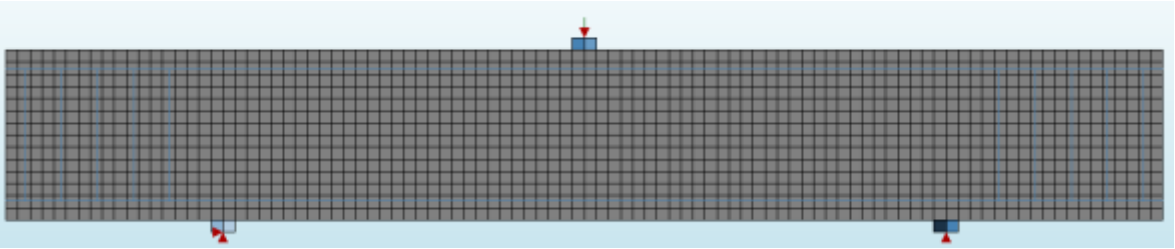

Figure 3. 16 Finite element Mesh for full scale test

The beam was loaded with a total displacement of 3.5mm, applied over increments of 0.1 mm. Comparative force vs displacement curves, from the experiment and MATLAB analysis can be seen in Figure 3. 17

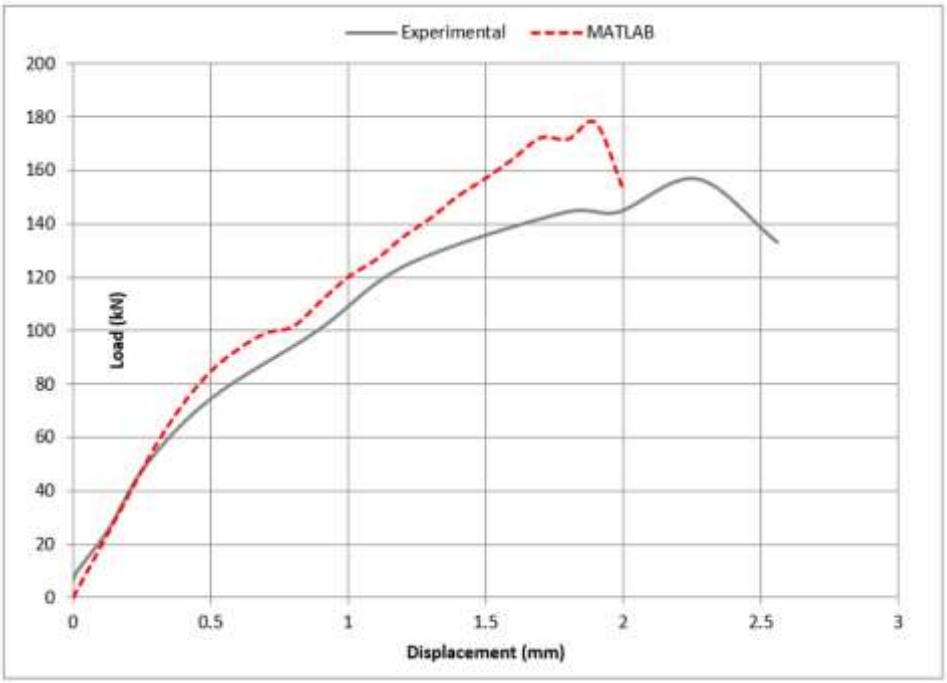

Figure 3. 17 Experimental and Computational Load vs Displacement comparison

As seen from the figure, there is a good agreement in the linear regime. This was expected, since the Young's modulus was estimated from the linear region of the experimental curve. There is a slight over prediction of capacity and stiffness, although the global behaviour of the beam is captured well. To further compare, the analysis with the experiment, numerical crack patterns are visualised at peak load-steps. Figure1, shows the major principal stresses plotted in the beam at load step 19(1.9mm displacement) and step 20(2mm displacement) of the computational analysis and compared with the experimental crack pattern. The value 0.0257 in the colour legend is the ultimate strain for concrete.

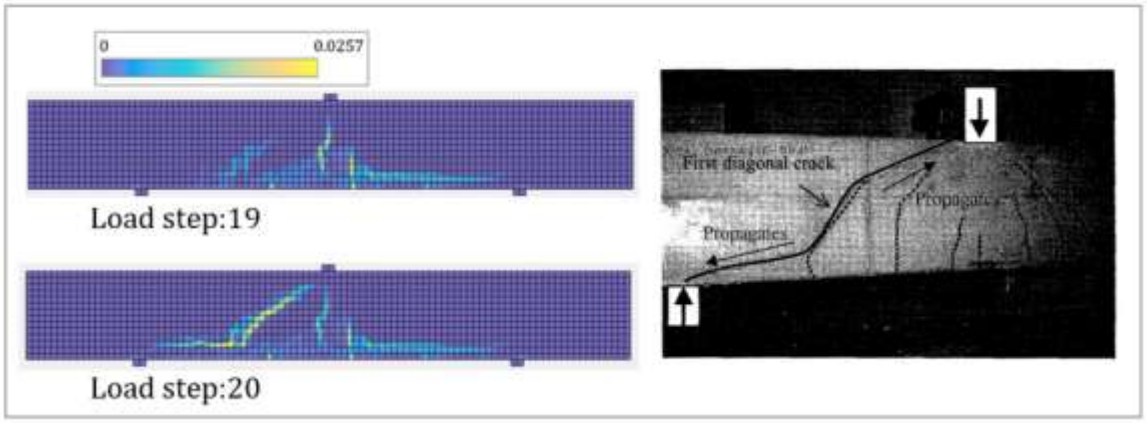

Figure 3. 18 Major principal strains vs experimental crack patterns plotted at load step 19(1.9mm) and load step20(2mm)

It can be seen that the diagonal crack is initiated at step 19 and suddenly propagates in step 20 causing failure. This is in very good agreement with the experimental observations, therefore affirms the validity of the obtained finite element analysis solution. Converged solution was obtained for all considered steps.

3. 7 Image analysis of damaged domain

The best fit line algorithm discussed in chapter 2, to obtain crack orientations from images of damaged domain was implemented and coupled with damage input for finite element analysis. In order to obtain binary images from digital images of specimens, the image processing software ImageJ [18] was used. Using the same software, the binary image was scaled such that (1x1) mm length corresponds to (1x1) pixel in the image. This implies, the geometry of domain under study is represented by a matrix with number rows equal to length of domain and number of columns equal to the height of the domain. Since the read image is binary, each entry of the matrix is either 0(white) or 255(black).

The virtual gird of boxes is set up by dividing the rows and columns into divisions of size r. Here, r represents the box-size which can be varied to obtain the desired refinement. Upon fixing the element size, the matrix entry (row and column number of the vertices) of boxes with black pixels in them were stored as damaged elements. The slope of the best fit line of the black pixel distribution inside each box was stored as the orientation of the crack in the element. The coupling with the finite element mesh was achieved by comparing the global co-ordinates of the element-centres with the centre of the boxes, derived from the corresponding matrix entries.

3.8. Discussion

A finite element tool was set up on MATLAB to include the material model for damaged concrete. The highlights of the implementation were discussed. The code was verified by testing concrete structures at various scale. Satisfactory results were obtained for all tests. To this end, the developed tool will now be used to simulate experiments on pre-damaged RC structural members. The results from the full-scale experiment will be recalled as a reference undamaged beam analysis in the next chapter.

4.Computational analysis of experimental specimens

4. 1 Introduction

The implemented FE tool was used to simulate two experiments found in literature, on pre-damaged RC structural members [4], [28] in order to draw conclusion about the modelling strategy adopted in the study. The first experiment, is treated as a calibration example. The full-scale test described in the previous chapter is treated as the undamaged specimen from the experiment. The pre-damage specimen is modelled using the same finite element mesh, but with an added input for pre-damage. The second experiment is a more realistic case of pre-damage. The image analysis algorithm discussed in the previous chapters is utilised for damage inputs. A number of sensitivity studies are conducted to explore the model's range of application. For each experiment, the computational study is reported in the following format:

- Description of the experiment
- Finite element modelling using damage input strategy
- Results and discussion
- Sensitivity study

4. 2 Experiment 1: Influence of vertical pre-cracking on reinforced concrete in shear [4]

4.2. 1 Description of the experiment

This experiment consists of a series of tests conducted on pre-cracked beams, to study the influence of vertical cracking on the structural response. The experiment involves two phases.

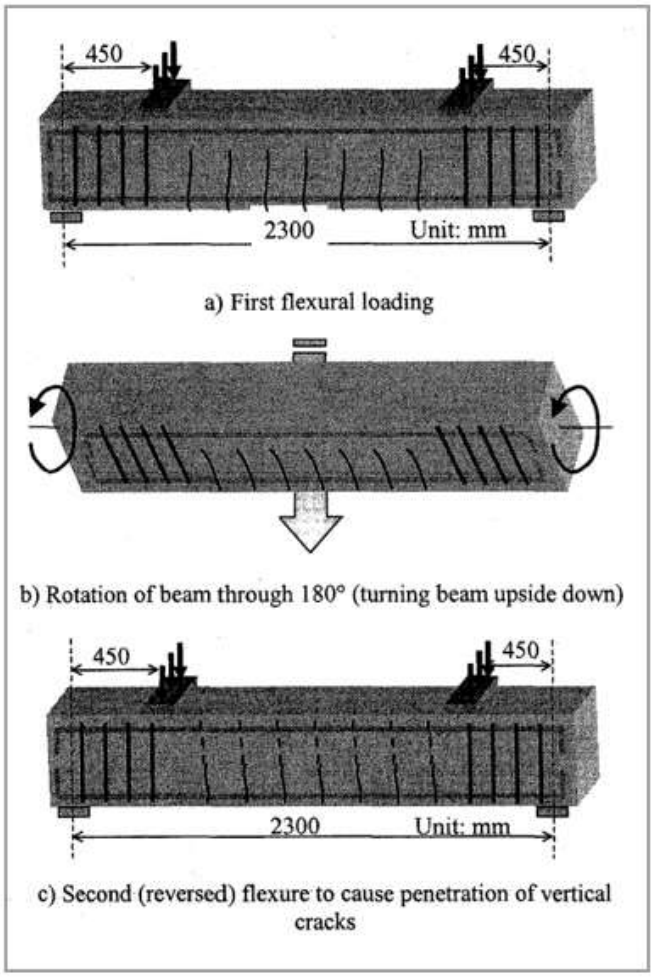

Figure 4. 1 Set up for reverse flexural loading [1]

❖ Phase 1: Application of reverse flexural load to generate vertical pre-cracks

The set up for this phase can be seen in Figure 4. 1. The beam is loaded in flexure by applying a 2-point load. Flexural cracks are allowed to generate vertically. The beam is then rotated by 180°, in order to allow the cracks to penetrate throughout the section of the beam. The shear span of the beam is kept unreinforced, in order to force the formation of the cracks in the shear span. Sufficient shear reinforcement is provided near the supports so as to avoid shear cracking at the ends. Multiple specimens were loaded in such a manner with varying amount of reverse flexural loading, in order to obtain pre-cracked beams with varying degree of cracking. The condition of the shear spans of the specimens after application of reverse flexural loading was recorded. A schematic representation is provided in the experiment and can be seen in Figure 4. 1

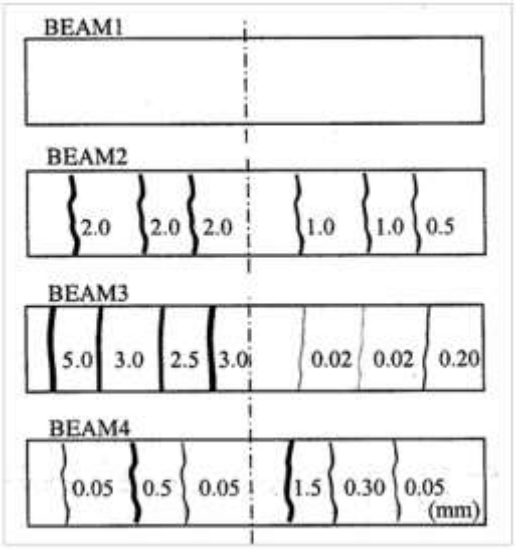

Figure 4. 2 Condition of shear spans after reverse flexural loading [4]

The numbers next to each crack signify the residual crack-width measured in mm. BEAM1, is a reference undamaged specimen which was not loaded in reversed flexure, therefore contains no cracks. The cracks in BEAM2, were reported to be more or less equally spaced. BEAM3 and BEAM4 exhibited varying severity of cracking on the left and right side [4].

❖ Phase 2: Application of shear load on pre-cracked beams

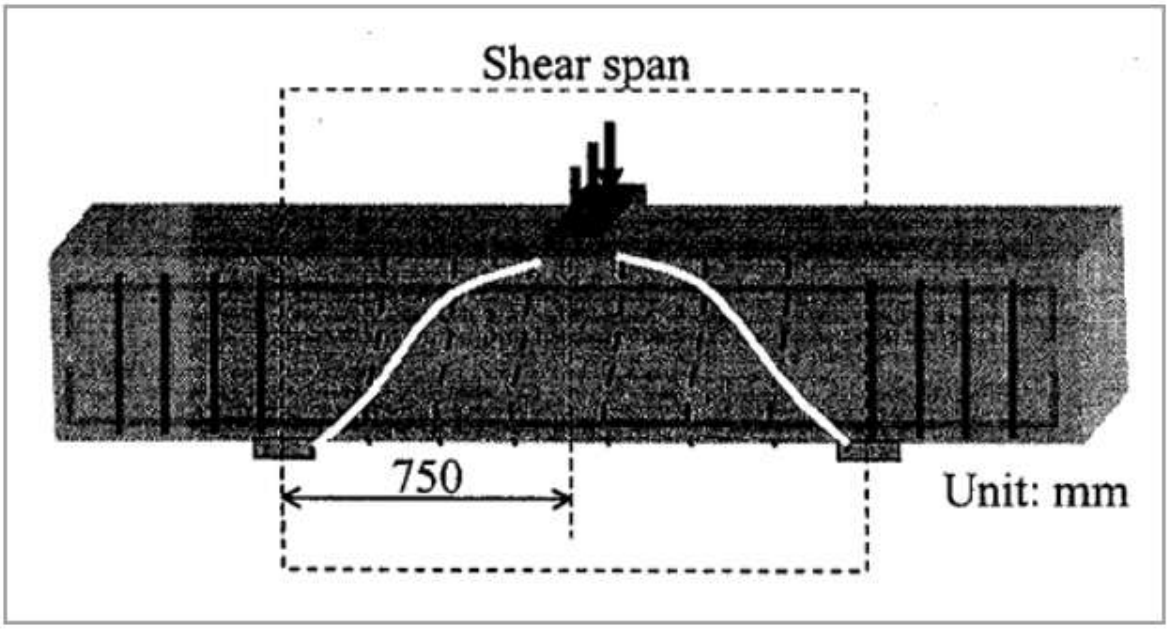

Figure 4. 3 Set up for shear loading [4]

The set up for this phase of the experiment can be seen in Figure 4. 3. The support conditions are altered in order to induce shear load. The load is applied through one point in the centre of the beam span.

Beam	Loading capacity(KN)	Percent load increase(%)	Side at which shear failure took place
Beam1(non pre-cracked, reference test)	157.0	0.0	Left
Beam 2	233.5	48.8	Right
Beam3	184.9	17.8	Right
Beam4	217.3	38.4	Left

Figure 4. 4 Results of the shear test [4]

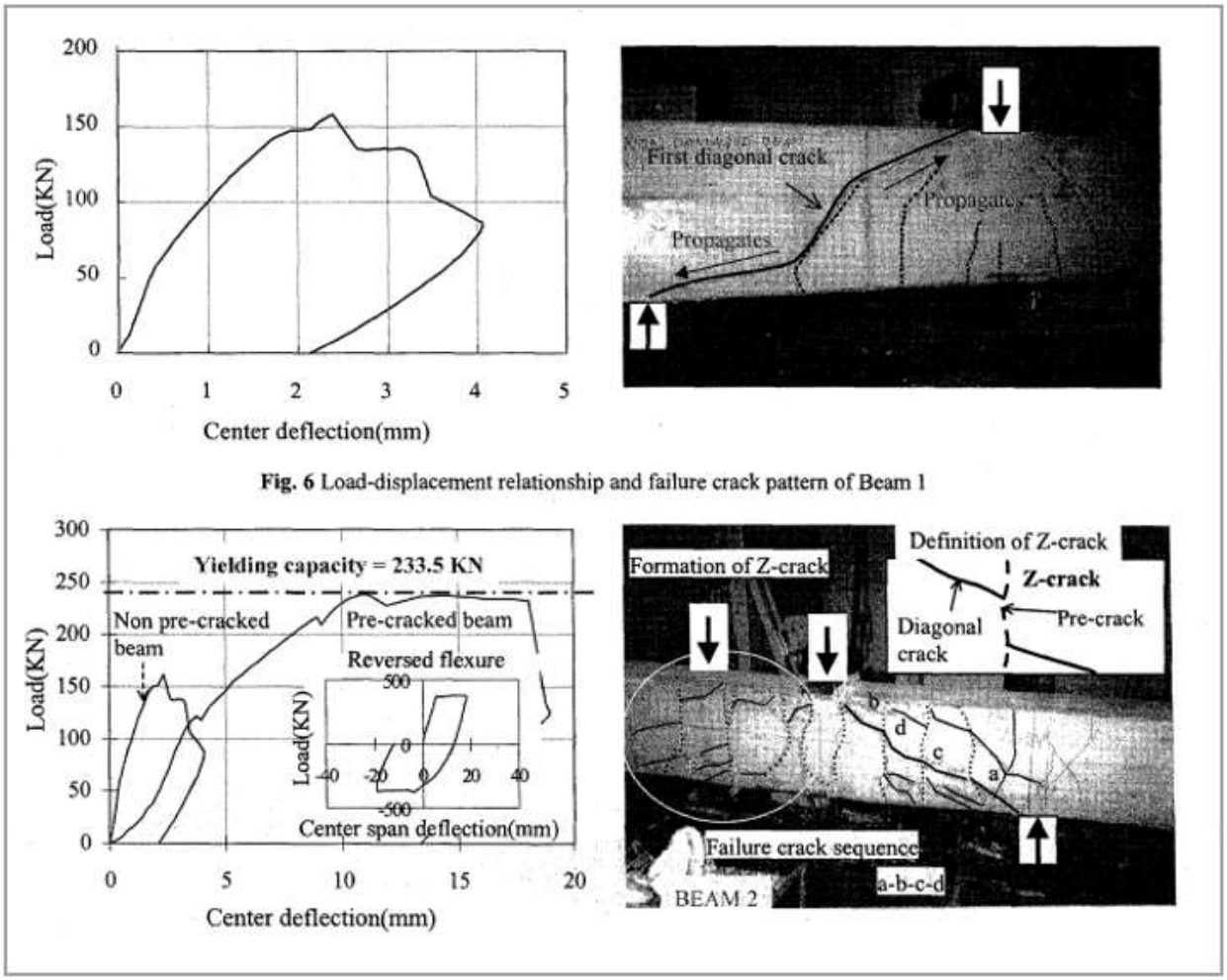

Figure 4. 5 Load-displacement curve and failure mode for beam1 and beam2 [4]

The results of the shear test are enlisted in Figure 4. 4. It can be observed that an increase in shear loading capacity was reported with respect to the reference undamaged beam(BEAM1). Figure1 shows the load-displacement relationship and the failure crack patterns for BEAM1 and BEAM 2.

The failure of the reference beam(BEAM1) is finalised by the propagation of a single diagonal crack which joins the point of load application and the support. BEAM 2 exhibits a different failure mode. Cracks a-b-c-d seen in Figure 4. 5 form independently at different load steps, throughout the application of the load, to finalise the failure path. This allows the beam to carry load even after the formation of diagonal cracks, thereby increasing the over-all shear capacity

and ductility of the beam [4]. A qualitative force vs displacement comparison for non pre-cracked and pre-cracked beam can be seen in Figure 4. 6

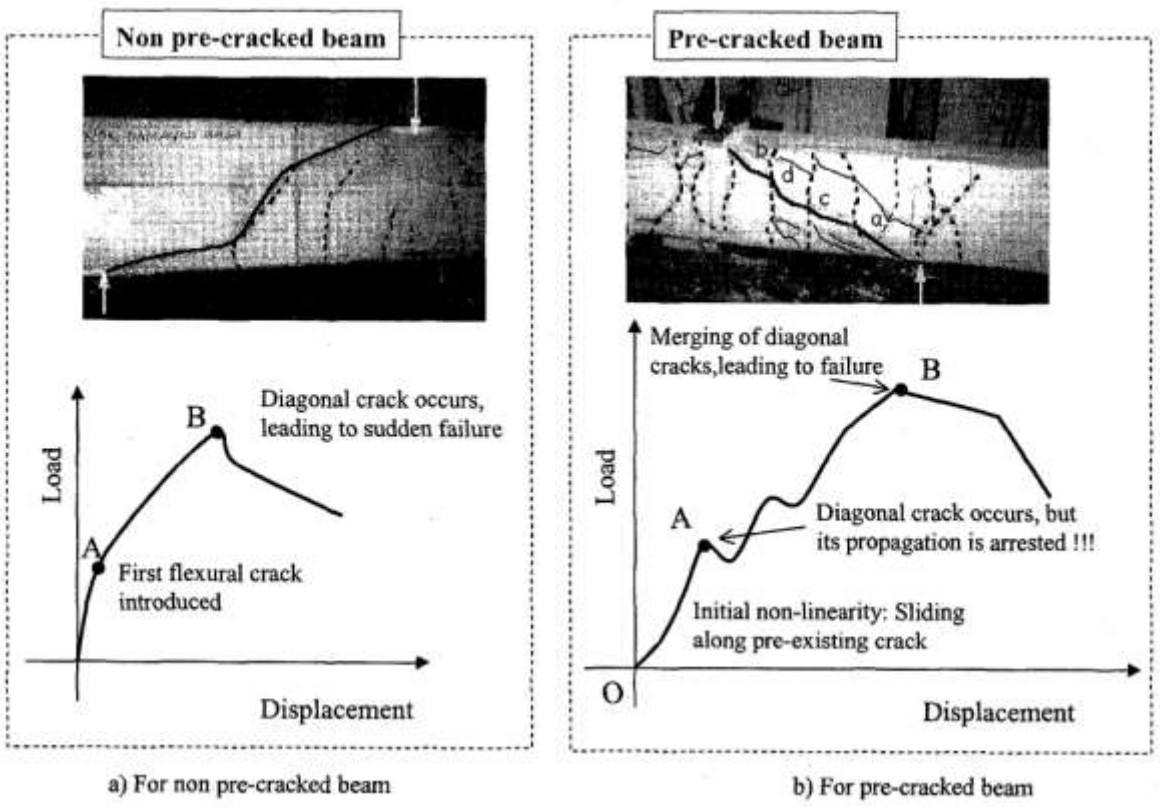

Figure 4. 6 Qualitative force vs displacement comparison for non pre-cracked and pre-cracked specimen [4]

4.2. 2 Finite element modelling using damage input strategy

The finite element model and the results of the computational analysis for the reference beam without any pre-cracks (BEAM1) was discussed in chapter 3. BEAM2, which was reported to have more or less equally spaced cracks was chosen for the computational study of the damaged specimen. The damaged beam was modelled using the same finite element mesh as BEAM1, but with an added input for damage to account for the existing pre-cracks. Six bands of perfectly vertical, equally spaced cracks were modelled in the shear span of the beam. The crack-widths for this beam were correlated to the tensile damage variable in the normal direction – d_{nt}. All the crack-widths were large enough to yield a value of 1 form the stress-crack opening relationship, used in the analysis. Damage was thus assumed to be purely tensile and cracking was assumed to be perfectly vertical, hence all other damage variables including the direction of damage were set to zero. A total displacement of 18mm was prescribed to the loading point in 7 steps of 0.5mm followed by 58 steps of 0.25mm. The principal strains plotted over the finite element mesh at the first load step can be seen in Figure 4. 7.

Figure 4. 7 Finite element mesh for damaged specimen(BEAM2) at load step 1(0.5mm)

4.2. 3 Results and discussion

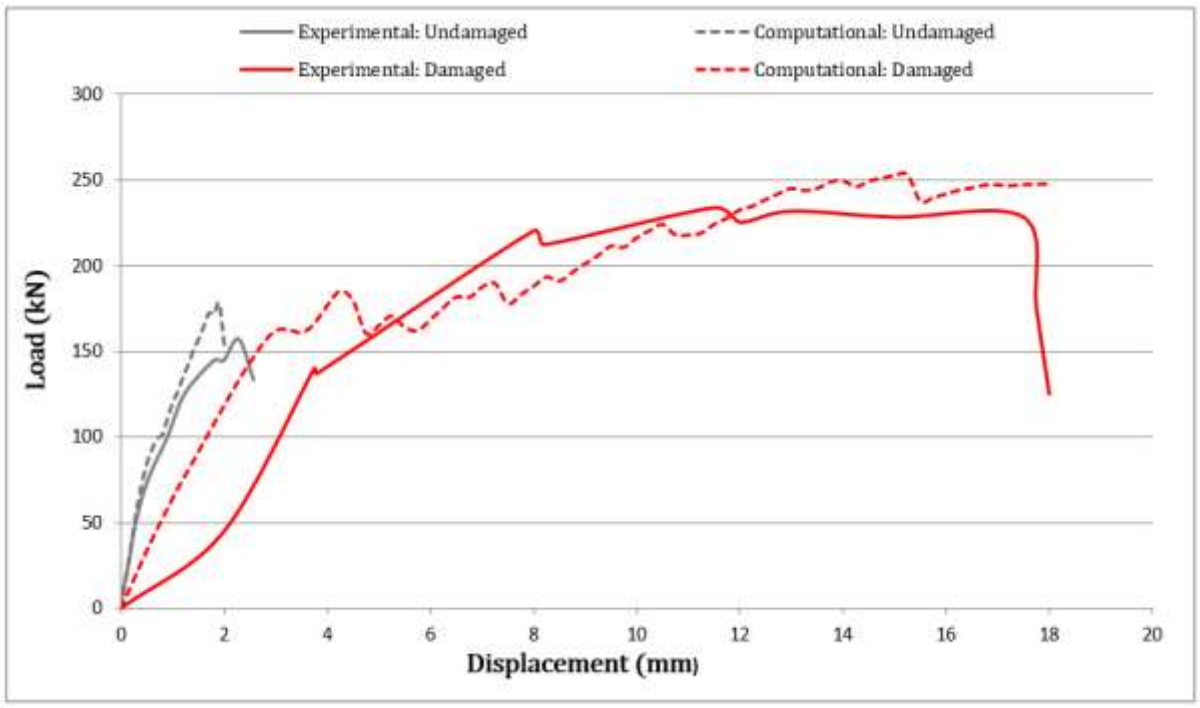

Figure 4. 8 Force vs Displacement comparison for undamaged and damaged beams

Comparative experimental and computational force vs displacement curves for the undamaged reference BEAM1 and damaged BEAM2 can be seen in Figure 4. 8. As can be seen from the figure, drastically different behaviour of damaged and undamaged beam is observed in the force displacement curve. To investigate this behaviour further, numerical crack patterns at characteristic load-steps were studied. Figure 4. 9 shows the major principal strains at load step 3 plotted on the deformed finite element mesh. The scale of deformation is exaggerated by a factor of 20. The value 0.0129 in the colour legend represents the ultimate tensile strain of concrete.

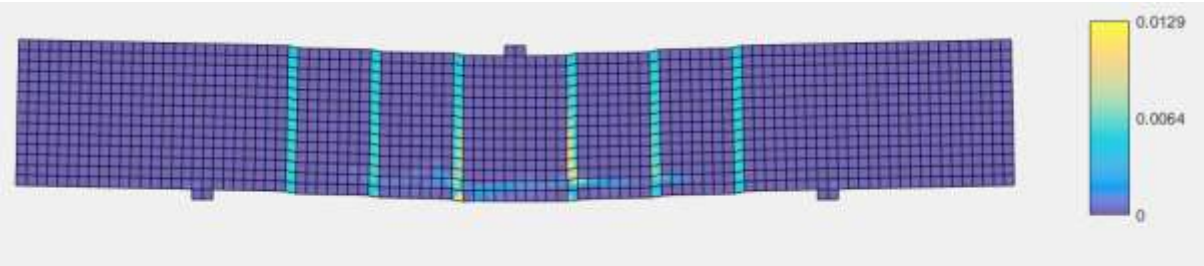

Figure 4. 9 Major principal strains on deformed mesh at load step 3(1.5mm)

It can be seen that relative sliding occurs between the cracks. Strain starts to localise in the already damaged elements. This explains the initial low stiffness observed in the force vs displacement curve in **Error! Reference source not found.**. Formation of new cracks is also seen around the damaged elements. Figure 4. 10 displays the major principal strains plotted at load steps 6 and 7.

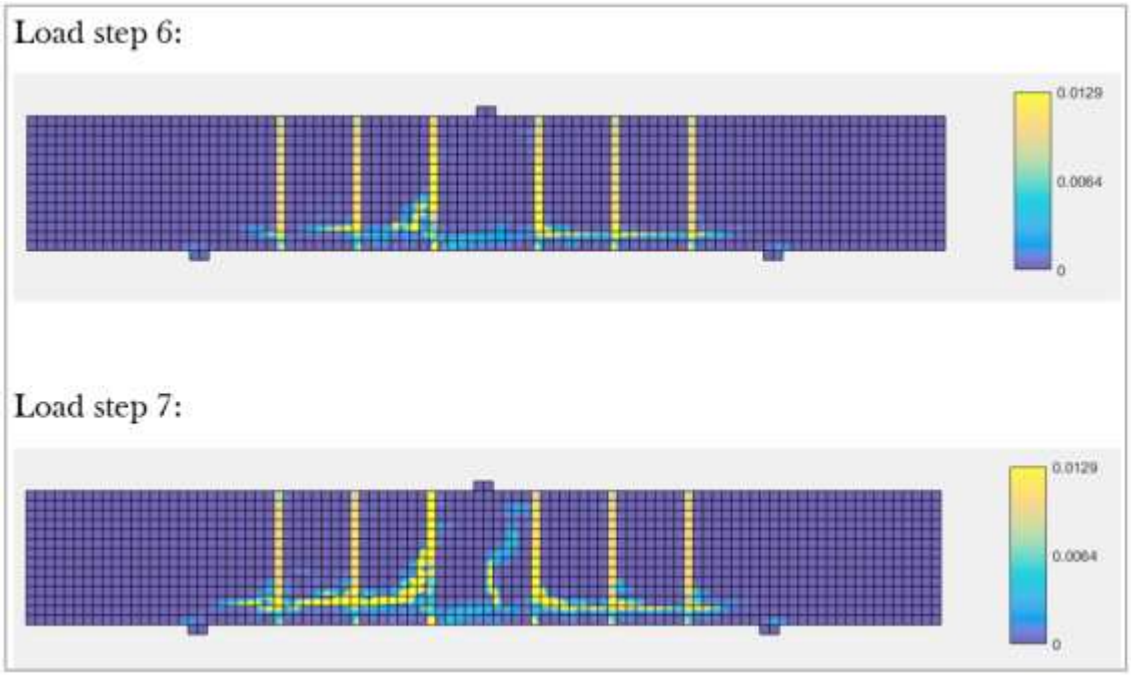

Figure 4. 10 Major principal strains at load step 6(3mm) and 7(3.5mm)

Load step 6 signifies the first peak in the computational force vs displacement curve seen in Figure 4. 5. It marks the onslaught of the first diagonal crack. In load step 7, the propagation of this crack is arrested by the already existing damage. This continues to take place for newly formed diagonal cracks until load step 10. The load drops temporarily, and rises again until load step 11 where diagonal cracks start forming on the other side of the already existing damage. Major principal strain plots for load step 10 and load step 11 can be seen in Figure 4. 11.

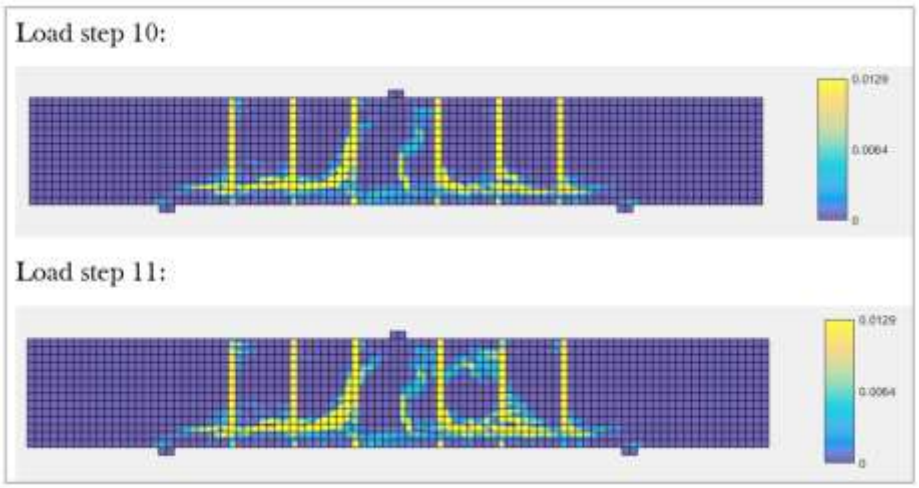

Figure 4. 11 Major principal strains at load step 10(4.25mm) and 11(4.5mm)

In the subsequent load steps, the force vs displacement curve drops and rises successively, upon formation and arrest of new diagonal cracks. The evolution of is visualised by plotting the major principal strains for load steps 15, 25 and 55. The scale is altered from the previous plots to incorporate high strain values in order to aid visualisation. The value of 0.0386 in the colour legend represents three time the ultimate tensile strain of concrete.

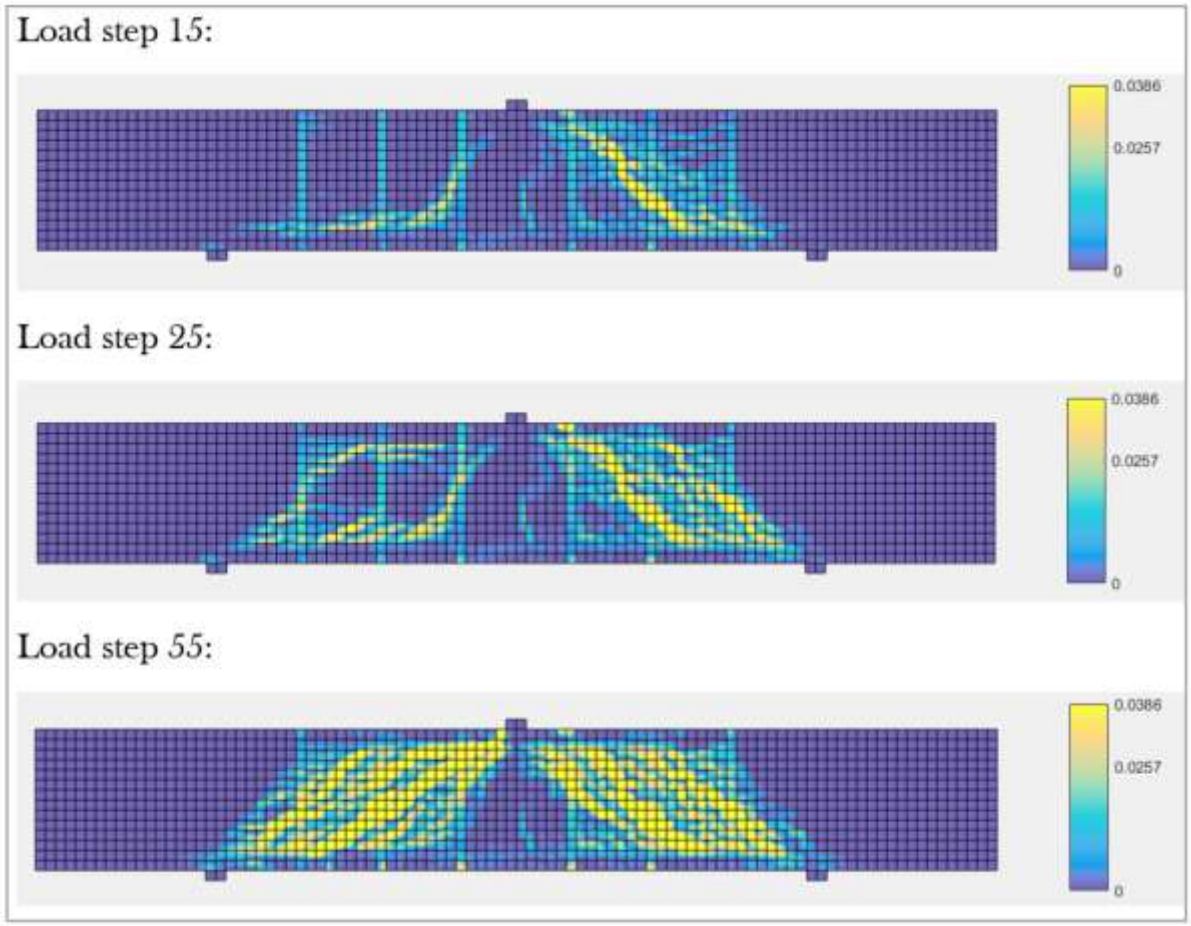

Figure 4. 12 Major principal strains at load step 15(5.5mm), 25(8mm) and 55(15.5mm)

Multiple diagonal cracks merging to form a failure path is observed, although a clear localised path is not obtained. Yielding of the longitudinal reinforcement begins at load step 52. A plot of stresses in the reinforcement can be seen in Figure 4. 13.

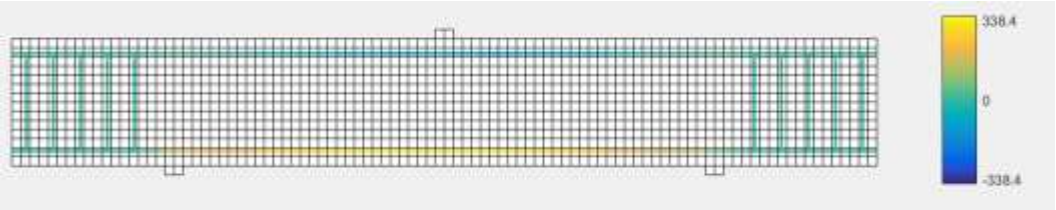

Figure 4. 13 Reinforcement stress at load step 52(14.75 mm) (fy = 338.4N/mm2)

After this step, a drop is observed in the force vs displacement curve following which a plateau is observed. The computational shear capacity of the beam can be estimated to be around 250 KN observed at a mid-point displacement of 15.5mm, which is in good agreement with the experimental observation.

4.2. 4 Sensitivity study

The computational analysis was unable to capture the initial non-linearity in the force vs displacement curve. This non-linearity is attributed to the relative sliding of the pre-existing cracks in the experimental observations [4]. A constant shear retention of 0.01 was used in the previous analysis to model this phenomenon. Physically more appealing is the damaged based shear retention model in which the shear modulus of the cracked elements is assumed to degrade at the same rate as the normal stiffness. Thus, the analysis was carried out again using a damaged based shear retention model, keeping all other parameters unchanged. A minimum shear retention of 0.005 was set in order to avoid numerical difficulties. A comparison of force vs. displacement curves can be seen in Figure 4. 14.

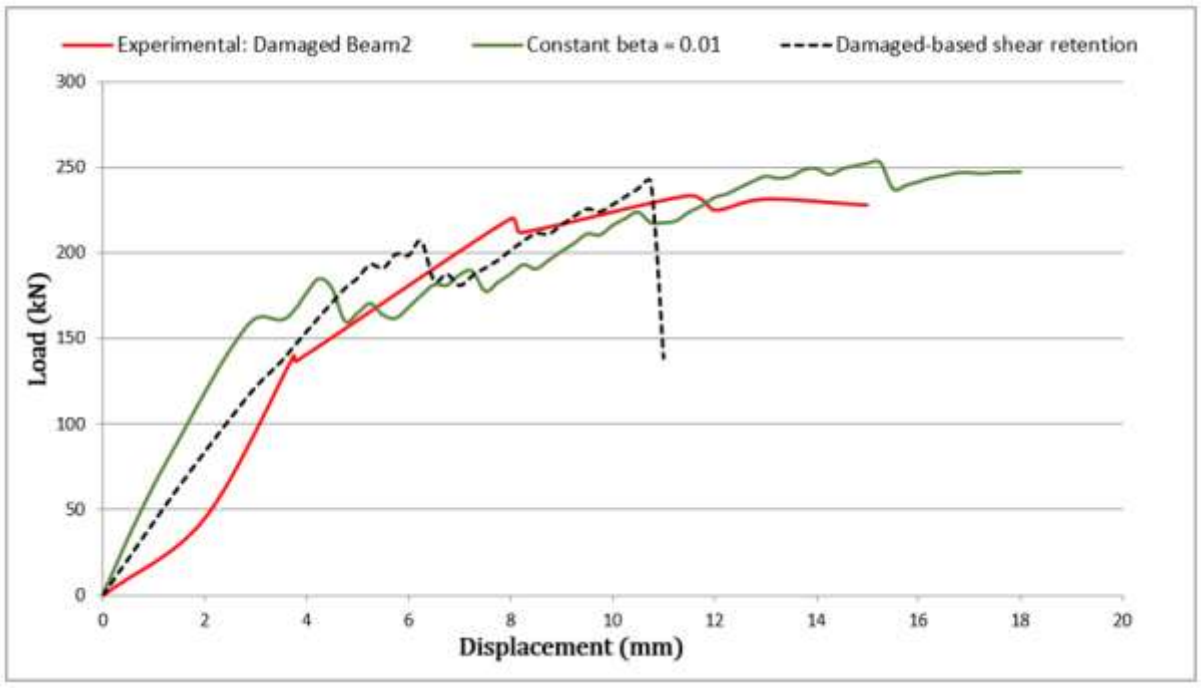

Figure 4. 14 Comparative force vs displacement curves for constant and damaged based shear retention

A drop in the initial stiffness of the beam can be observed. This is not unexpected, since the pre-cracked elements now have half the shear stiffness than the previous analysis. Although there is a closer estimation of initial stiffness, the nonlinear behaviour as per the experiment is still not captured. The part of the force vs displacement curve after which diagonal cracks start forming, is characterised by a stiffer behaviour than the previous analysis. This can be attributed to the fact that, using a damaged based shear retention implies a gradual decline of shear stiffness for elements which are not damaged from the start of the analysis. Thus, the initial part of the curve is dominated by sliding of existing cracks and the latter by initiation, propagation and arrest of diagonal cracks, giving rise to the peculiar failure mode. The evolution of crack pattern is visualised in Figure 4. 15 by plotting major principle strains at characteristic load steps.

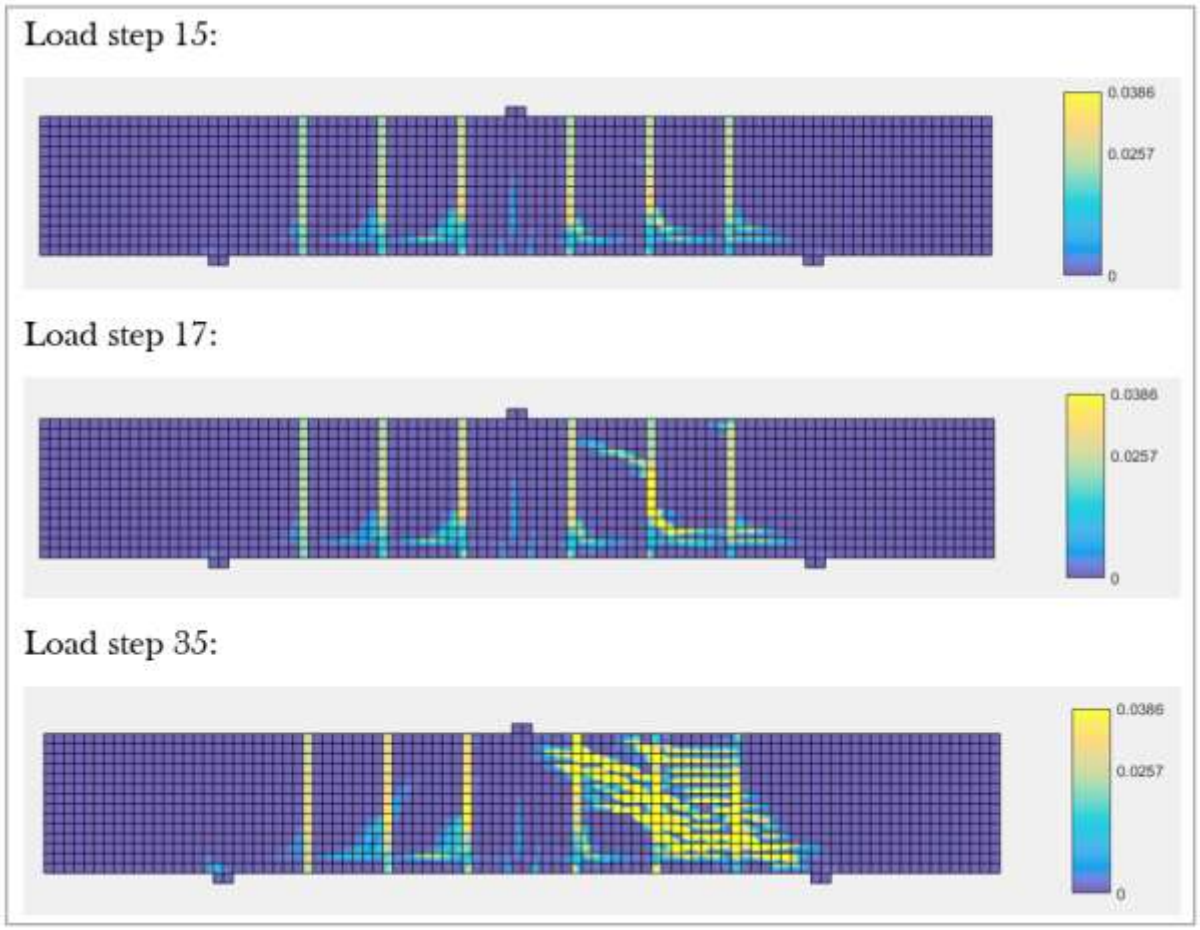

Figure 4. 15 Major principle strains at characteristic load steps for damaged based shear analysis

The Z-shape crack geometries observed in the experiment are captured until load step 36. A plot of reinforcement stresses seen in Figure 4. 16 reveals initiation of yielding for the longitudinal rebars at this step.

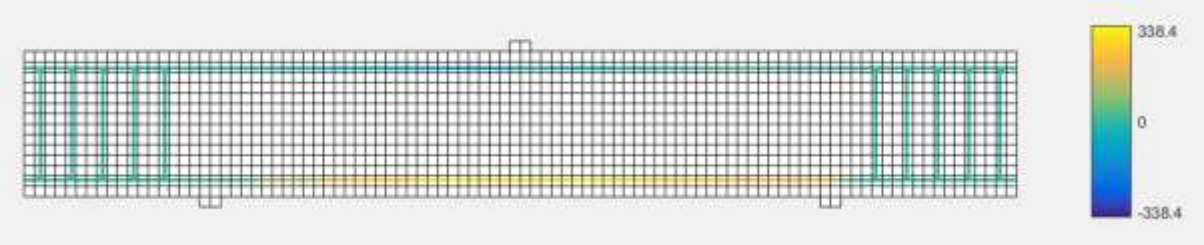

Figure 4. 16 Reinforcement stress at load step 35(10.55 mm) using damaged based shear retention (fy = 338.4N/mm2)

The finite element solution beyond this load step is discarded as numerical failure of the analysis is observed which is marked spurious deformations of a row of elements. This is responsible for the sudden drop observed in the load vs displacement curve. Assuming the solution valid until step 35, a computational shear capacity of around 240 KN at a displacement of 10.5mm is obtained using a damaged based shear retention factor.

4. 3 Experiment 2: Investigation of vmin based on experimental research [5]

4.3. 1 Description of the experiment

This experimental programme consists of a number of tests conducted on RC beams of varying depth, reinforcement ratio, boundary and loading conditions to assess the shear capacity. Two specimens with the same geometry and material properties from a small series of tests from this programme were selected for computational analysis. These will be referred to as specimen1 and specimen2. The geometry, support and loading conditions of the specimens can be seen in Figure 4. 17. The reinforcement layout is seen in Figure 4. 18.

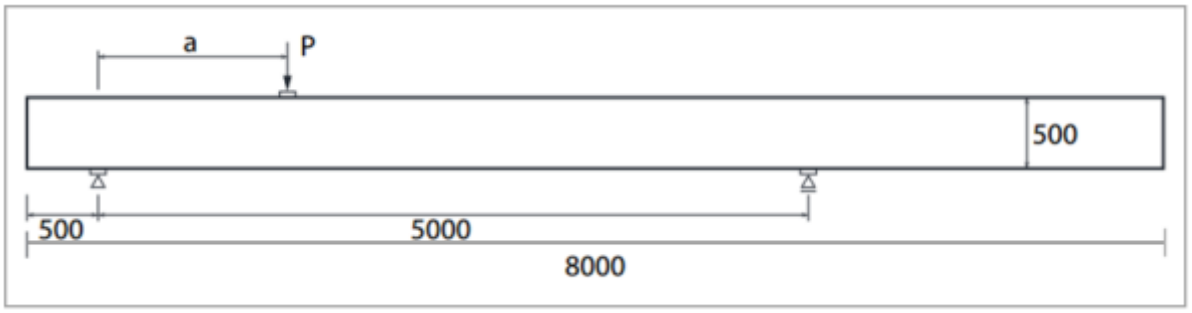

Figure 4. 17 Geometry, support and loading conditions for specimens from experiment 2(Unit: mm) [5]

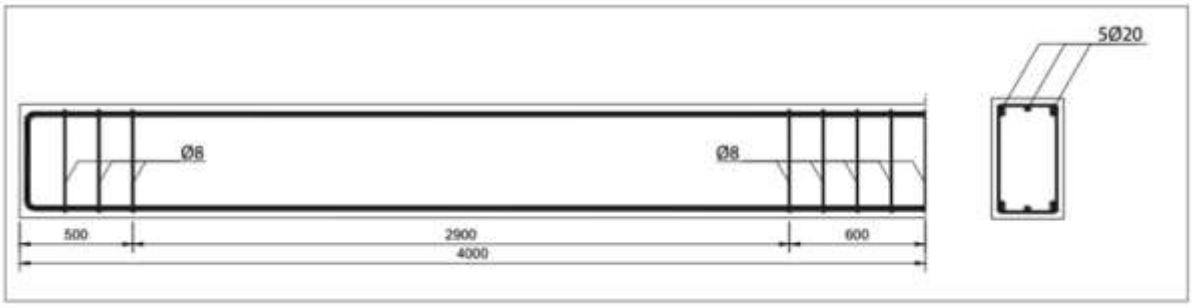

Figure 4. 18 Reinforcement layout for specimen from experiment 2(Unit: mm) [5]

The test consists of two phases:

- **Phase 1:**

  In this phase, the distance 'a' as seen in Figure 4. 17 is set to 2000mm for specimen1 and 1250mm for specimen2 and the beam is loaded in until failure. A flexure failure mode is obtained at the end of phase1 for both specimens. Images of the crack pattern around the loading point for specimen1 and specimen2 can be seen in Figure 4. 19 and Figure 4. 20.

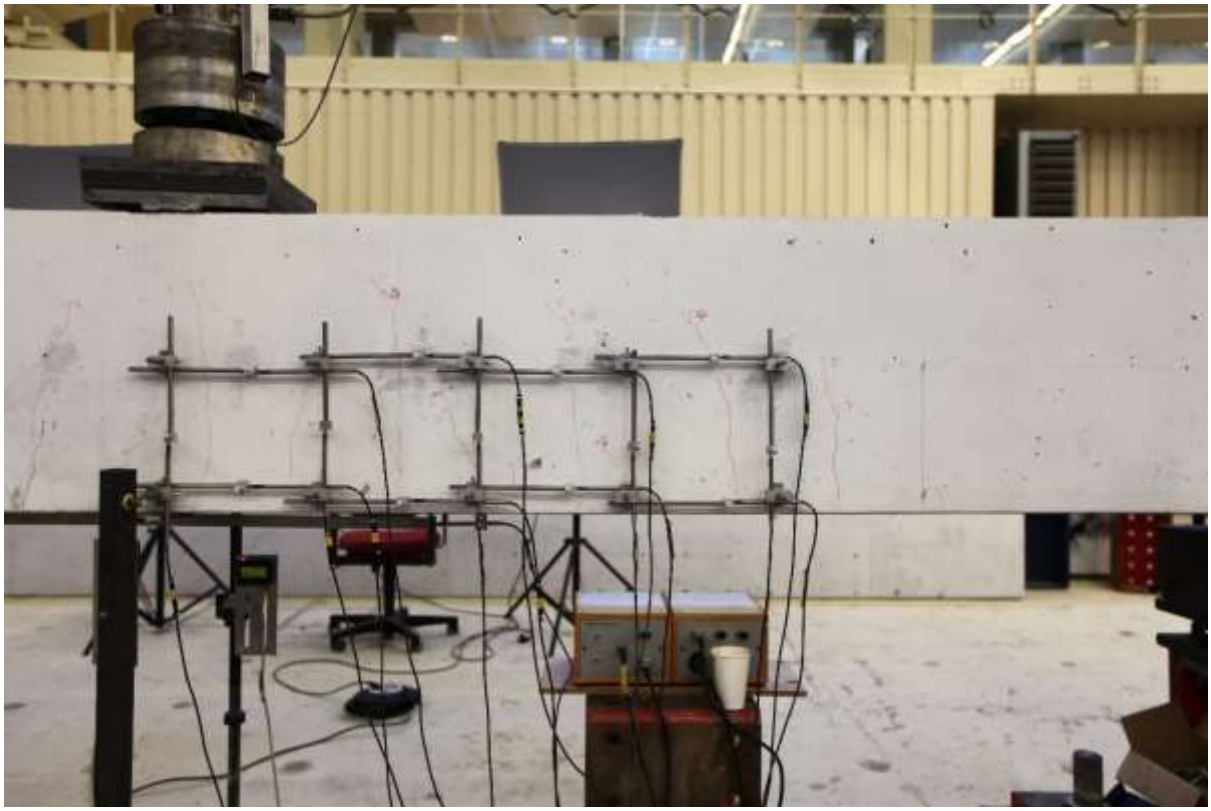

Figure 4. 19 Crack pattern at the end of phase 1 for specimen1(Back end of the specimen) [5]

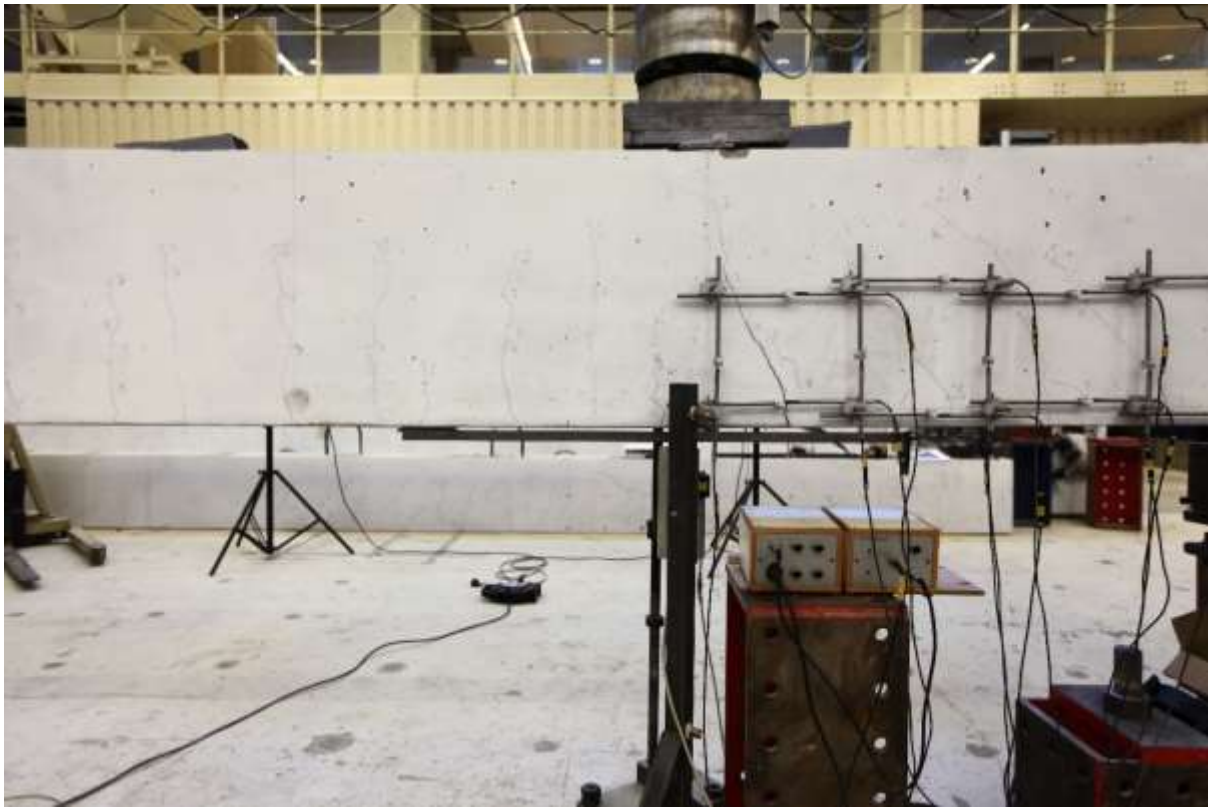

Figure 4. 20 Crack pattern at the end of phase 1 for specimen2(Back end of the specimen) [5]

❖ **Phase 2:**

In this phase the distance 'a' is set to 1250mm for specimen1 and 1000mm for specimen2. Specimen1 is strengthened between the previous loading point and the far support using metal strips glued with pleximon and pre-stressed on two places. The beams were then loaded until failure. Shear failure due to propagation of a newly formed diagonal crack is observed in specimen1, whereas flexural failure is observed for specimen2. An image of the failure crack pattern and the force vs displacement curve for specimen1 and specimen2 can be seen in Figure 4. 21 and Figure 4. 22 respectively.

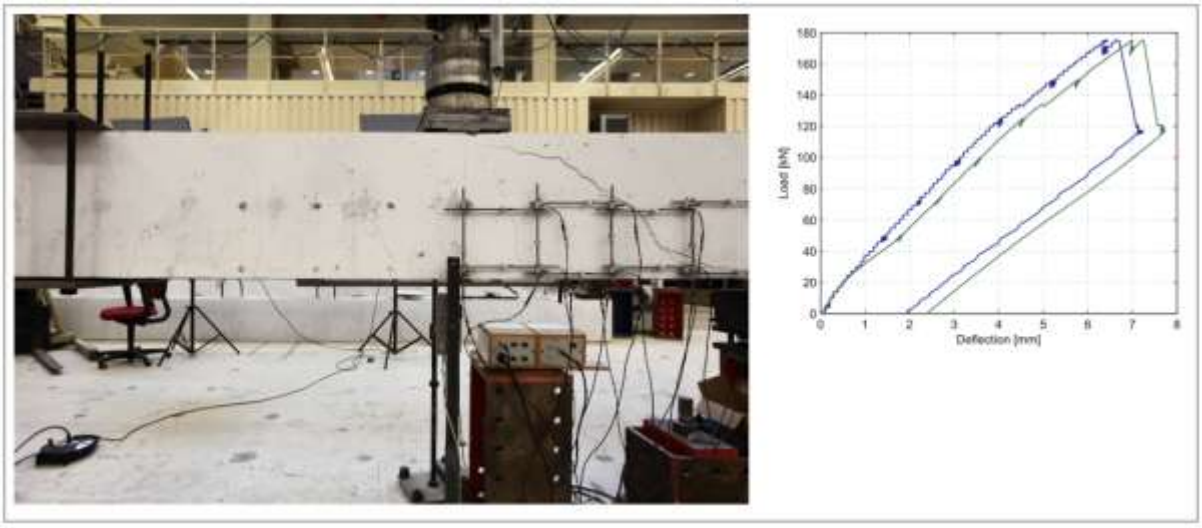

Figure 4. 21 Crack pattern and load deflection curve at the end of phase 2 for specimen1(Back end of the specimen) [5]

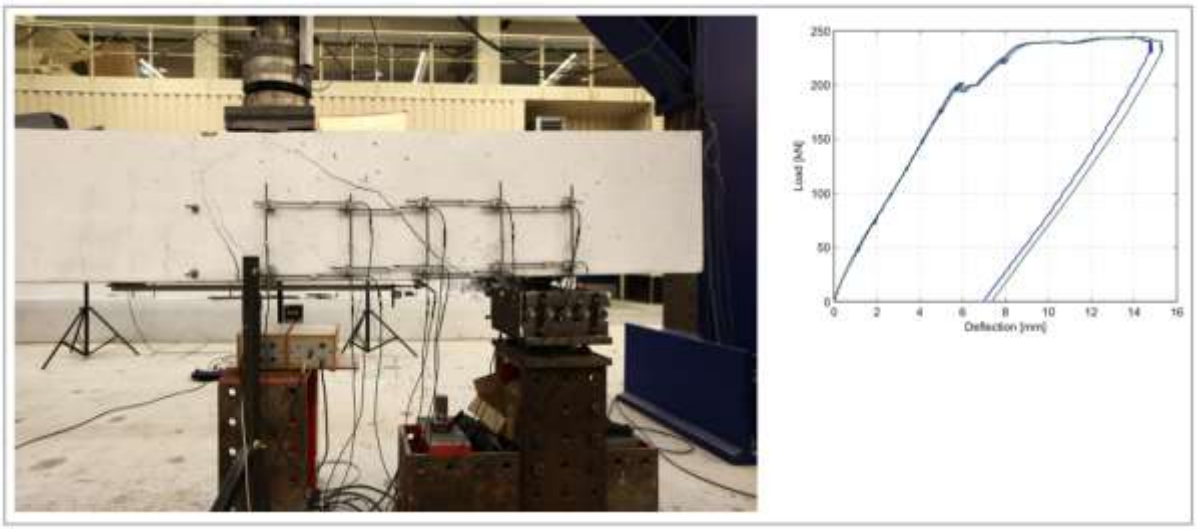

Figure 4. 22 Crack pattern and load deflection curve at the end of phase 2 for specimen2(Back end of the specimen) [5]

4.3. 2 Finite element modelling

The specimens were treated as damaged at the end of phase 1. Phase 2 was modelled with the damage from phase 1 as input.

The experimental report mentions C65 as the concrete class and plain steel bars with a yield strength of 250 N/mm^2 as the reinforcement class of the specimens. A characteristic compressive strength value(f_{ck}) of 65N/mm^2 was assumed for concrete and characteristic yield value of 250 N/mm^2 was assumed for reinforcement. Material properties for concrete and reinforcement were calculated from these values using guidelines for nonlinear finite element analysis of concrete structures [23]. The tensile strength was calculated using the formula for $f_{ck} > 40$, given in the fib model code [29].

The calculated material properties and assumed finite element parameters are seen in Table 4. 1.

Thickness(t)	300 mm
Young's modulus(E)	41707 N/mm^2
Poisson's ratio(ν)	0.15 (Damaged based)
Compressive strength (f_c)	73 N/mm^2
Tensile strength(f_t)	4.17 N/mm^2
Compressive fracture energy(G_c)	39.51 N/mm
Tensile fracture energy(G_f)	0.158 N/mm
Element size	50 mm
Crack bandwidth(h)	50 mm
Crack orientation	Fixed
Tensile behaviour	Hordijk tension softening
Compressive behaviour	Parabolic softening
Shear behaviour after cracking	Constant (β=0.01)
Element type	CQ16M
Integration scheme	4-point Gauss
Convergence criteria	Displacement norm: 1e-3 mm Force norm: 1e-6 mm
Maximum no. of iterations	50
Yield stress for reinforcement (fy)	250 N/mm^2
Young's modulus for reinf. (Es)	200000 N/mm^2
Hardening modulus for reinf. (Eh)	4000 N/mm^2

Table 4. 1 Material properties for concrete and reinforcement for computational analysis of phase 2

Since specimen1 was strengthened between the old loading point and the far support, the cracks in the strengthened part (not visible in Figure 4. 19) were not considered as pre-damage. For specimen2 all cracks visible in Figure 4. 20 were considered as pre-damage. Image analysis was used as a means to estimate damage data for the finite element mesh. A binary image of the crack pattern of the damaged region was developed by estimating the crack trajectories from the original image. The binary image was then covered with a grid of box size 50. The direction of the best fit line for black pixel points inside a box was considered as the direction of damage for the box. The process is shown schematically in

Figure 4. 23. The damage data was then mapped onto the finite element mesh. The obtained direction of each box, was thus used as direction of damage θ for the elements. Damage was assumed to be purely tensile. d_{nt} was set to 1 for all damaged elements keeping other variables to 0. A total displacement of 15 mm was prescribed at the loading point in 30 steps of 0.5mm for specimen1. Total displacement of 20mm was prescribed for specimen2 in steps of 0.5mm. The major principal strain plotted over the finite element mesh at the load step 1 for specimen1 and specimen 2 can be seen in Figure 4. 24 and Figure 4. 25 respectively.

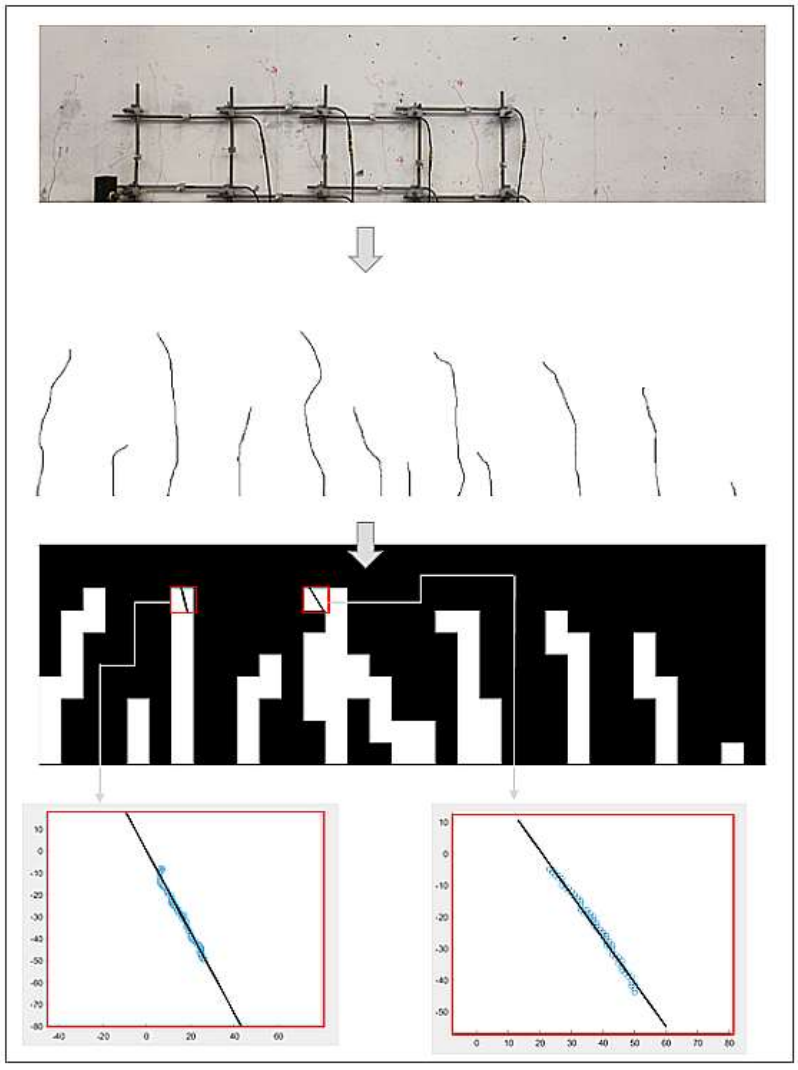

Figure 4. 23 Estimation of crack trajectories using image analysis

Figure 4. 24 Major Principal strain over Finite element mesh at load step 1(0.5mm) for specimen1

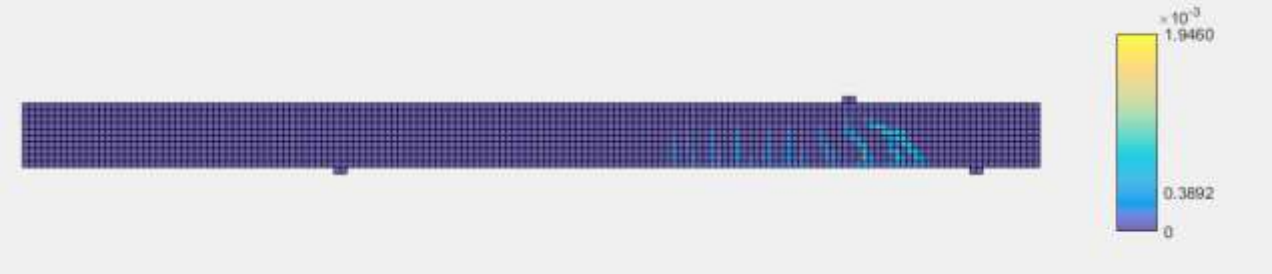

Figure 4. 25 Major principal strain over Finite element mesh at load step 1(0.5mm) for specimen2

4.3. 3 Results and discussion

Comparative force vs displacement curves for both specimens can be seen in Figure 4. 26.

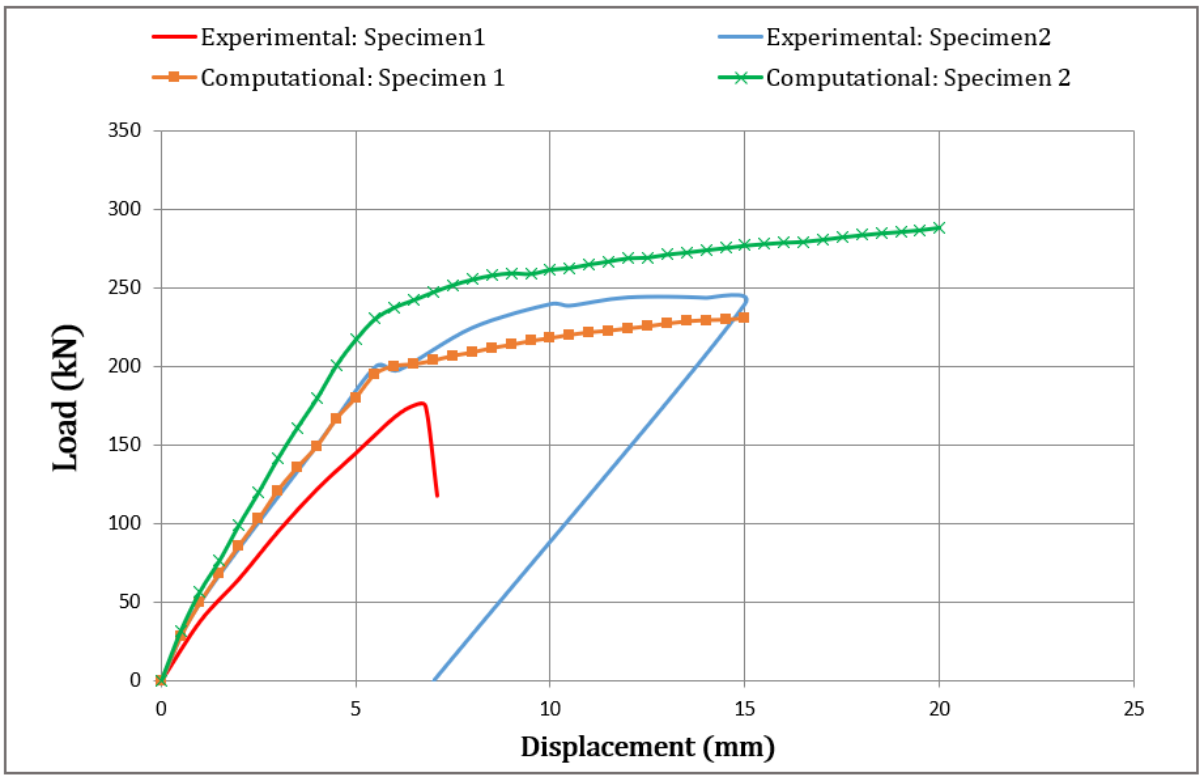

Figure 4. 26 Comparative Force vs displacement curve for specimen1 and specimen 2

Over-prediction of stiffness is observed for both specimens. To explore the computational behaviour further, major principal strains are plotted to visualise the evolution of the crack patterns. The strain plots for specimen 1 can be seen in Figure 4. 27.

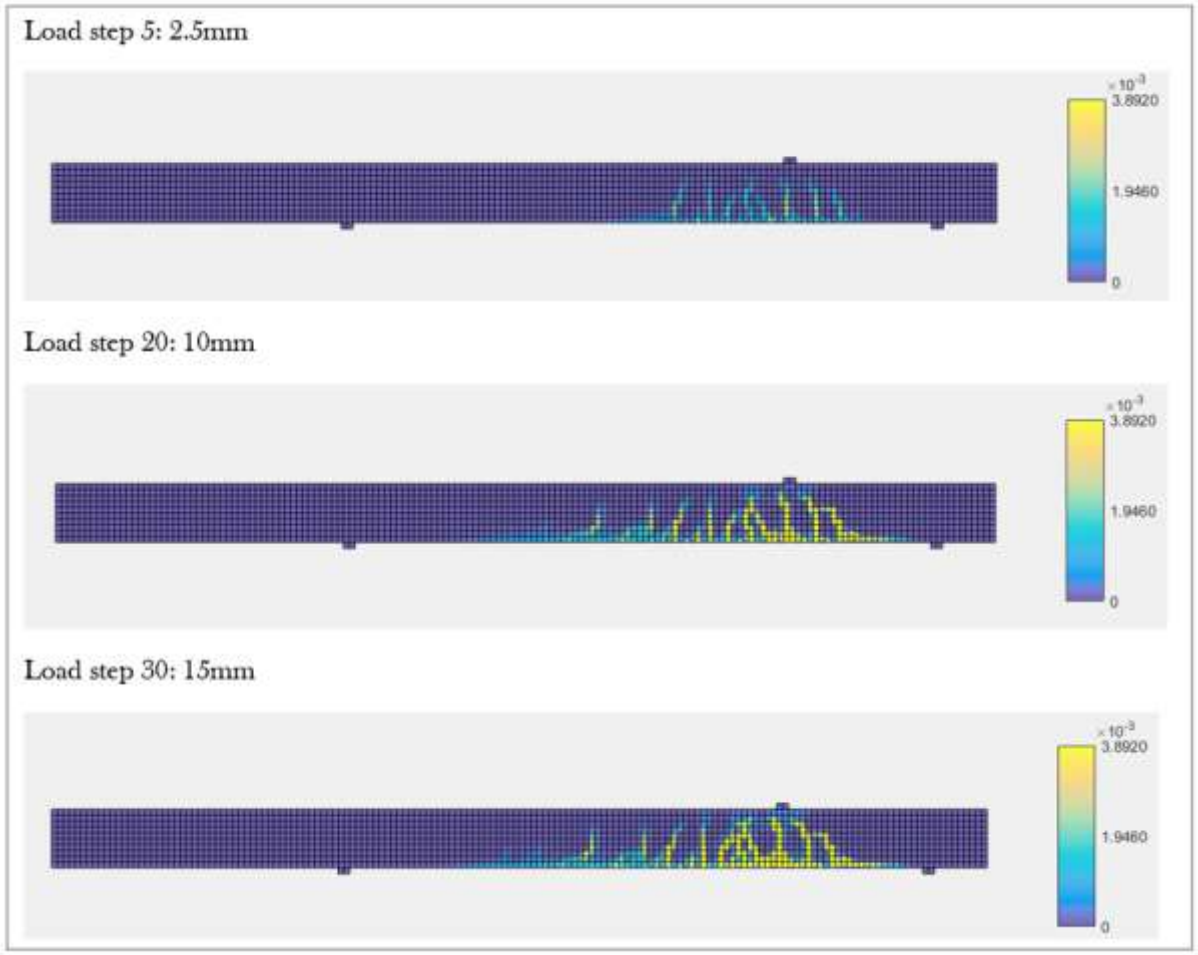

Figure 4. 27 Major principal strains at characteristic load steps for specimen1

As seen in Figure 4. 25 strain localises in the already existing damage and the cracks widen as the load goes on increasing. Reinforcement yielding is initiated at load step 12. The plot of reinforcement stresses is seen in Figure 4. 28

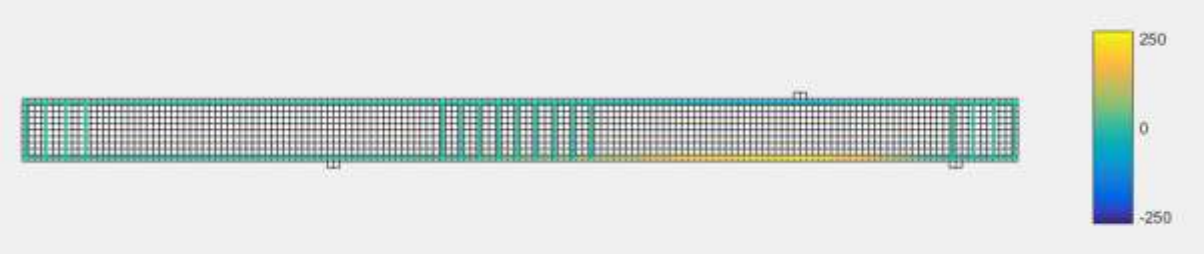

Figure 4. 28 Stresses in reinforcement at load step 12 (6mm) for specimen 1(fy = 250n/mm2)

This is the point after which the computational force-displacement curve shows a plateau. Considering 0.5% allowable strain in the reinforcement, the ultimate stress value is observed at load step 18, which corresponds to a displacement of 9mm. A load capacity of 220KN could be estimated assuming failure due to breaking of the longitudinal reinforcement. This however is

not in agreement with the experimental observations, in which sudden failure occurs due propagation of a new diagonal crack joining the loading point and the near support. As seen in Figure 4. 27, formation of new diagonal cracks between the loading point and the near support is not predicted by the finite element solution until the final load step.

The principal strain plots for specimen2 can be seen in Figure 4. 29

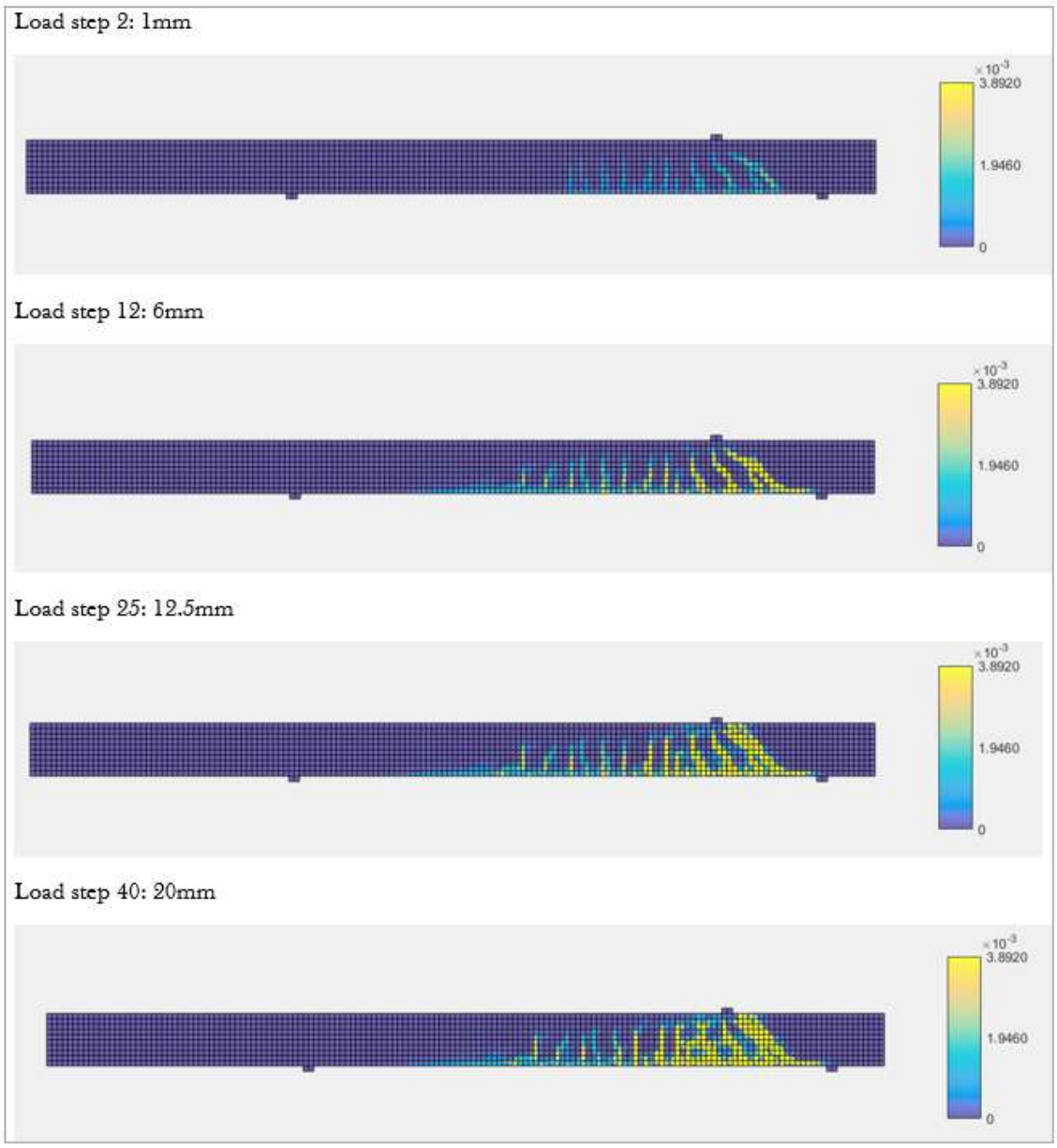

Figure 4. 29 Major principal strains at characteristic load steps for specimen2

It can be observed that strain localises in the already damaged elements. Propagation of the right most existing crack is observed as the load goes on increasing. This is in good agreement with the experimentally observed failure crack pattern. Reinforcement yielding is initiated at load step 12, which corresponds to a displacement of 6mm. A plot for reinforcement stresses can be seen in Figure 4. 30

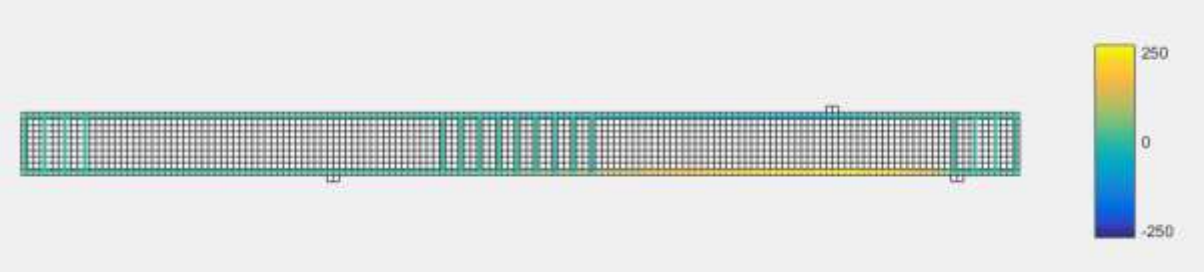

Figure 4. 30 Stresses in reinforcement at load step 12 (6mm) for specimen 2 (fy = 250n/mm2)

Ultimate stresses value assuming 0.5% allowable strain is attained at load step 16, which corresponds to a displacement of 8mm and a load of around 255KN. The capacity is in reasonable agreement with the experimental observations.

4.3. 4 Sensitivity study

A number of sensitivity studies were performed in order to examine the influence of the damage input parameters in the prediction of the structural response. The modelling strategy and the results obtained for specimen1 and specimen2 in the previous section are treated as reference analyses for comparison.

First, in order to study the impact of the pre-damage input itself, an undamaged analysis was performed by removing the damage inputs from the reference analysis of specimen1. Comparative force vs. displacement curves can be seen in Figure 4. 31.

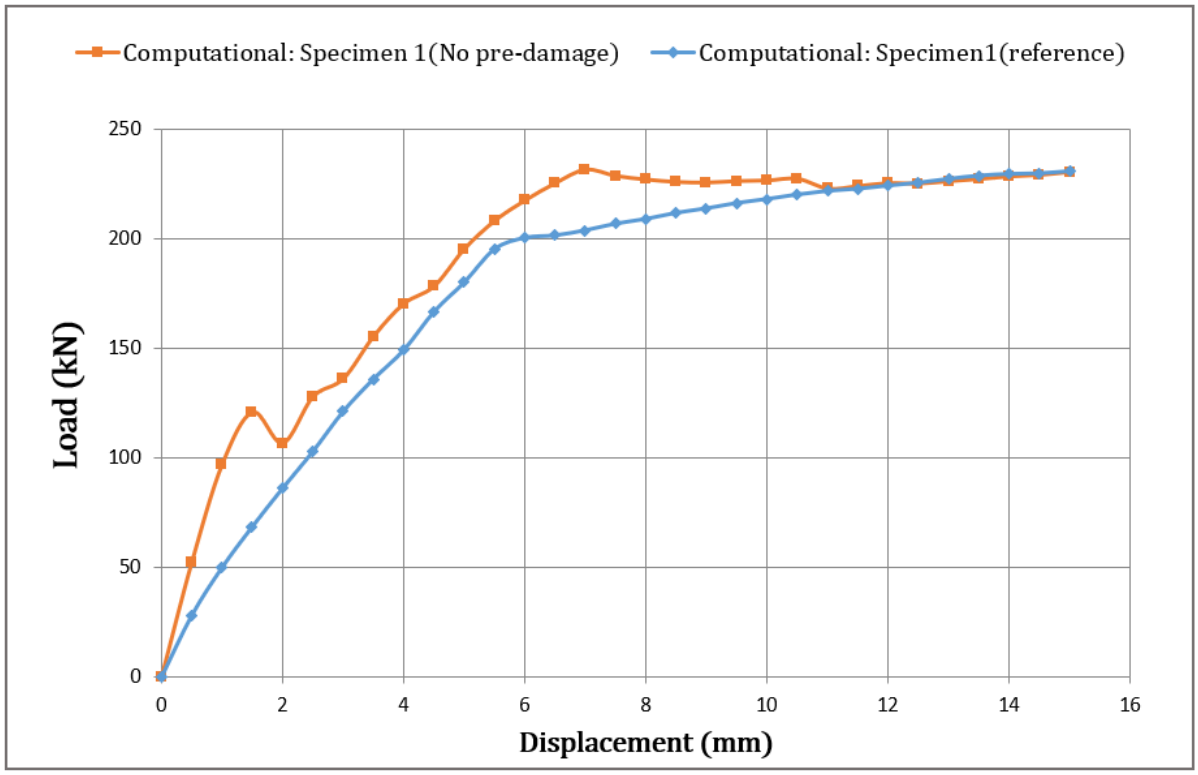

Figure 4. 31 Force vs displacement curve for specimen 1 with and without pre-damage

Reduction in the initial stiffness due to pre-damage input can be observed in the figure. Additionally, a delayed initiation of yielding of longitudinal reinforcement can be inferred.

To study the sensitivity of tensile damage input parameters d_{nt} and d_{tt} and the direction of damage input θ, two analyses were performed with the following variations from the reference analysis:

1. $d_{nt} = 1$, $d_{tt} = 0$ and $\theta = 0$
2. $d_{nt} = 1$, $d_{tt} = 1$ and $\theta = 0$

Comparative force vs displacement curves for specimen 1 and specimen 2 can be seen in Figure 4. 32 and Figure 4. 33 respectively.

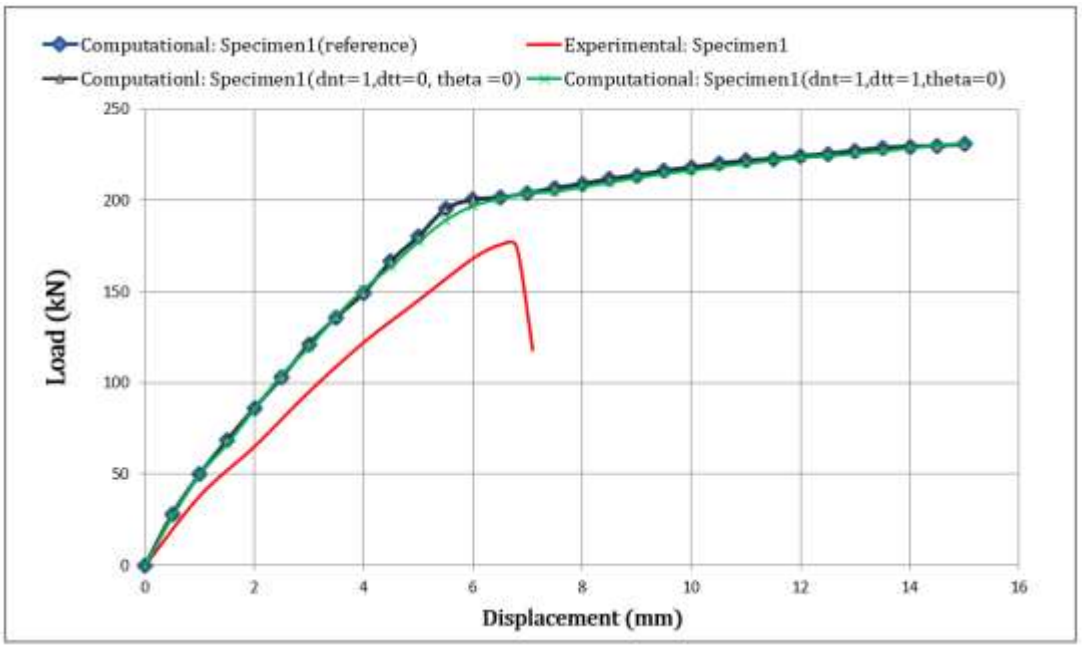

Figure 4. 32 Force vs displacement curves for input parameter sensitivity study (specimen 1)

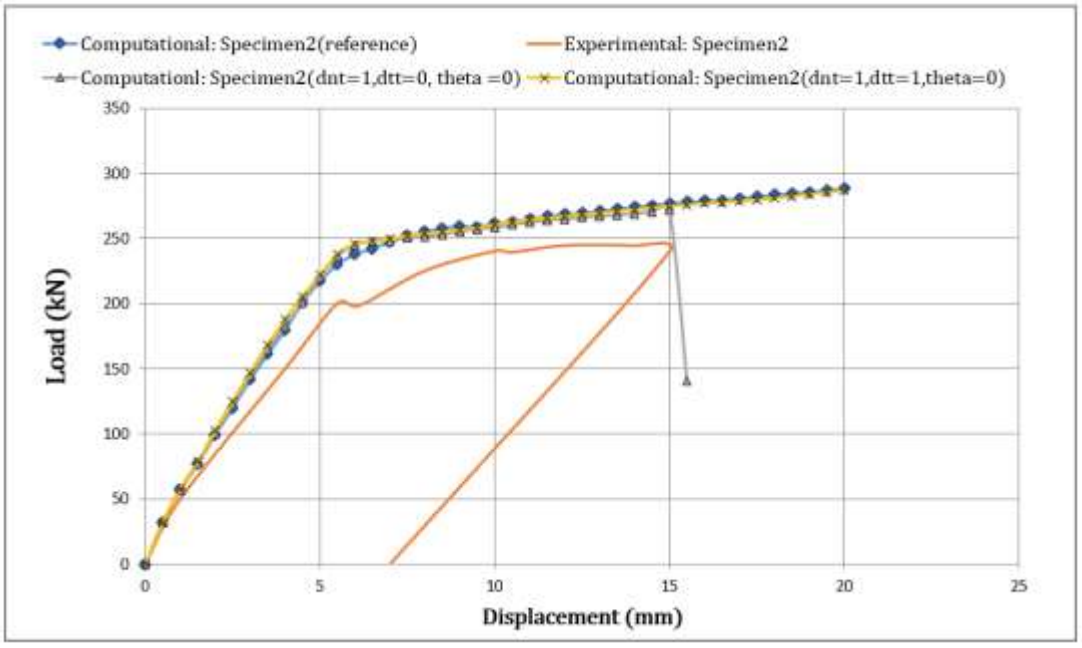

Figure 4. 33 Force vs displacement curves for input parameter sensitivity study (specimen 2)

No significant influence due to inclusion of direction of damage can be inferred from the plots.

A preliminary test was carried out using the damage zone input discussed in chapter 2, by considering the parts of the specimens visible in Figure 4. 19 and Figure 4. 20 as damaged zones. A trial damage input of d_{nt} = 0.5, d_{tt} = 0.5 was set. For the direction of damage, θ = 0 was set initially and the orientation of the nt-axes system for an element was fixed upon the first rotation. A total displacement of 20 mm was prescribed in 80 steps of 0.25mm. All other parameters were kept unchanged from the reference analyses. Comparative force vs displacement curve for specimen1 can be seen Figure 4. 34.

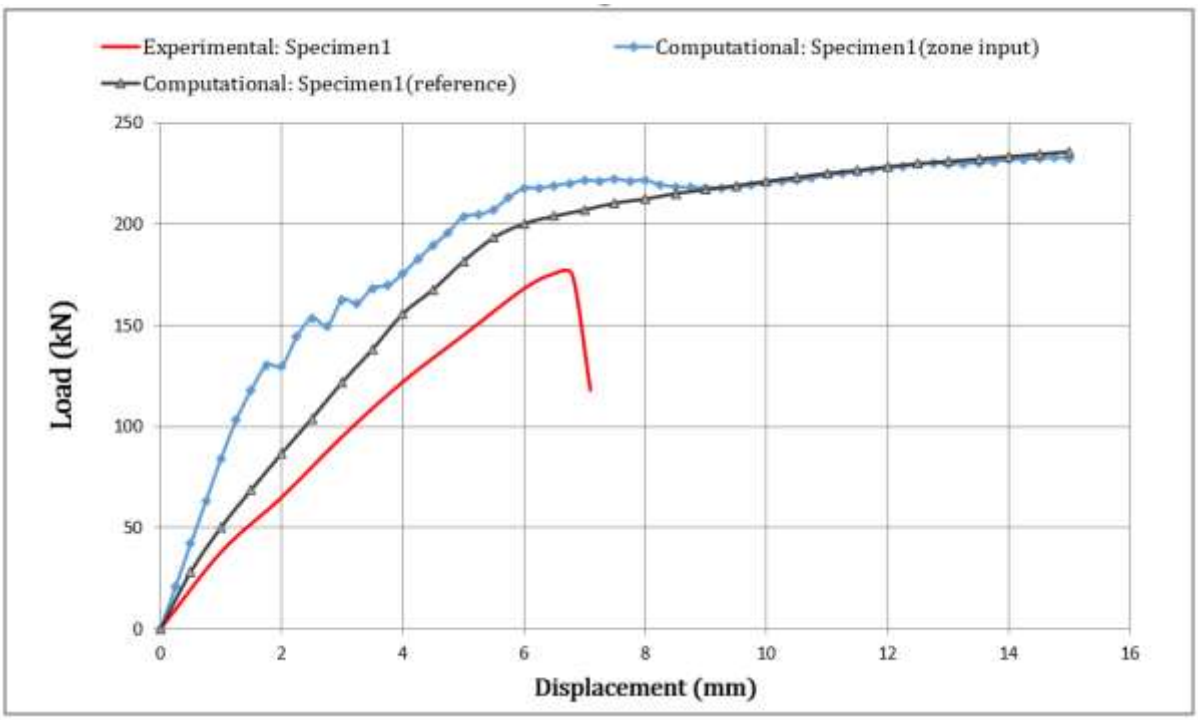

Figure 4. 34 Force vs displacement curves for Damage zone input test(Specimen1)

Stiffer initial response than the reference analysis can be observed. The solution returns to the path of the reference analysis at a displacement of 9mm. The crack pattern at this step in the respective analysis is compared by plotting major principal strains in Figure 4. 35.

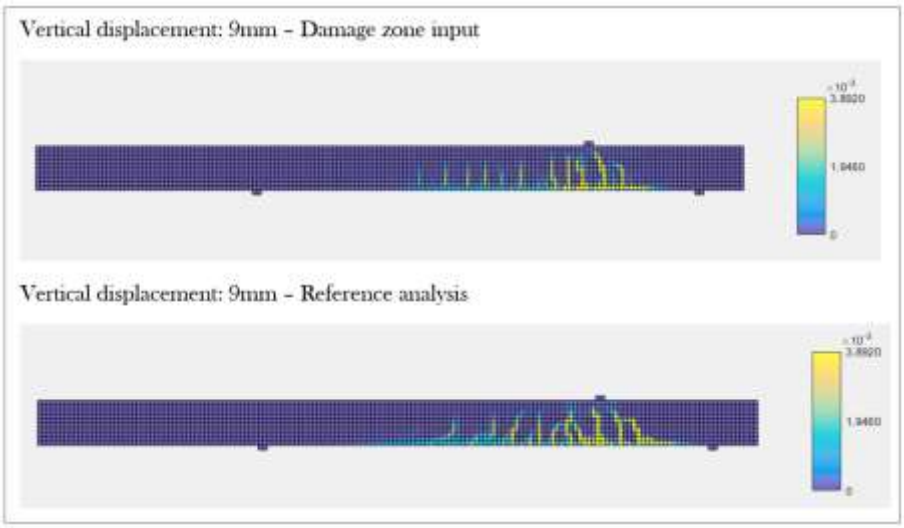

Figure 4. 35 Crack pattern at merging point in the force displacement curve (Specimen1)

Some similarity can be inferred from the comparison. Initiation of reinforcement yielding takes places at a vertical displacement of 6mm for both analyses.

Similar observations can be made for specimen2. The initial part of the curve is characterised by a stiffer response than the reference analysis and the force displacement curves merge at a displacement of 7.5mm giving comparable localisation of strain. The force vs displacement curve and crack pattern comparison at a displacement of 7.5mm for specimen 2 can be seen in Figure 4. 36 and Figure 4. 37 respectively.

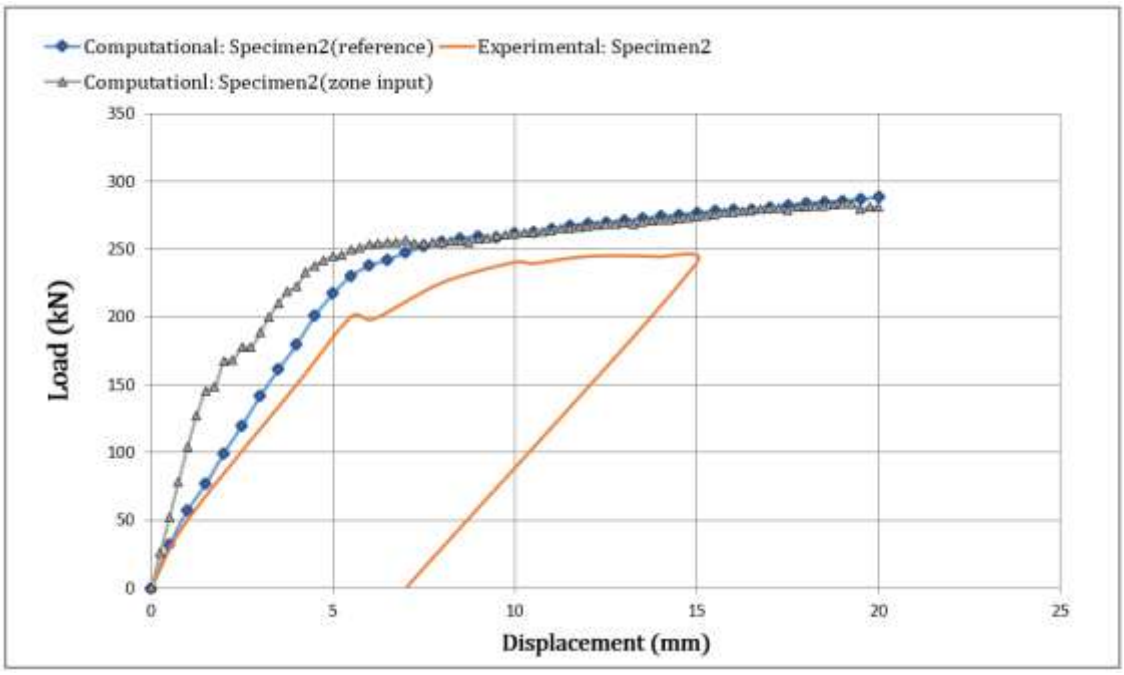

Figure 4. 36 Force vs displacement curves for Damage zone input test(Specimen2)

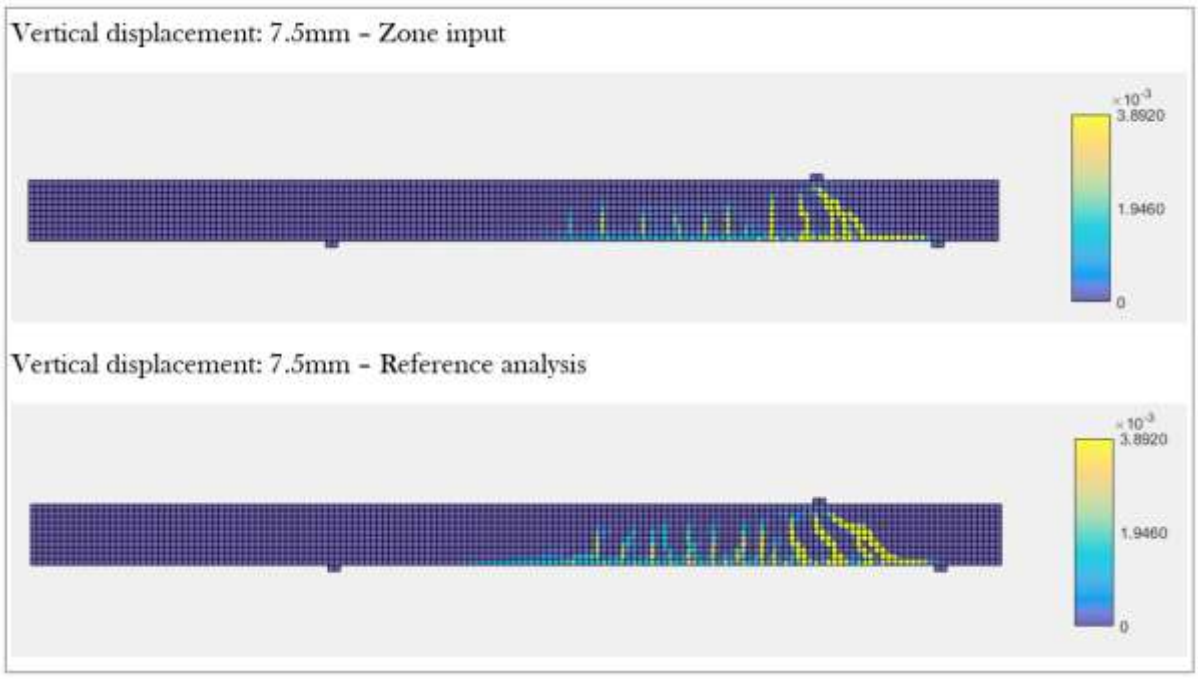

Figure 4. 37 Crack pattern at merging point in the force displacement curve (Specimen2)

In order to compare the adopted modelling strategy with a conventional method for modelling pre-damage in RC structures, the reference analysis of specimen 1 was compared with results from phased analysis performed using DIANA. The finite element mesh for phased analysis can be seen in Figure 4. 38

Figure 4. 38 Finite element mesh for phased analysis (Specimen1)

The is load applied in two phases as in the experimental procedure. In phase1, loading point 1(marked P1 in Figure 4. 38) was prescribed a total downward displacement of 10 mm in 20 steps of 0.5mm. The same loading point was then unloaded with 12 steps of -0.5mm. The crack pattern at the end of phase1 can be seen in Figure 4. 39

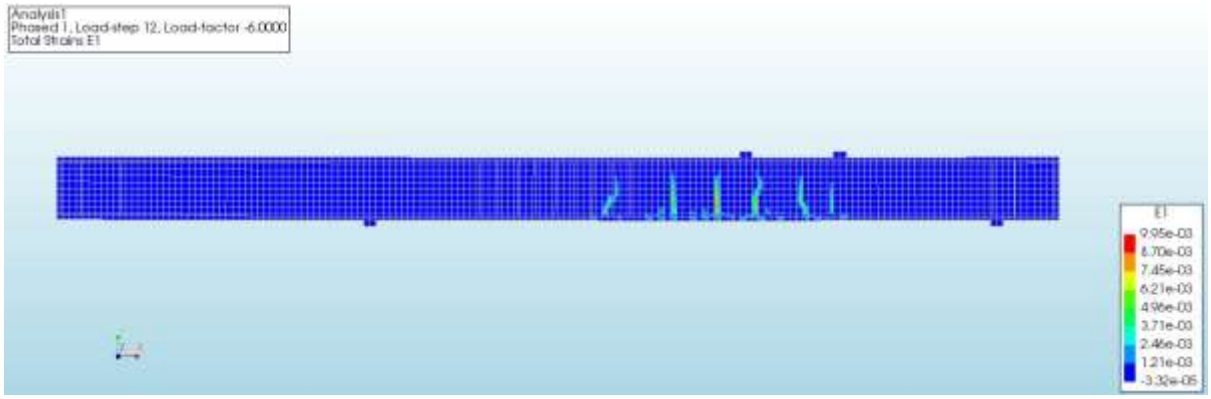

Figure 4. 39 Crack pattern at the end of loading phase1 (Computational Specimen1)

Fair agreement can be seen with the experimental pattern at the end of this phase seen in Figure 4. 40

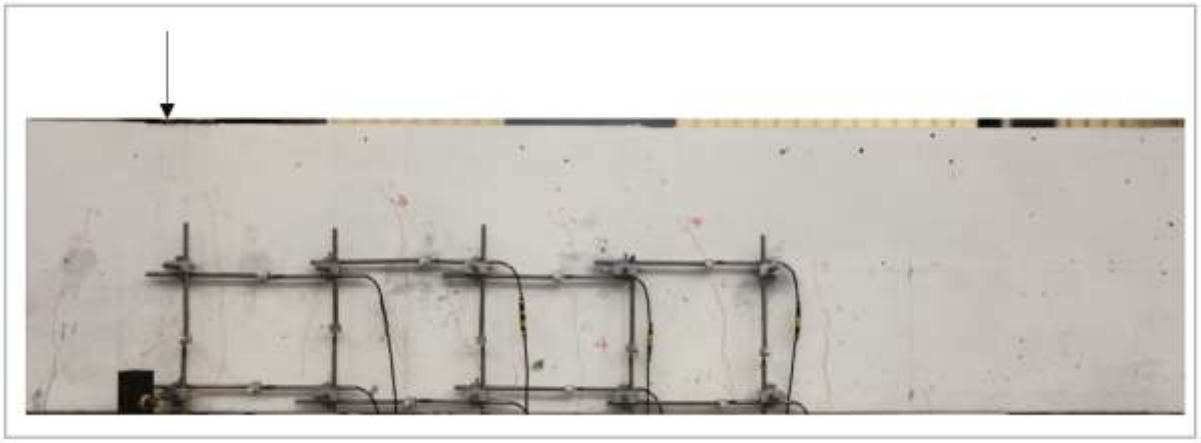

Figure 4. 40 Crack pattern at the end of loading phase1 (Experimental Specimen1)

In phase 2, a total displacement of 15mm was prescribed to loading point 2 in 30 steps of 0.5mm. Comparative load vs displacement curves can be seen in Figure 4. 41

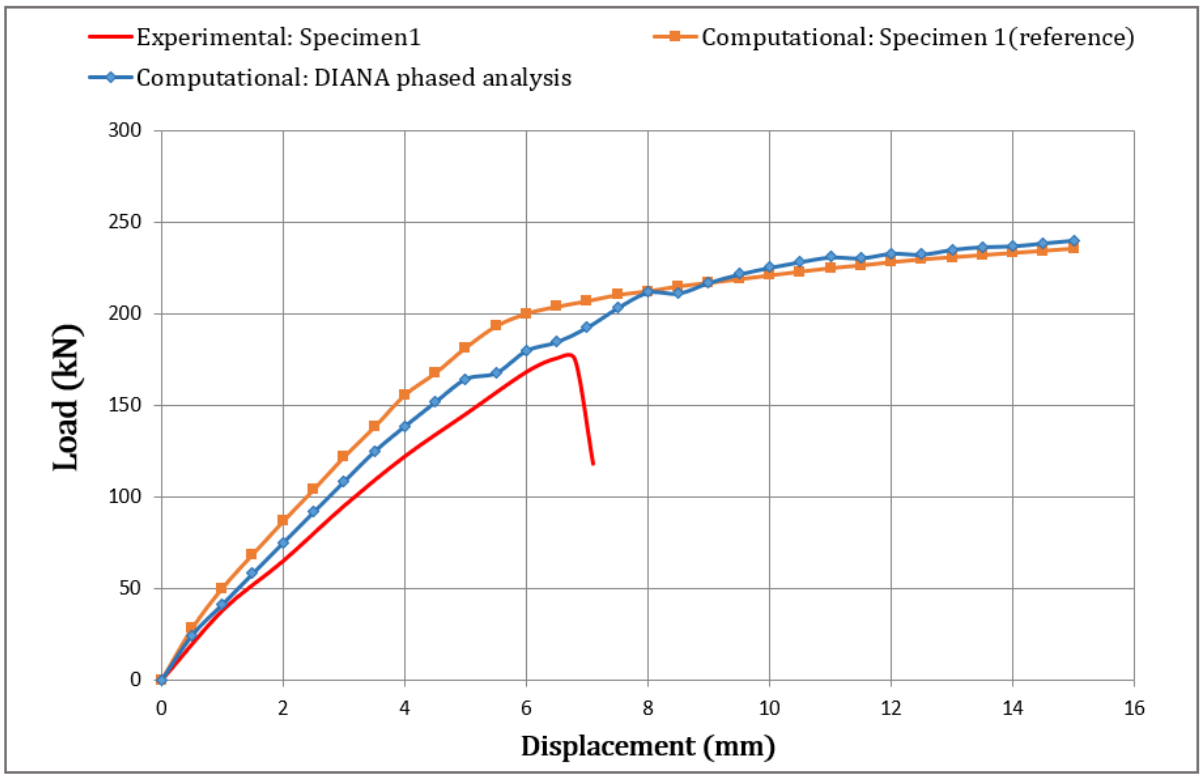

Figure 4. 41 Force vs displacement comparison with phased analysis approach

A better prediction of initial stiffness is observed for phased analysis compared to the computational reference solution. The two curves converge to a more or less similar path after a displacement of 8mm. Plot of reinforcement stresses at a displacement of 9.5mm for phased analysis shows initiation of reinforcement yielding.

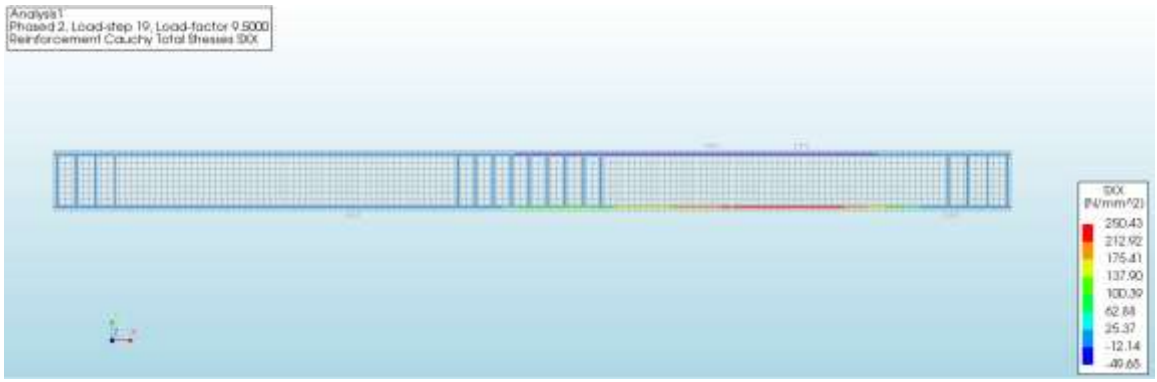

Figure 4. 42 Reinforcement stresses at displacement of 9.5mm for phase2 of DIANA phased analysis

A comparison of the experimental failure crack pattern and major principal strains at the final load step for both approaches can be seen in Figure 4. 43. Both computational analyses exhibit similarity in crack pattern, however neither is in agreement diagonal shear failure mode observed in the experiment.

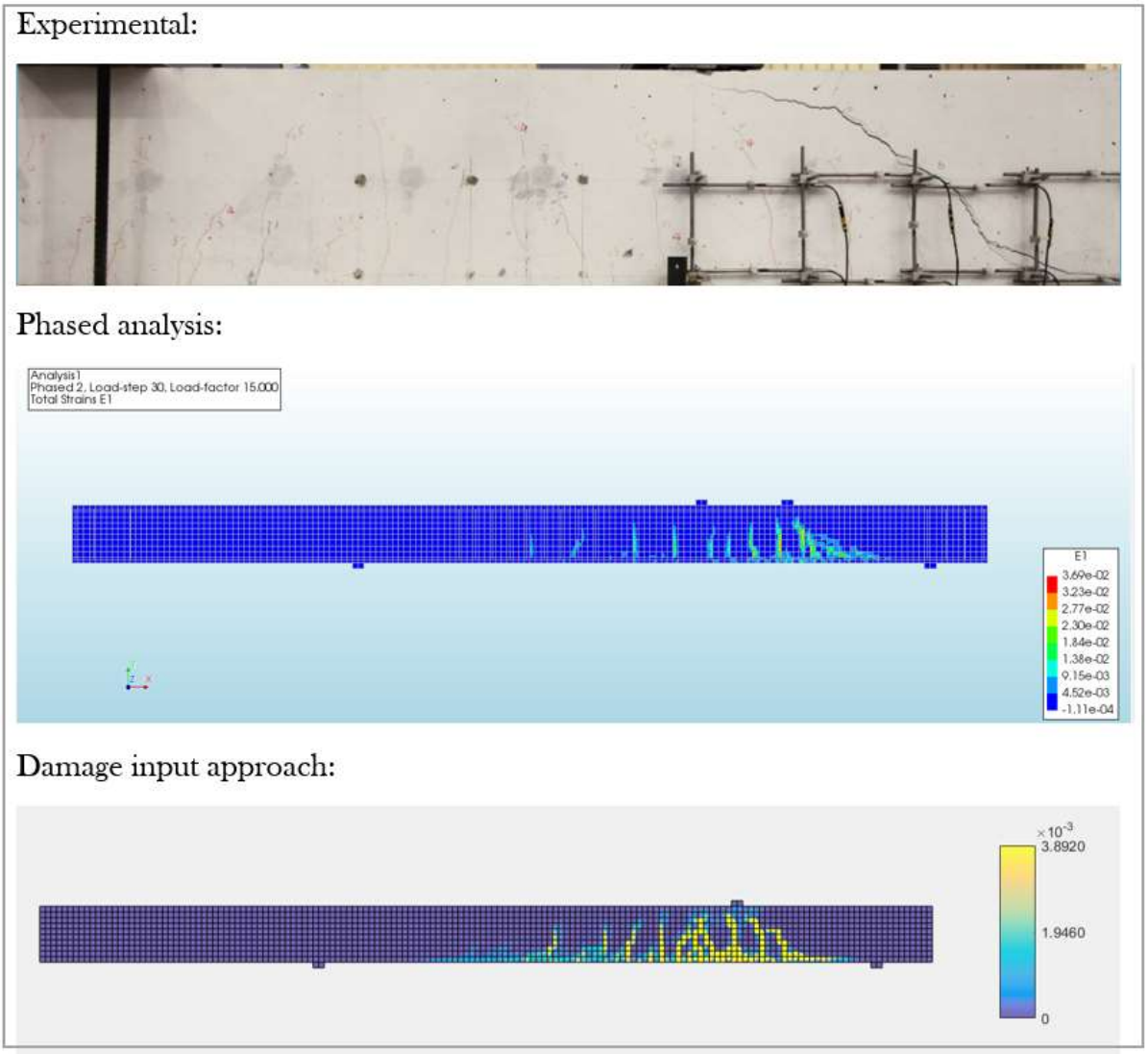

Figure 4. 43 Comparison of experimental failure crack pattern with computational analyses

4.4. Discussion

The implemented material model was used to simulate two experiments on pre-damaged RC structural members. The modelling strategy discussed in the previous chapters was tested via a number of sensitivity studies. Inclusion of pre-damage variables in the analysis resulted in impacts on structural response like reduction of stiffness and alteration of capacity and failure modes. However, a clear sign of ultimate failure was generally not obtained in the computational analyses. The point where longitudinal reinforcements break, was estimated as the ultimate capacity. Separate discussion for each experiment follows next:

❖ Experiment 1: Influence of vertical pre-cracking on reinforced concrete in shear [4]

The existing damage and newly formed cracks interact resulting into a drastic alteration of the structural response. The shear sliding along existing cracks play a vital role in determining the final failure crack pattern. Although, the specimen is a somewhat unrealistic case of pre-damage, its peculiar and unexpected failure mode underlines the importance of accounting for existing

concrete damage in structural analysis. With assumptions of perfectly vertical global and local cracking (θ=0), full element damage in the normal direction(d_{nt}=1) and no element damage in the tangential direction(d_{tt}=0), the essential features of this experiment were captured reasonably well by the finite element solution. The same shear model was used for both damaged and undamaged elements. A comparison of constant shear retention (beta = 0.01) and damaged based shear retention (minimum beta = 0.005) shows that, the point of interaction of pre-damage and new cracks is delayed in the analysis using damaged based shear retention. Before, this point however a better estimate of stiffness of the specimen is obtained. Use of an appropriate shear model for pre-damage is still an open question. Relative sliding along pre-existing cracks can be influential in determining the failure mode, as seen in the experiment. Use of a low shear retention of 0.01 did provide reasonable solutions to the particular problem, although a more consistent shear model still needs to be sought which accounts for a combined effect of crack-width and crack-tortuosity. Using different shear retention models for damaged and undamaged elements could provide a refined alternative strategy.

Experiment 2: Investigation of vmin based on experimental research [5]

In Experiment 2, more realistic cases of pre-damage were tested. Comparison of analysis with crack-orientation θ and vertical crack-orientation (θ =0) resulted in almost the same solution. This was also observed for comparison between analysis with damage in normal direction versus damage in both normal and tangential direction. In all cases, the crack-trajectories from the image of the specimen were used to assign damaged elements. This suggests that the over-all distribution of damage over the finite element mesh, impacts the analysis more, than the input for local reduction of stiffness and local crack-orientations. Therefore, the damage zone approach could be developed towards more effectively accounting for the over-all distribution of damage over the structure rather than refined inputs for local stiffness loss and crack-orientations. Finally, a comparison with phased analysis approach was conducted, in which good agreement was obtained with the results of the damage-input approach. Thus, it could be a viable alternative, when phased analysis is difficult to perform.

5. Conclusions and recommendations

The research question set in the introductory chapter is discussed here. Conclusions are drawn based on the computational analyses carried out in the previous chapter. The primary assumptions, limitations and applications of the study are reflected upon and recommendations for future research are provided.

5. 1 Research question:

How can the information obtained from visually observed crack patterns in RC structures be included in finite element analyses?

A methodology was set up to account for information obtained from visually observed crack pattern into finite element analysis. The methodology involves three essential components:

1. Image analysis of photos of crack patterns to obtained damage information.
2. Translating the obtained information into input, for a material model for damaged concrete.
3. Carrying out finite element analysis using the material model to obtain structural response.

Two ways of inputting damage were conceived:

1. Single crack input – in which stiffness loss due to damage is evaluated for every single individual crack.
2. Damage zone input – in which stiffness loss due to damage is evaluated over a region of the structure.

The single crack input was tested with an assumption of binary pre-cracking, i.e. an assumption that damage input variables in the material model do not take up values between 0 and 1, the methodology was tested in an orthogonal smeared cracking system for a few experimental specimens. Characteristic impacts of concrete damage, on the structural response were observed in the finite element solutions, along with insightful numerical crack patterns. Correct failure mode and reasonable residual load-carrying capacity was predicted for two out of three specimens. Fair agreement was obtained for a comparative test conducted with the phased analysis approach. Sensitivity studies indicate, that the distribution of the over-all crack pattern has a greater impact on the analysis than the local information about stiffness loss and crack-orientation. Possibilities to drop the assumption of binary cracking were explored by considering extraction of crack-width information from images. The resolution requirements for such an extraction may be unreasonably high. Damage zone input could serve as an alternate strategy to overcome this restriction. A trial analysis using the damage zone input was conducted. A need for further exploration for the calibration of this type of input exists.

5. 2 Outlook towards structural application

As discussed in introductory chapter, a desired characteristic of the investigated modelling approach is, practicality in application to real-life RC structures. The developed methodology assumes surface features to be fully correlated to the internal damage in the structure. This seems to be a reasonable assumption for structural cases where the response can be reliably obtained by performing a 2-d analysis. In real-life structures however, it likely that such a representation is inadmissible and a 3-d representation of the structure is required to obtain a reliable response. Image analysis of the surface crack distribution as a detection technique, cannot provide adequate information for such cases. Therefore, other damage detection techniques, e.g. acoustic tomography could supplement or replace image analysis in the developed method, in order to obtain information on the internal distribution characteristics of damage.

The success of the developed methodology also, relies on the availability of an image which reflects the damage characteristics of the domain under study. In consideration of practical feasibility, this effectively necessitates a scaled high-resolution image of the damaged domain of the structure. This can be a challenge in real-life applications due to large sizes of real structures, different surface textures for different structures and restrictions concerning the visibility of the damaged domain. However, a workable solution can be found by using drones equipped with high-resolution cameras. These could be used to capture multiple pictures from the same range in order to construct an over-all scaled image of the damaged domain, which can be processed for required features.

5. 3 Recommendations for future research

For a practical damage zone input, the complex crack pattern geometries observed on concrete surfaces are required to be captured. This could be a potential application for fractal geometry, as it provides quantitative descriptions of highly complex patterns and processes. Due to its inherent feature of discretising the domain under study into a grid of boxes, multifractal analysis can provide a scale invariant link between the measure of damage and the finite element mesh. Literature indicates correlations between the multifractal measures of surface crack pattern and the mechanical properties of the RC structure. A deeper understating of these correlations along with image-resolution requirements to be able to capture the multifractal distribution of crack patterns could be obtained through new experimental setups. This could lay the foundation for linking the multifractal measures to the damage variables in a concrete material model. A study utilising the developed methodology with varying element sizes could provide further insight into its limit/scope of application. It could also, help in deciding the suitability of either inputs for different scenarios of pre-damage. The methodology could be extended to incorporate effects of other type of concrete damage mechanisms, e.g. alkali-silica reaction, which exhibit distinct surface features.

Appendix A

A. 1 Introduction

Finite element method is a numerical technique used to solve partial differential equations. The displacement-based version of the method can be used to solve the equilibrium equations of continuous bodies by transforming it to virtual work equations. The geometry of the structure is discretised into a finite number of elements for which the nodal displacements are considered to be the fundamental unknowns. A relation between the nodal forces and displacements can be derived via a constitutive relationship between stresses and strains, which is assumed to be a material property. An appropriate assembly of the elements and application of boundary conditions gives rise to a system of equations which describes the equilibrium of the structure. These equations can then be solved using an appropriate solution technique in order to calculate the displacement of the entire structure. Under this framework many constitutive models exist which can be used to simulate the highly non-linear behaviour of RC structures. These can be based on experiments or can be idealised stress-strain curves. The formulation of these models can vary depending on the phenomena to be modelled and the required degree of sophistication. This appendix describes formulations based on total strains. The parameters used to describe the behaviour of concrete are briefly discussed. Following that, different concepts within this formulation to numerically model cracking are discussed, with emphasis on smeared cracking, which serves as a point of departure for the proposed model.

A. 2 Total strain based formulation

In a total strain based formulation, an injective relationship is assumed between stress **σ** and strain **ε** [20]. Figure A. 1 shows a typical qualitative example for uniaxial tension and compression for reinforced concrete.

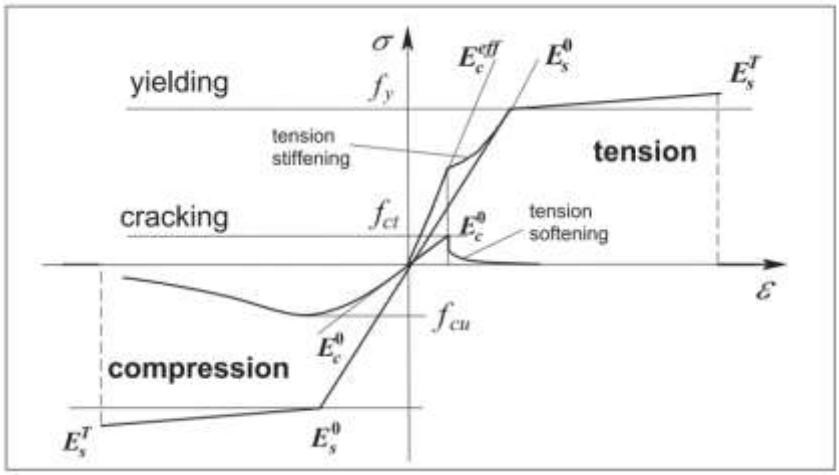

Figure A. 1 Qualitative material model for RC [2]

In tension, the point at which concrete reaches its tensile strength (f_{ct}) signifies the onslaught of cracking. Before this point, concrete is assumed to be a linear elastic material and its behaviour is governed by the Young's modulus (E) and Poisson's ratio(ν). After cracking, the material is assumed to soften gradually and the initial stiffness of concrete ($E = E_c^0$) decreases with increasing strain. Similar behaviour can be assumed in compression, where the concrete begins to soften after reaching its compressive strength (f_{cu}). The area under the stress-strain curve is termed as the fracture energy of the material and is defined as the amount of energy dissipated during fracture per unit of newly created fracture surface area. The fracture energy in tension (G_f) and in compression (G_c) are assumed to be material properties.

The reinforcement, wherever present can be modelled using a separate constitutive relationship. Figure A. 1 shows a hardening model of the reinforcement in which the initial steel stiffness (E_s^0) drops to hardening stiffness (E_s^T) after the yield stress (f_y) is exceeded. The summation of stiffness contributions from concrete and steel reinforcement is considered as the effective stiffness of RC (E_c^{eff}).

In the elastic regime, the behaviour of concrete in shear is governed by the shear modulus (G). It is related to the to the Young's modulus through the relation,

$$G = \frac{E}{2(1+\nu)}$$

After cracking, the initial shear stiffness ($G_0 = G$) declines to a damaged shear stiffness(G_d). Many possibilities exist to define shear retention relations [30]. The considered relations are discussed in chapter 3.

A. 3 Crack concepts

Owing to its limited tensile capacity, cracking in concrete significantly impacts the stress distribution within RC structures and is one of the main causes of nonlinearity in the analysis. Different approaches to numerically model cracking exist, each with a unique perspective on a 'crack'. The classical concepts of discrete crack and smeared crack are discussed in this section.

A.3. 1 Discrete crack concept

In the discrete crack approach, a crack is modelled as a geometrical discontinuity. Interface elements with rigid connection between overlapping nodes can be provided along a predefined cracking path. The initial stiffness of the elements is assigned a large dummy value to simulate the uncracked stage. Upon violation of the condition of crack initiation, element stiffness is changed and a constitutive model for discrete cracks is activated. The constitutive law links the tractions $\mathbf{t}^{cr}$ along the crack to relative displacement $\mathbf{u}^{cr}$ across the crack via $\mathbf{C}^{cr}$, which represents nonlinear material phenomena.

This approach is most suitable in analysis when the crack path is already known. From a pre-damage point of view, it is potentially applicable to cases where the behaviour of the structure is dominated by very well-defined cracks. The biggest drawback of this approach is that it implies a continuous change in the nodal connectivity, which does not fit well the nature of finite element

displacement method. Also, this approach is not suitable in cases of distributed fracture since it only allows modelling of individual localised cracks.

A.3. 2 Smeared crack concept

In the smeared crack approach, cracked concrete is imagined as a continuum such that the notions of stresses and strains remain valid. Instead of a discrete separation, the crack is 'smeared' over an area such that nodal connectivity is maintained [25]. The length over which the strain localises is incorporated as an input parameter termed the crack bandwidth(h) or sometimes, internal length(h_{eq}). This could be conceived as the length of the fracture process zone of the crack. Bandwidth for a few element-shapes and crack orientations is depicted in Figure A. 2.

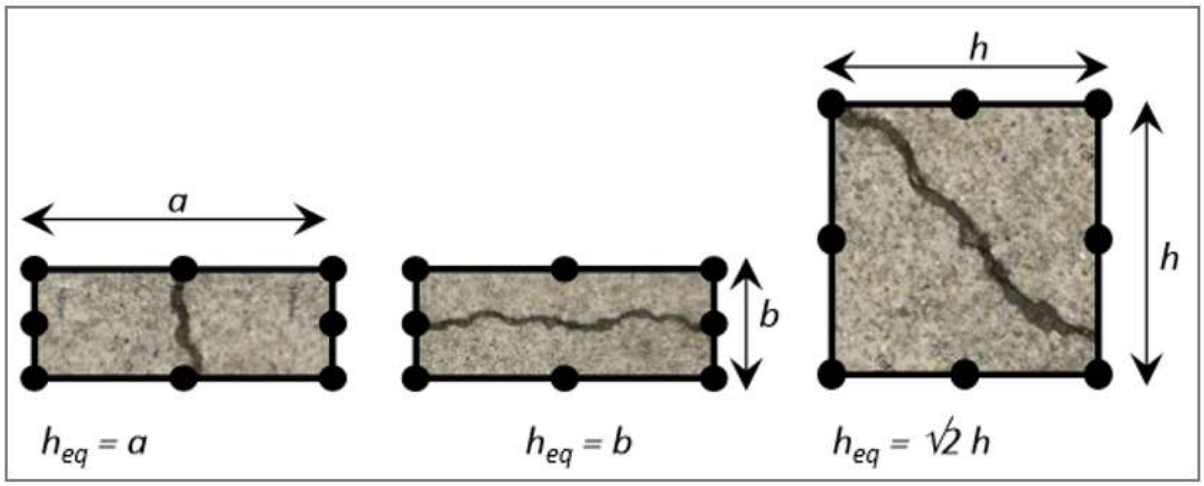

Figure A. 2 Crack Bandwidth or equivalent length [23]

When starting from an uncracked state, concrete is treated as a linear-elastic isotropic material. For a two-dimensional case, the constitutive relationship can be expressed as,

$$\boldsymbol{\sigma}_{xy} = \mathbf{D}_e \, \boldsymbol{\varepsilon}_{xy} \qquad \text{(eq.A.1)}$$

Where, *xy* represents the global co-ordinate system. $\mathbf{D}_e$ represents the linear-elasticity stiffness matrix.

When the principle tensile stress in a material point exceeds the tensile strength of concrete, a crack is initiated perpendicular to the direction of the principle stress. The initial isotropic relationship (Eq.2.2) is switched to an orthotropic relationship with nt-axes of orthotropy wherein, n is the direction normal to the crack and t, the direction tangential to the crack (Figure A. 3).

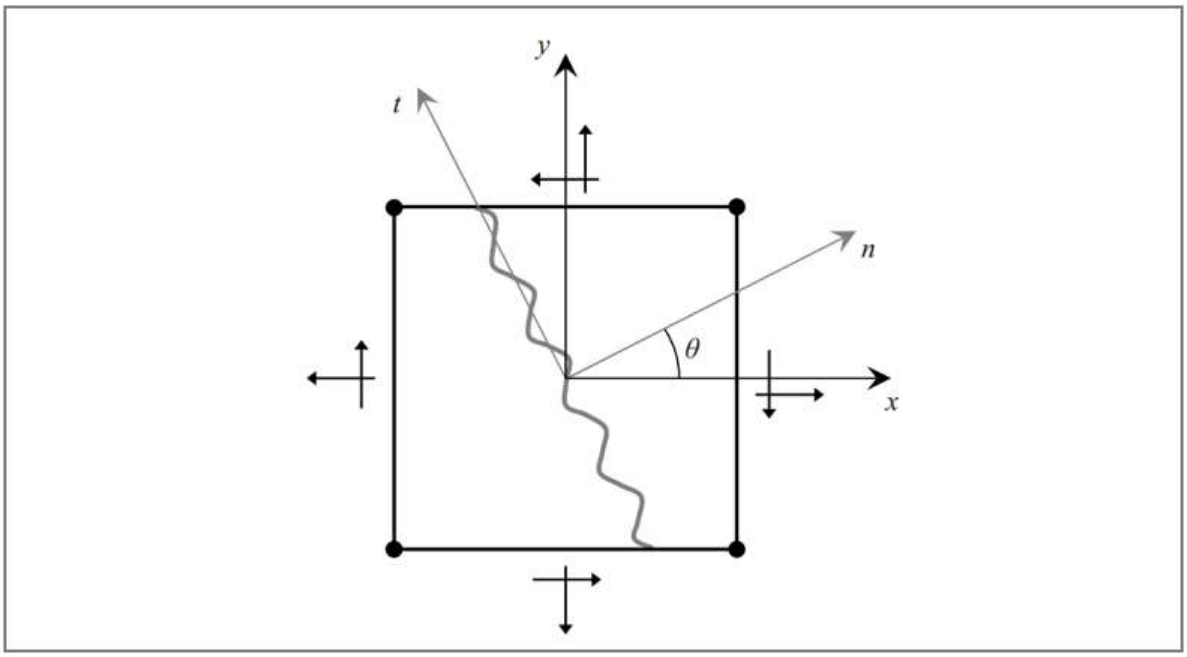

Figure A. 3 Axes of cracking for a concrete element with a single crack [21]

The stress-strain relationship in the nt-axes system is now written as,

$$\boldsymbol{\sigma}_{\mathrm{nt}} = \mathbf{D}_{\mathrm{nt}}\,\boldsymbol{\varepsilon}_{\mathrm{nt}} \qquad \text{(eq.A.3)}$$

Where $\mathbf{D}_{\mathrm{nt}}$ represents the secant or tangent material stiffness matrix.

If θ is the angle between the x-axis and n-axis, the following relation can be set up between the components of $\boldsymbol{\sigma}_{\mathrm{nt}}$, $\boldsymbol{\varepsilon}_{\mathrm{nt}}$ and $\boldsymbol{\sigma}_{\mathrm{xy}}$, $\boldsymbol{\varepsilon}_{\mathrm{xy}}$,

$$\boldsymbol{\sigma}_{\mathrm{nt}} = \mathbf{T}_{\sigma}(\theta)\,\boldsymbol{\sigma}_{\mathrm{xy}} \qquad \text{(eq.A.4)}$$

$$\boldsymbol{\varepsilon}_{\mathrm{nt}} = \mathbf{T}_{\varepsilon}(\theta)\,\boldsymbol{\varepsilon}_{\mathrm{xy}} \qquad \text{(eq.A.5)}$$

Where, $\mathbf{T}_{\boldsymbol{\sigma}}$ and $\mathbf{T}_{\boldsymbol{\varepsilon}}$ are transformation matrices.

Combining (Eq.2.2), (Eq.2.3), (Eq.2.4) and (Eq.2.5) yields,

$$\boldsymbol{\sigma}_{\mathrm{xy}} = \mathbf{T}_{\sigma}^{-1}(\theta)\mathbf{D}_{\mathrm{nt}}\,\mathbf{T}_{\varepsilon}(\theta)\boldsymbol{\varepsilon}_{\mathrm{xy}} \qquad \text{(eq.A.6)}$$

(eq.A.6) gives a relation between stresses and strains in the *xy* coordinate system via the material stiffness matrix in the nt co-ordinate system.

If the angle θ is fixed upon the initiation of the first crack, the approach is referred to as fixed smeared cracking. The fixing of angle of the nt co-ordinate system entails misalignment of the principal direction of stresses and strains. Thus, an appropriate shear retention relationship is required after cracking, in this approach [25].

When the angle θ is continuously aligned with the direction of principal strains, it is referred to as rotating smeared cracking. Here, co-axiality is enforced between principal directions of stresses

and strains and the expression for shear stiffness after cracking is derived from the principal values [25].

Refinements to this formulation involving decomposition of the strains which allows multiple cracking directions within one element are also possible [20] [25], but are not treated in this thesis. The treatment here is limited to orthogonal cracking, in which upon initiation of the crack, only normal and tangential strains in the element are monitored and their effects are transferred to the global axis system of the analysis.

Smeared cracking approach has a major advantage of computational simplicity as it preserves the topology of the finite element mesh. Material descriptions for similar elements are enough to model cracking, thereby circumventing the need to introduce special interface elements in the mesh, like in the case of discrete cracking. Also, crack bandwidth 'h' enters the description of the material, which can be given a physical interpretation of the width of the crack fracture zone, allowing modelling of distributed fracture. These advantages make this approach a suitable candidate for a generic modelling approach for damage in RC.

Appendix B

B. 1 Introduction

The damage mechanisms studied in the literature review in order to characterise damage in reinforced concrete are described in detail in this appendix.

B. 2 Damage due to mechanical loading

Concrete is a heterogenous material in which aggregates are dispersed in a matrix of hydrated cement paste. There exist weak interfacial transition zones at the boundary between the aggregates and the cement paste. Moreover, prior to application of mechanical loading there may already exist randomly oriented micro-defects and air-voids [10]. For most design purposes, these are neglected, and concrete is treated as an isotropic homogenous material. However, these defects serve as potential locations for initiation of damage in the structure upon application of load.

Due to the fact that the tensile strength of concrete is drastically lower than its compressive strength, micro-cracks are formed locally, at points of highest tensile stress. As the load goes on increasing, micro-cracks continue to develop at points where the tensile stress exceeds the tensile strength. These micro-cracks coalesce together along the path of least resistance to form macro-cracks, which are visible on the surface of the structure. [10], [31]. Thus, macro-cracks represent the change of internal micro-structure of the material leading to the localisation of damage. Therefore, the presence of macro-cracks induces anisotropy, which influences the stress distribution within the structure [32]. In the experiment conducted by Maekawa and Pinnamas the effect of vertical pre-cracks on the shear capacity of beams under mechanical loading is studied. It is observed that the response of pre-cracked RC beams changes considerably as compared to the undamaged beam. It is also seen that the structural response is sensitive to the width, location and orientation of the cracks.

Figure B. 1 shows a schematic representation of typical cracks observed in RC structures which can be attributed to load history. Shear and flexural cracking in unreinforced areas of high tensile stress is commonly observed. Splitting cracks may be observed in areas with compressive strut action.

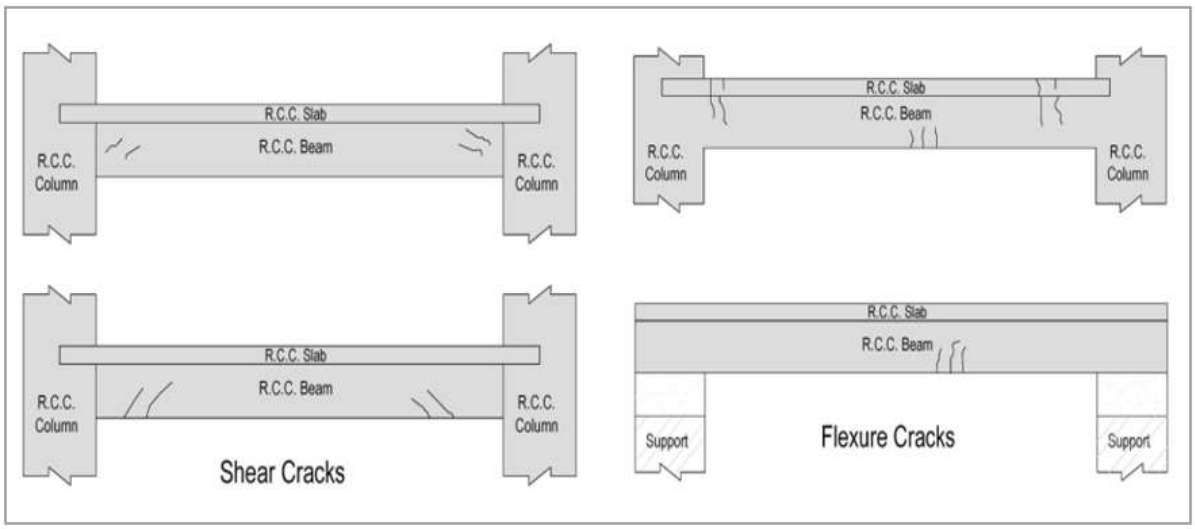

Figure B. 1 Typical cracks in RC members due to external load [43]

B. 3 Damage due to reinforcement corrosion

Concrete in structural applications is most commonly reinforced with embedded steel bars in order to resist the tensile stresses developed in the structure. Steel bars may also be present in the compressive zones, which are provided for a more efficient load transfer to limit the size of cross-section of structural members.

Steel is not a naturally occurring material, but is manufactured by smelting and refining iron-ore. Corrosion is the electro-chemical reaction by which steel releases energy to revert back to its original state, i.e. Iron-oxide(rust). Thus, reinforcement corrosion is characterised by loss of rebar area. Rust occupies more volume than steel, thereby exerting expansive pressure on the surrounding concrete. Continual production of rust leads to increasing expansive pressure which may exceed concrete tensile strength, leading to cracking along the rebar and eventual spalling of concrete cover [33]. The process is schematically shown in Figure B. 2. This may impact the bond strength between steel and concrete and thereby adversely affect the load-carrying capacity of the structural member [34].

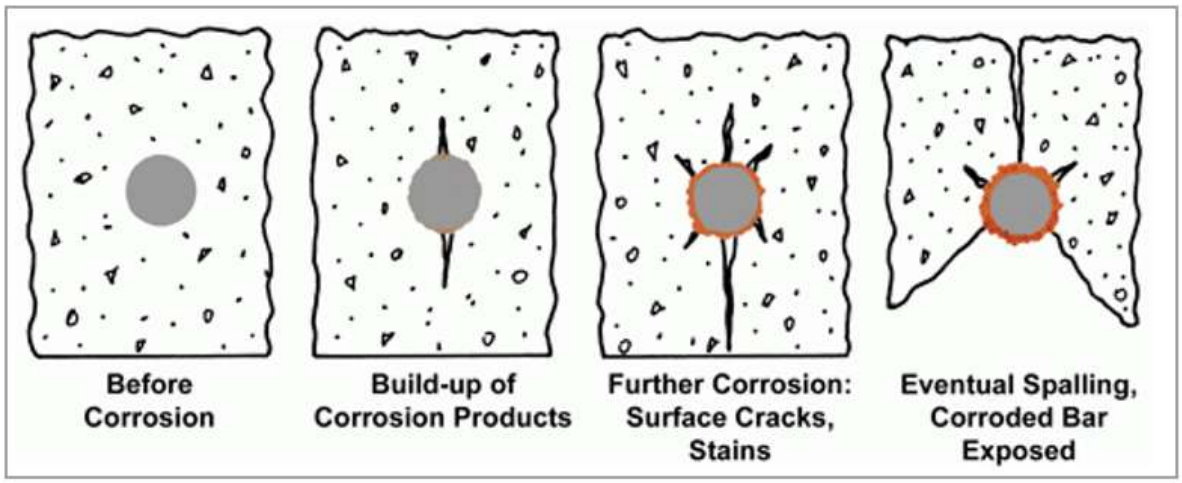

Figure B. 2 Evolution of corrosion damage in RC [8]

Corrosion in RC is a highly time-dependent process. It requires the presence of water and oxygen and is generally accelerated by chloride and carbonation attack. The degree of corrosion may vary spatially, from locally corroded areas called pitting corrosion to distributed corrosion along the rebar called uniform corrosion. The extent of damage due to corrosion can be broadly divided into three stages [33]:

I. Initial period, when negligible corrosion takes place due to a passive layer around the steel bar providing high alkalinity.
II. Propagation period, when the passive layer is destroyed by chloride and carbonation attacks and minor cracking can be observed in the concrete cover.
III. Acceleration period, when corrosion is accelerated due to easy access of oxygen causing widespread cracking with rust stains and concrete spalling

Figure B. 3 shows an RC member affected by reinforcement corrosion. Spalling of the cover and longitudinal cracks along the steel bar represents the damage to the concrete. Many models exist which correlate the weight loss of rebar to the mechanical properties of damaged reinforced concrete [35]. The weight loss along the rebar due to corrosion can be estimated directly by a number of measurement methods, e.g. Open circuit potential, Surface potential, Linear Polarisation resistance etc. [36].

Figure B. 3 RC member affected by reinforcement corrosion [9]

B. 4 Damage due to freeze-thaw cycles

The microstructure of concrete is characterised by a number of voids and capillaries. These may be present in the hardened cement paste or aggregates. When concrete is subjected to very low temperatures, the water inside the voids and capillaries freezes and expands to exert hydraulic pressure on the surrounding area. Also, the presence of soluble salts in the water lowers its freezing point. This may attract more water from surrounding cavities and upon freezing exerts internal osmotic pressure [10], [31]. Thus, alternate freezing and thawing cycles on concrete may cause deterioration and micro-cracking leading to degradation of mechanical properties of concrete. Figure B. 4 schematically describes the process inside the cement paste of concrete.

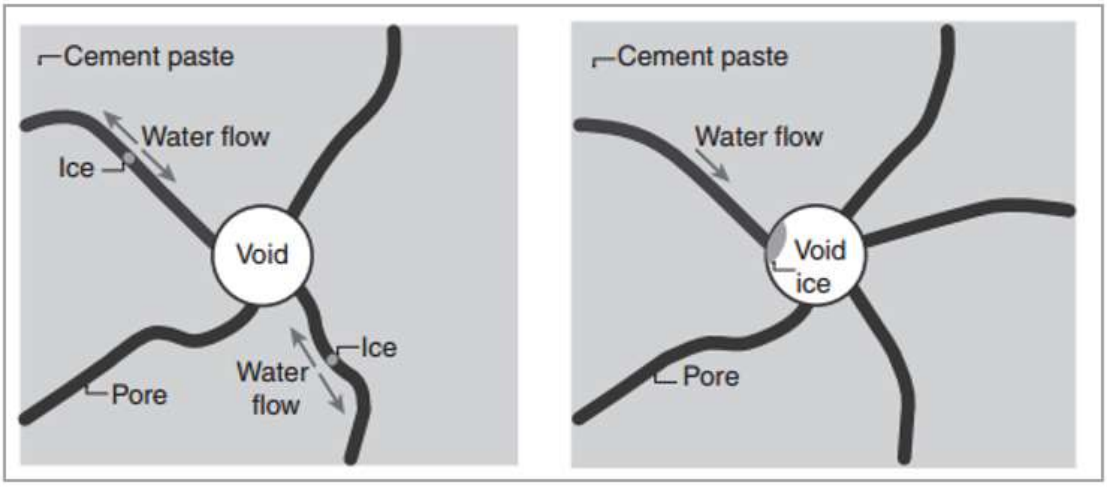

Figure B. 4 Freeze-thaw mechanism in the cement paste [10]

Damage due to freeze-thaw cycles manifests itself into two major forms:

I. Surface scaling (Figure B. *5*)
II. Internal frost damage

Surface scaling causes delamination of concrete cover usually leaving the rest of the structure unharmed [37]. The extent of damage can be visually observed. Delamination of concrete cover may accelerate reinforcement corrosion in the structure.

Figure B. *5* Surface scaling of concrete due to freeze-thaw cycles [11]

Internal frost damage is a more dangerous outcome of freeze-thaw cycles and leads to degradation of mechanical properties of concrete. It is usually difficult to access the precise extent of damage by mere visual observations and drilled cores may be needed to evaluate the properties of damaged concrete.

Internal frost damage is highly dependent on the micro-structure of the concrete and the environmental conditions of the surroundings. Many studies and models have been developed to take into account the effect of internal frost damage on the structural properties of reinforced concrete [37], [31], [38], [39]. The current degree of saturation of concrete is suggested to be a prime factor in accessing the extent of damage [37]. G Fagerlund of the Swedish Concrete and Cement Research institute proposed a methodology which links the degree of saturation of concrete to the degraded elastic modulus [37], [10]. Permeability of the aggregates and air-entrainment of the cement paste, presence of de-icing salts can be other major controlling factors [10].

B. 5 Damage due to Alkali-Silica Reaction

A wide variety of siliceous aggregates used in concrete are vulnerable to attack by alkaline pore fluid in the concrete. This reaction produces a hygroscopic gel which expands as it absorbs water. Upon considerable expansion, the swelling pressure might be sufficient to crack aggregates or cement paste. These cracks may propagate upon continued expansion of the gel, leading to further damage of the material. [10].

ASR is a chemical process which has mechanical consequences [40]. Therefore, the distribution of reactive sites, localisation and extent of damage may depend on numerous inter-dependent factors like, the rate of reaction, expansion of the gel, availability of moisture, temperature, presence of pre-existing micro-cracks etc. [40].

Figure B. 6 ASR map-cracking and cracks preferentially oriented along the main reinforcement [7]

Visibly, on the macro-scale damage due to ASR is characterised by a network of randomly oriented cracks known as map-cracking. It may be accompanied by presence of dissected silica gel in the cracks. In cases where the expansive force of the reaction is restrained due to reinforcement, the cracks may be preferentially oriented along the main reinforcement (Figure B. 6) [7].

Although, ASR damage exhibits visible characteristics on the surface of the structure, petrographic evidence on drilled cores are often needed to attribute ASR as the primary cause of damage [41]. The Damage Rating Index (DRI) for quantification of ASR damage, proposed by Dr. P. E. Grattan-Bellew of the National Research Council of Canada, enlists the following characteristics of the reaction as petrographic evidence:

- Coarse aggregate with crack
- Coarse aggregate with crack and gel
- Coarse aggregate de-bonded
- Reaction rim around aggregate
- Cement-paste with crack
- Cement-paste with crack and gel
- Air void lined with gel

In this system, the above characteristics are attributed weights according to their order of importance, allowing for an estimation of the degree of damage of a sample [42].

The Stiffness Damage Test (SDT) allows estimation of the loss of elastic modulus of an ASR affected specimen through cyclic compressive loading and has been advocated as a powerful tool for assessing damage in concrete due to ASR [43].

References

[1] A. Slobbe, *ERP Structural Intergrity - Stochastic structural analysis of corroded RC structures,* 2016.

[2] "DIANA 10.2 User's Manual," FEA DIANA BV, Delft, 2017.

[3] "MATLAB," [Online]. Available: https://nl.mathworks.com/products/matlab.html.

[4] A. Pimanmas and K. Maekawa, "Influence of pre-cracking on reinforced concrete behaviour in shear," *Concrete Library of JSCE No.38,* December 2001.

[5] Y. Yang, C. van der Veen and D. Hordijk, "Investigation of vmin based on experimental research".

[6] "Types & Summary of Cracks in Reinforced Concrete Beams," [Online]. Available: https://gharpedia.com/types-summary-of-cracks-in-reinforced-concrete-beams/.

[7] G. E. Blight and M. G. Alexander, Alkali-Aggregate Reaction and Strctural damage to concrete, CRC Press/Balkema, 2011.

[8] [Online]. Available: https://www.galvanizeit.org/transportation-seminar/hdg-steel-benefits/maintenance-free/in-concrete.

[9] "PCI – PENETRATIVE CONCRETE CORROSION PROTECTION," [Online]. Available: http://technokotes.com/project/concrete-corrosion-protection-pci/.

[10] P. K. Mehta and P. J. Monteiro, Concete: Microstrcutre, properties and materials, Third ed., 2006.

[11] "Freeze Thaw Damage In Bricks And Concrete: How To Prevent It," [Online]. Available: https://www.makewoodgood.com/freeze-thaw-damage/.

[12] M. Cao, Q. Ren and P. Qiao, "Nondestructive Assessment of Reinforced Concrete Structures Based on Fractal Damage Characteristic Factors," *Journal of Engineering Mechanics,* Vols. 132, No. 9, 2006.

[13] B. Mandelbrot, The Fractal Geometry of Nature, 1982.

[14] M. Kulenovic, "Applications of Fractal Geometry," [Online]. Available: http://fibonacci.math.uri.edu/~kulenm/honprsp02/index.html.

[15] A. Farhidzadeh , E. Dehghan-Niri, A. Moustafa, S. Salamone and A. Whittaker, "Damage Ass ssment of Reinforced Concrete Structures Using Fractal Analysis of Residula Crack Patterns," *Society for Experimental Mechanics ,* 2013.

[16] A. Ebrahimkhanlou, A. Farhidzadeh and S. Salamone, "Multifractal analysis of crack patterns in reinforced concrete shear walls," *Structural Health Monitoring,* 2016.

[17] A. B. Chabbra and R. V. Jensen, " Direct determination of the f(α) singularity spectrum and its applicaltion to fully developed turbulence".

[18] "Image Processing and Analysis in Java," ImageJ, [Online]. Available: https://imagej.nih.gov/ij/index.html.

[19] D. Kondo, H. Welemane and F. Cormery, "Basic concepts and models in continuum damage mechanics," *Revue européenne de génie civil,* vol. 11, no. (n° 7-8). pp.. ISSN 17747120, pp. 927-943, 2007.

[20] R. de Borst and L. Sluys, Computational Methods in Non-linear Solid Mechanics, 2015.

[21] A. Slobbe, "Propagation and band width of smeared cracks," 2015.

[22] B. Sluys and R. De Borst, Computational Methods in Nonlinear Solid Mechanics (CIE5142), TU Delft, 2015.

[23] M. Hendriks, A. de Boer and B. Belleti, "Guidelines for Nonlinear Finite Element Analysis of Concrete Strucutres," Rijkswaterstaat Centre for Infrastructure, 2016.

[24] D. A. Hordijk, H. W. Reinhardt and H. W. Cornelissen, "Experimental determination of crack softening characteristics ofnormalweight and lightweight concrete".

[25] J. G. Rots and J. Blauwendraad, "Crack models for concrete: Discrete or smeared? Fixed, Multi-directional or Rotating," *Heron,* vol. 34, 1984.

[26] "Gauss Quadrature," [Online]. Available: http://www2.mae.ufl.edu/haftka/structII/chap4-2.pdf.

[27] "28 Stress Recovery," [Online]. Available: http://www.colorado.edu/engineering/CAS/courses.d/IFEM.d/IFEM.Ch28.d/IFEM.Ch28.pdf.

[28] R. T. Koekkoek and Y. Yang, "Measurement Report on the Transition between Flexural and Shear Failure of RC Beams without Shear Reinforcement," TU Delft, Delft, 2016.

[29] fib Model Code for Concrete Strucutures 2010.

[30] A. F. Pruijssers , "Description of the stiffness relation for mixed-mode fracture problems in concrete using the rough-crack model of Walraven," TU Delft.

[31] Z. Yang, "Assesing cumulative damage in concrete and quantifying its influence on life cycle performance modelling," 2004.

[32] A. Pimanmas and K. Maekawa, "Finite element analysis and behaviour of pre-cracked reinforcement concrete members in shear," *Magazine of concrete research,* vol. No.4, no. August, 263-282, 2001.

[33] J. R. Mackechnie and M. G. Alexander, *Repair principles for corrosion-damaged reinforced concrete structures,* Department of Civil Engineering, University of Cape Town, 2001.

[34] M. Tahershasmi, "Structural Effects of Reinforcement Corrosion in Concrete Strucutures," Department of Civil and Environmental Engineering, Chalmers University of Technology, 2016.

[35] Y. Zhao, J. Yu and W. Jin , "Damage analysis and cracking model of reinforced concrete structures with rebar corrosion," *Elsevier,* 2011.

[36] H.-W. S. Song and V. Saraswathy, "Corrosion Monitoring of Reinforced Concrete Structures - A review," *International Journal for Electrochemical Science,* vol. 2, 2007.

[37] G. Fagerlund, "Fagerlund, G. (1995). Frost damage on concrete : estimation of the future deterioration.," *The Residual Service Life of Concrete Structures,* vol. Vol. 3067, no. BRITE/EURAM project BREU-CT92-0591, 1995.

[38] H. Muttaquin, H. Okuyama, Y. Sato and T. Ueda, "Stress-strain relationships of concrete damaged by freezing and thawing," *Journal of Advanced Concrete Technology,* vol. 2, no. 1, pp. 89-99, 2004.

[39] K. Z. Hanjari, P. Utgenannt and K. Lundgren, "Experimental study of the material and bond properties of frost-damaged concrete," *Cement and Concrete Research 41,* pp. 244-254, 2011.

[40] A. Giorla, C. Dunant, A. Guidoum and K. Scrivener, "Experimental and Numerical Study of Alkali-Silica reaction under multi-axial load," 2012.

[41] B. Godart, M. d. Rooij and J. G. Wood, "Guide to Diagnosis and Appraisal of AAR Damage to Concrete Structures - Part 1 Diagnosis (AAR 6.1)," RILEM, 2013.

[42] P. Rivard, B. Fournier and G. Ballivy, "The Damage Rating Index Method for ASR Affected Concrete—A Critical Review of Petrographic Features of Deterioration," *Cement Concrete and Aggregates,* 2002.

[43] L. F. Sanchez, B. Fournier, M. Jolin and J. Bastien, "Evaluation of the stiffness damage test (SDT) as a tool for assessing damage in concrete due to ASR : Test loading and output responses for concretes incorporating fine or coarse reactive aggregates," *Cement and Concrete Research,* 2013.

[44] W. B. Kratzig, Y. S. Petryna and F. Stangenberg, "Measures of structural damage for global failure analysis," *International Journal of Solids and Structures (2000)* , vol. 37, 2000.